An Investigation of the Seismic Response of Earthen Levees with Cutoff Walls with a Focus on the Development of a High Performance Cutoff Wall Material

by

Adam J. Lobbestael

A dissertation submitted in partial fulfillment
of the requirements for the degree of
Doctor of Philosophy
(Civil Engineering)
in the University of Michigan
2014

Doctoral Committee:

Assistant Professor Adda Athanasopoulos-Zekkos, Co-Chair
Professor Victor C. Li, Co-Chair
Professor Roman D. Hryciw
Associate Professor Veera Sundararaghavan
Associate Professor Dimitrios Zekkos

ACKNOWLEDGEMENTS

I would like to take this opportunity to thank the many people who have helped me throughout graduate school and who have made this dissertation possible. First and foremost, I would like to thank my doctoral advisor, Professor Adda Athanasopoulos-Zekkos. Through the course of my research project and graduate school she has been an exceptional mentor, not only concerning the technical aspects of my research, but also with regard to several other areas, ranging from writing and presentation skills to career and personal development. I admire her dedication to and passion for our field of study as well as engineering education. She is the kind of researcher, scientist, educator, and advisor that I aspire to be.

I also would like to thank Professor Dimitrios Zekkos, who has also been an important mentor to me. Professor Zekkos has had a profound impact on my life in several ways, beginning with encouraging me to go to graduate school and pursue a PhD. I never imagined that this was even a remote possibility for me and will always be grateful to him for the opportunities that this has opened up to me. The other members of my committee, Professor Li, Professor Hryciw, and Professor Sundararaghavan also deserve recognition, both for their help with this research as well as for being excellent teachers in the classroom.

Several other members of the faculty and staff in the College of Engineering have helped me in a variety of ways. Professor Michalowski and Professor Woods have been excellent teachers

and it has been a pleasure to learn from and to work with both of them. I would like to thank Dr. Montgomery for her excellent course on Teaching Engineering and for all of her help with career development and the faculty position application process. Rebi Varghese has come to my assistance for computer matters countless times, and I am grateful for his help and patience. I also would like to thank Sherry Breuger and Kimberly Smith for their help with many administrative matters over the years, as well as for their kindness and cheerfulness.

I also would like to thank the many graduate students with whom I have shared my time here at Michigan, for their camaraderie and support. It has been invaluable to have peers who understand the rollercoaster that graduate school has been. They include David Saftner, Yongsub Jung, Mustafa Saadi, Sid Nadukuru, Athena Gkrizi, Clinton Carlson, Andhika Sahadewa, Yao Zhang, Hyon-Sohk Ohm, Jonathan Hubler, and Nick Brandt, among others.

Lastly, I want to thank my family for the love and support they have shown and the patience they have had with me. Not only have they kept my spirits high, but they have helped me keep my life in perspective, continually reminding me of what is most important. Many thanks go to my parents, my grandparents, my brothers and their wives, and my sisters. Finally, all of my nieces and nephews have brightened so many of my days, and I could never thank them enough. Janae, Sylvie, Rory, Leif, Lew, Garon, Evalyn, and Marie: Thanks for taking my mind off school and making me smile countless times.

TABLE OF CONTENTS

LIST OF TABLES

LIST OF FIGURES

ABSTRACT

In recent years, flood protection systems across the nation have undergone extensive investigation into their current state and adequacy regarding various potential hazards. These investigations have revealed that 1) many existing levees are vulnerable to excessive under- and through-seepage due to the insufficient state or length of their cutoff walls, and 2) seismic activity poses serious risks to many existing levees. Traditional cutoff walls (e.g. slurry-type walls and steel sheet pile walls) have a variety of shortcomings, particularly for levees in seismic regions. This project investigates the feasibility of using a new cutoff wall material that overcomes many of the shortcomings associated with traditional cutoff wall materials. The proposed cutoff wall material is from a family of high performance fiber-reinforced cementitious materials called Engineered Cementitious Composites (ECC). ECC possesses several characteristics that make it ideal for use as a cutoff wall material in seismic regions, including high tensile ductility and small crack width, among others.

The initial portion of this study focuses on characterizing the dynamic response of levees with conventional cutoff walls. Two sets of parametric analyses are conducted to investigate how the presence of a cutoff wall affects the dynamic response of a levee and what type of demands are placed on the cutoff wall during the seismic event. One set of analyses is conducted for levees founded on non-liquefiable soils and the other is for levees founded on liquefiable soils. In collaboration with materials science researchers, an ECC material is then tailored for use in the

construction of levee cutoff walls. The results of materials testing on the resulting candidate mix design are then used as input in further numerical modeling, in which the dynamic response of levees with ECC cutoff walls is investigated. These analyses are used to assess the feasibility of the candidate mix design.

Conclusions regarding the feasibility of using such a material for levee cutoff walls are presented, with recommendations for a candidate ECC mix. Also, revisions to existing levee seismic design guidelines are proposed, based on the results of the parametric analyses of the dynamic response of levees with conventional cutoff walls

CHAPTER 1

Introduction

Throughout the history of the United States, water resource and flood management projects have played a critical role in our development and vitality. Not only have water management projects allowed for the rise of prolific societies at the interface between land and water, such as the Mississippi River Valley and the Great Lakes Region, but they have also enabled the great American West to flourish in what was once a barren desert. Society however must strike a delicate balance between water use and protection from the very same water that it so heavily depends upon. Society depends on its close proximity to something that, while altogether essential, possesses tremendous destructive power, as has been witnessed through floods, hurricanes, and tsunamis. As our nation and economy continue to grow, there is ever increasing life, property, agriculture, and livelihood that become dependent upon this balance and it becomes more necessary for us to invest in and improve our water infrastructure. Prompted by the destruction that resulted from Hurricane Katrina, the research study presented in this dissertation investigates the feasibility of a new risk mitigation technique for flood protection systems, in an effort to address a facet of the need for flood protection improvements.

1.1 Motivation and Problem Statement

A stark reminder of just how much we depend on our flood protection systems and how much they are protecting was provided by the devastation that followed Hurricane Katrina in the late summer of 2005. Widespread failure of the flood protection system around New Orleans, Louisiana contributed significantly to the heavy losses resulting from the hurricane and subsequent flooding; a death toll greater than 1,600 and economic losses on the order of $150 billion. The causes and results of the approximately 40 levee failures that occurred in New Orleans are well documented by Seed et al in a set of 4 companion papers (2008a, b, c, and d). Figure 1-1 presents a selection of images of the destruction that the hurricane caused to the levee systems.

This catastrophic performance of the levees in New Orleans prompted organizations and regulatory agencies across the country to take a closer look at the state of their flood protection systems. The investigation by the American Society of Civil Engineers (ASCE) warranted a grade of *D*- for levees on the ASCE infrastructure report card, the lowest grade. The California Department of Water Resources (DWR) also commissioned a broad investigation into the current state and reliability of levees in their jurisdiction. The report resulting from this investigation indicated the potential implications of an additional layer of complexity that could seriously challenge levees; seismic activity. Figure 1-2 presents a seismic hazard map of the United States, which highlights this vulnerability, indicating that California is a very seismically active region. However, it can also be seen on this map that the Mississippi River Valley, heavily protected by levees, coincides with another seismically active region; the New Madrid seismic zone. The coincidence of the nation's regions with the most levees and the nation's most seismically active zones underscores the importance of considering the seismic vulnerability of levees.

The results of the analyses of the Sacramento-San Joaquin river delta area, conducted as part of the DWR investigation, provide a strong example of how seismically-induced levee failures could result in calamitous damages. The Sacramento-San Joaquin river delta area lies at the confluence of the Sacramento and San Joaquin rivers in central California and serves as a fresh water source for approximately 23 million people. Within the delta area there are approximately 60 "islands" which are below sea level due to land subsidence, which are protected by roughly 1,100 miles of levees. The elevation of these island ranges from 5 to 30 feet below sea level, as shown in Figure 1-3. The investigation concluded that "A major earthquake of magnitude 6.7 or greater in the vicinity of the Delta Region has a 62% probability of occurring sometime between 2003 and 2032. This could cause multiple levee failures, fatalities, extensive property destruction and adverse economic impacts of $15 billion or more" (URS 2007).

The repercussions of failures of these levee systems not only include the disaster associated with widespread flooding, but would also severely compromise this vital fresh water source. The fresh water from the river delta flows into the Pacific Ocean and accordingly there is a salinity gradient between the two water bodies. This gradient is regularly subject to slight shifts due to tidal trapping mechanisms, but could be severely shifted in the event of levee failures in the delta. Figure 1-4 shows the results of a hydrologic model investigating a scenario in which 20 levee breaches result from a seismic event (NEES EOT 2014). Figure 1-4 (a) shows the delta region prior to levee breaching and (b) shows several of the delta islands flooded shortly after levee breaching, with the salinity. Figure 1-4 (c) shows the salinity of the delta region approximately 8 days after the seismic event. As a result of the backflow from the ocean, the salinity has intruded all the way into the delta and essentially decimated the fresh water resource. This scenario further underscores the importance of seismic resilience of levees.

A key component of levee resilience is the inclusion of cutoff walls to protect against excessive under- and through-seepage (illustrated in Figure 1-5), which was identified as the failure mechanism for several of the levee breaches in New Orleans following Hurricane Katrina, due to the insufficient length or state of the existing cutoff walls (ILIT 2006). These findings, coupled with the DWR investigation reports suggesting that seismic activity may seriously challenge the current state of levees, introduce the issue of the seismic performance of cutoff walls and levee systems with cutoff walls. Typical levee cutoff walls are constructed using the slurry wall construction method and are composed of various soil, bentonite, and cement mixtures. However, these are brittle materials and therefore may crack during a seismic event, rendering them ineffective as seepage barriers.

Conventional cutoff walls are subject to a range of other issues in addition to the concerns related to seismic performance. Excavations investigating slurry type cutoff walls have shown that vegetation and tree roots are capable of causing significant cracking, as shown in Figure 1-6. Burrowing rodents have also been shown to be very destructive to slurry cutoff walls. Steel sheet pile walls, another cutoff wall option, do not face these same concerns, but are not ideal for use in levee systems for other reasons. Due to the assembly method used for sheet pile walls, with continuous joints running the entire pile length, they are prone to leakage and it is very difficult to verify that a connection joint has remained intact through the construction process. Also, the extensive nature of levee systems, which run for several miles, often makes the cost of sheet pile walls prohibitive. Due to the shortcomings associated with conventional cutoff walls, seismic vulnerability and through-seepage risks may compound to result in catastrophic loss. Accordingly, there is a need to advance the state of the art and practice of levee analysis, design, and construction, particularly with regard to levee cutoff walls.

1.2 Proposed Solution and Research Approach

The study presented in this dissertation focuses on the investigation of the feasibility of a new cutoff wall material that overcomes the shortcomings associated with traditional cutoff wall materials. The proposed material is from a family of high-performance fiber reinforced composites called engineered cementitious composites (ECC). ECC materials exhibit several properties that make them a desirable choice for a cutoff wall material that would be resilient against seismic activity. Chief of these is the superior ductility that ECC possesses, as demonstrated in Figure 1-7. Additional benefits and more details on this material are presented in depth in a later chapter.

The development of a new ECC-type cutoff wall material has been a multidisciplinary endeavor, approached through a series of stages, combining numerical modeling and physical material testing. The numerical modeling was conducted using FLAC – Fast Lagrangian Analysis of Continue (Itasca 2011), a 2D explicit finite difference program designed for continuum modeling of geotechnical analysis of rock, soil, and structural support. This software package was selected for a variety of features that make it ideal for the challenges presented by modeling the dynamic response of levee systems, including the ability to model liquefaction and soil-structure interaction. The explicit finite difference formulation ensures that physical instability does not result in numerical instability, allowing for the ability to accurately model large deformations and flow. FLAC also has a built in programming language, FISH, which enables the user to easily define new variables and functions allowing for parametric study automation, assignment of unique property distributions, and powerful command over the implementation of the program. The numerical modeling components of this study were conducted in conjunction with a material tailoring and testing process, performed by materials science researchers at the Advanced Civil Engineering Material Research Laboratory (ACE-MRL) at the University of Michigan. The goal

of the material tailoring process was to develop an ECC-based material that is suitable for use as a levee cutoff wall, meeting the restraints imposed by performance, construction, and economic considerations.

The first portion of the research study focuses on characterizing the dynamic response of levees with conventional cutoff walls. Prior to this study, little or no research had been conducted on the dynamic response of earthen levees with cutoff walls. Understanding the influence of a cutoff wall on levee response and the demands placed on a cutoff wall during a seismic event were the first tasks of this research study. This portion of the study consisted of two parametric analyses, one for levees founded on non-liquefiable soils, and one for levees founded on potentially liquefiable soils. The parametric analyses investigate a broad range of combinations of input motions, wall types, and soil properties and were conducted to identify the critical parameters influencing the dynamic response of levees with cutoff walls.

The first portion of the study also provided a starting point for the subsequent material tailoring process by providing insight into the demands that a seismic event places on a levee cutoff wall and accordingly what demands an ECC cutoff wall would need to be able to sustain. Initial target values for a range of performance parameters (e.g. ductility, tensile strength, permeability, cost) for the new ECC material were designated based on the results of the first portion of the study as well as review of existing research. ECC mix designs were developed, tested, and subsequently revised to achieve a mix design meeting the performance targets. The material testing results were also used as numerical model inputs in the final portion of the study.

The final portion of the study again used numerical modeling to investigate the dynamic response of a levee system with a cutoff wall, this time composed of the new ECC material. A third parametric analysis was conducted using a range of input motions and soil profiles, all with

ECC cutoff walls. The results of this analysis were used to verify the feasibility of the ECC mix design and to propose recommended revisions and improvements.

1.3 Overview of Dissertation

The details of each portion of the research study, as overviewed above, are presented in the following 5 chapters:

Chapter 2 presents the setup and results of the parametric analyses of levees with conventional cutoff walls (sheet pile walls and soil cement bentonite walls). The parametric analysis presented in this chapter investigates levees founded on soils which are not considered to be liquefiable. The results of this parametric analysis are compared to existing recommendations for the evaluation and design of the seismic performance of levees.

Chapter 3 is similar to Chapter 2, however it includes the added complexity of soil liquefaction, modeled using the state-of-the-art UBCSAND soil model. Again, a parametric analysis is conducted for levees with conventional cutoff walls and the results are compared to existing recommendations.

Chapter 4 presents a background on ECC materials and the properties that make them ideal for the application of cutoff walls for levees in seismic regions. This is followed by a summary of the material tailoring and testing process. Finally, considerations necessary to capture the behavior of the new ECC material in a numerical model are discussed.

Chapter 5 presents the setup and results of the numerical modeling of the dynamic response of levees with ECC cutoff walls. In this parametric analysis, both liquefiable and non-liquefiable soils are considered.

Chapter 6 presents a summary of and the conclusions of this study, regarding the feasibility of the use of the ECC material for levee cutoff walls. Limitations of this research study, as well as areas for further research are also presented.

(a)  (b) 

(c) 

Figure 1-1, Levee failures in New Orleans resulting from Hurricane Katrina (a) Levee erosion along St. Bernard Parish frontage (Seed et al 2008a), (b) Emergency repairs at the 17th Street Canal levee breach (Seed et al 2008c), and (c) Lower 9th Ward Inner Harbor Navigation Canal Levee Failure *(with emergency repair levee in place)* (Seed et al 2008b)

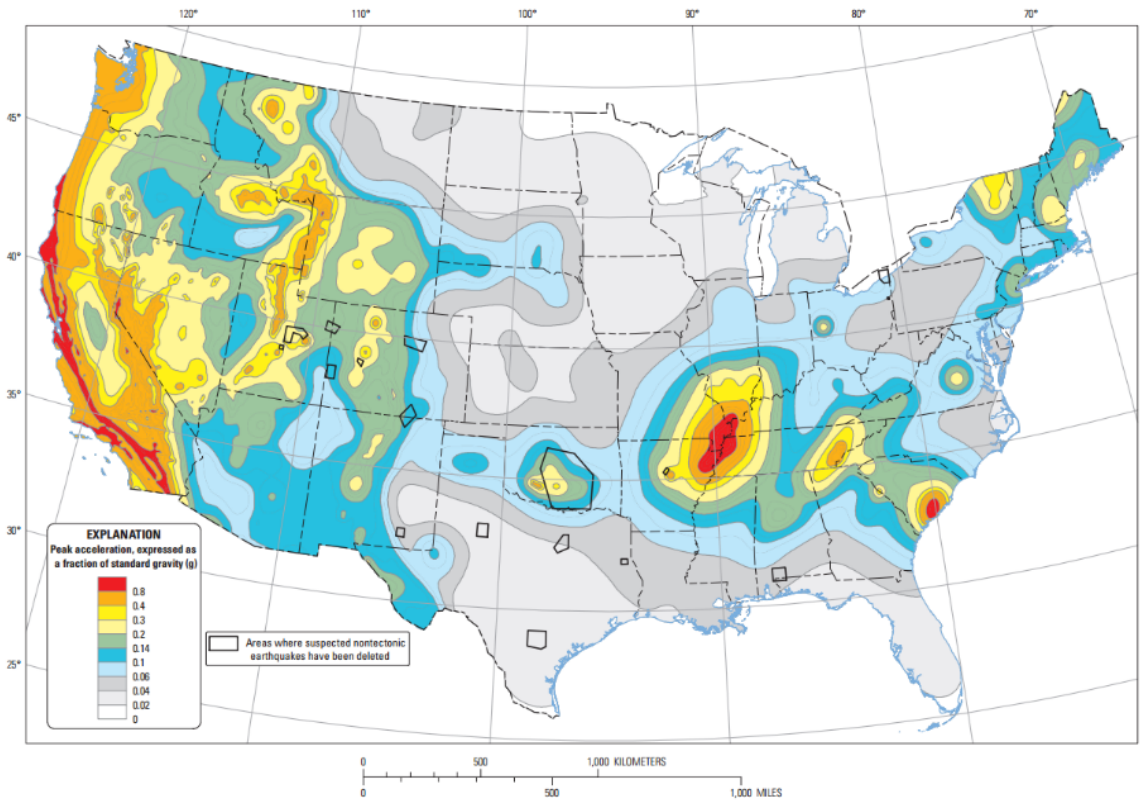

Figure 1-2, Seismic hazard map of the United States indicating peak ground acceleration values with 2% probability of exceedance in 50 years (Petersen et al 2014)

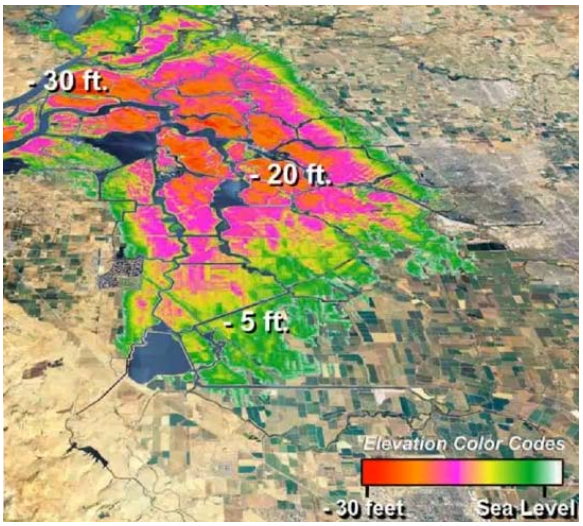

Figure 1-3, Land elevations above sea level in the Sacramento-San Joaquin river delta region (NEES EOT 2014)

(a)

(b)

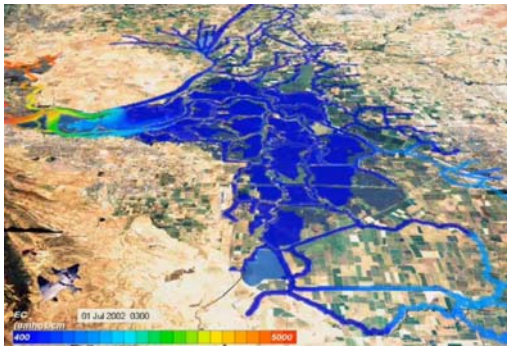

(c)

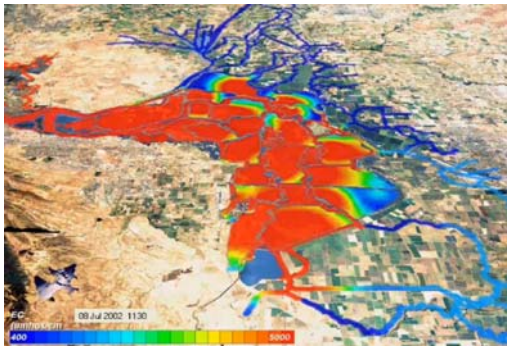

Figure 1-4, Hydrologic modeling of a flood event in the Sacramento-San Joaquin river delta resulting from a seismic event: (a) prior to flooding, (b) salinity directly after flooding and (c) salinity 8 days after flooding (NEES EOT 2014)

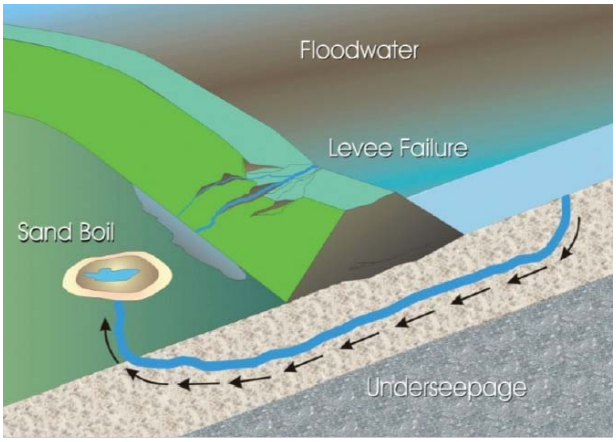

Figure 1-5, Schematic of levee failure due to excessive under seepage (ILIT 2007)

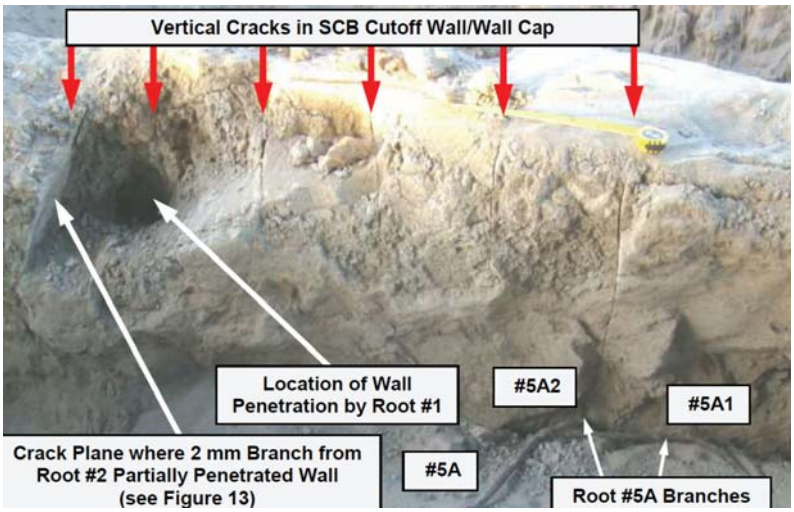

Figure 1-6, Cracks revealed in an exploratory excavation adjacent to a soil-bentonite cutoff wall (Harder et al 2009)

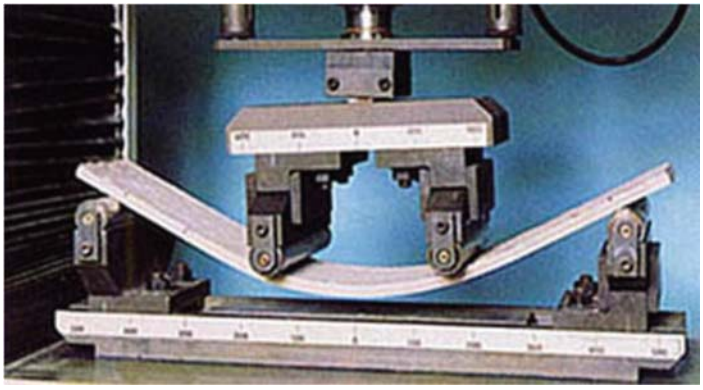

Figure 1-7, 4-point bending test on an ECC specimen

CHAPTER 2

Dynamic Response of Levees with Conventional Cutoff Walls

As an initial step in the process of developing a new material for use as levee cutoff walls for seismic risk mitigation, a parametric was conducted to investigate the dynamic response of earthen levees with conventional cutoff walls (i.e. steel sheet pile walls and soil cement bentonite slurry walls). Significant work has been done to understand the response of earthen levees to seismic activity (e.g. Athanasopoulos-Zekkos, 2008), but there has been no previous work to investigate how the presence of a cutoff wall affects the dynamic response of an earthen levee. Furthermore, it is unknown what demands a seismic event may place on a levee cutoff wall. This portion of the study was conducted to provide insight into how the presence of a cutoff wall affects the dynamic response of a levee, and by extension to predict how an ECC cutoff wall could affect the response of a levee. The analyses of levees with conventional cutoff walls were separated into two broad categories, 1) levees founded on non-liquefiable soils and 2) levees founded on liquefiable soils, with the first category being the focus of this chapter and the second presented in Chapter 3.

As mentioned previously, the dynamic response of levees is not well understood and has only recently begun to be studied in depth. Furthermore, there are currently only limited seismic

design guidelines for levees, such as the guidelines recently put forth by the U.S. Army Corps of Engineers (2013), which only focus on susceptibility to liquefaction and seismic displacements of purely earthen levees. A 2D finite difference numerical modeling parametric analysis was conducted to address this need. Several levee soil profiles with two different cutoff wall types were analyzed using simplified ground motion inputs. The general response of the levee, in terms of slope displacements, earth pressures, and soil-structure interaction is presented and discussed. Analyses were also conducted using actual ground motion recordings for comparison to the results with simplified ground motion inputs.

The dynamic analysis and design of levees with cutoff walls lies at the intersection of several topics which have been previously studied in geotechnical engineering, such as geotechnical earthquake engineering and site response, dynamic soil-structure interaction, seismic slope stability, and seepage, among others. However, it also poses a new set of challenges to be studied and understood. Research has recently been conducted on the seismic response of earthen levees (Athanasopoulos-Zekkos, 2008 and Athanasopoulos-Zekkos and Seed, 2013), however the effect of an embedded cutoff wall was not included in the scope of this research. Engineers began researching the seismic loading of retaining structures and walls in the early twentieth century (Okabe, 1926 and Mononobe and Matsuo, 1929) and extensive work has been conducted in this field since. A review of the existing literature on this topic is provided by Sitar et al (2012). Preliminary research however has shown that the problem of the dynamic response of levees with cutoff walls is more complex than the superposition of seismic slope stability and seismic earth pressures. Not only does the soil surrounding a cutoff wall place demands on the structural element, but the presence of a cutoff wall was shown to alter the response of the levee under

dynamic loading in terms of topographic amplification as well as displacements and strains (Lobbestael and Athanasopoulos-Zekkos, 2013).

2.1 Numerical Model and Parametric Analysis Input

The parametric analysis was conducted using the 2D finite difference software FLAC 7.0 (Itasca, 2011). A generic levee profile geometry was used for all of the analyses conducted as part of the parametric analysis. This profile consisted of a 10.7-meter high, symmetric levee founded on 30.5 meters of soil. The levee had 3:1 (H:V) slopes and a 9.1-meter crest width. For the levee profiles with a cutoff wall, the cutoff wall extended to a depth of 19.8 meters below the levee crest. The finite difference grid was composed of quadrilateral elements with a maximum width of approximately 1.5 meters, shaped into an expanded grid (as shown in Figure 2-1), using a plane-strain formulation. This maximum grid dimension was selected to allow waves with significant frequency contents of up to 7 Hz to propagate without numerical distortion. Since the analyses were performed for generic levee cross sections, a fully coupled fluid-mechanical analysis was not used for the initial stress state calculation and an uncoupled fluid-mechanical analysis was used instead. This was only for the initial stress state however; a fully coupled formulation was used during the dynamic analyses. The model was initially stepped to equilibrium with no water and pore pressures were computed using an uncoupled fluid analysis with the waterside slope submerged to half of its height and the water table at the toe on the landside. The model was then again stepped to equilibrium with the effective stresses adjusted to reflect the pore pressures.

Two different types of cutoff walls were investigated in the parametric analysis; a steel sheet pile wall and a soil cement bentonite wall. The steel sheet pile wall, being a slender structural element, was modeled as a beam element (available in FLAC). The soil cement bentonite wall

however was modeled using finite difference zones with a constitutive model, since it is a soil-like material. This approach of modeling slurry cutoff walls using discretized continuum is similar to ones proposed by other researchers (e.g. Baxter and Filz, 2007). The stiffness contrast between the cutoff walls and the surrounding soil does result in a decrease in the timestep required for numerical stability (computed automatically by FLAC), but does not result in prohibitive computation times.

Both wall types were attached to the surrounding soil using glued interfaces. This is a simplification of the model, but was done in order to avoid including additional structural Rayleigh damping, which results in a prohibitively small computational time step (in the context of an extended parametric analysis). In order to ensure that this assumption does not invalidate the results of the parametric analysis, a selection of analyses were run with unglued interfaces and compared to the analyses with glued interfaces. The results of these analyses are presented at the end of the chapter in Section 2.2.7, *Supplemental Analysis for Validation of Interface Modeling Assumptions*. The supplementary analyses indicate that this assumption has relatively small effect on the response of the system for the purpose of this study. The simplification does result in the development of a small amount of unrealistic tension along the interface between the wall and soil near the levee crest, but only for very strong motions (i.e. $a_{max} > 0.4g$). This did not have a significant effect on shear strains, surface displacements, maximum lateral earth pressures, and failure mechanism characteristics. This simplification has also been made by other researchers performing similar types of analyses (e.g. Tsompanakis, 2009 and Veletsos and Younan, 1997).

The dynamic analysis was performed after the calculation of the initial stress state. Hysteretic damping in the soils was modeled using a 4-parameter sigmoidal model, fit to observed modulus reduction and damping curves. In addition to the hysteretic damping, a small amount of

stiffness-dependent Rayleigh damping (0.2% at 1.7 Hz) was included to minimize numerical noise. In order to account for the behavior at the lateral extents of the model, free field boundaries were applied during dynamic loading. Absorbing boundaries were applied along the base of the model and the ground motion was applied as a stress-time history along the model base. This effectively models a vertically propagating shear wave and a compliant base, as described by Mejia and Dawson (2006).

A wide range of parameter combinations was investigated in this study in which the soil properties, cutoff wall type, input motion frequency, and input motion intensity were all varied. Figure 2-2 presents a schematic of the parameter combinations that were part of this study. Six soil profiles were analyzed in the parametric analysis. The material properties used to model them, along with the material properties of the cutoff walls are presented in Table 2-1. Profile 1 was a uniform, medium-stiff clay profile and Profile 2 was a uniform, stiff clay profile. These simplified profiles were chosen to better identify the effects of the various input parameters. Profile 3 was a more realistic clay profile with linearly increasing shear strength and stiffness with depth. The effective stress formulation used in the FLAC dynamic module requires that drained strength and stiffness parameters be defined. To accommodate this, properties for the clay materials were estimated from undrained parameters using recommendations by Bjerrum and Simons (1960). Profiles 4, 5, and 6 were similarly selected, with Profile 4 being loose sand, Profile 5 being dense sand, and Profile 6 consisting of sand layers of increasing shear strength and stiffness with depth.

The parameters used to capture the hysteretic damping behavior of the soils are also presented in Table 2-1. These parameters were used in a 4-parameter sigmoidal model and were calibrated to match modulus reduction and damping curves available in the literature. For the clay profiles (Profiles 1-3), modulus reduction and damping curves were calibrated based on Plasticity

Index (PI)-dependent curves for clays presented by Vucetic and Dobry (1991). For the sand profiles (Profiles 4-6), the average modulus reduction and damping curves for sands presented by Seed and Idriss (1970) were used.

Two types of input motions were used in the parametric analysis; Ricker wavelets and sinusoidal motions. These input motion types were initially used so the effects of individual parameters (e.g. excitation frequency, intensity, etc.) on the response of the system could be studied. Ricker wavelets were selected as a first input motion due to their simplicity and smooth frequency content about a center frequency (Ricker, 1940). Ricker wavelets have been used in other studies to investigate the effect of frequency content on soil-structure interaction (e.g. Tsompanakis, 2009 and Razmkhah et al, 2008). Sinusoidal motions were then used to investigate the effect of multiple cycles of loading, while still maintaining a simple frequency content and waveform. For both the Ricker wavelets and sinusoidal inputs, a range of frequencies between 1.0 Hz and 5.0 Hz were used, as well as input intensities ranging from 0.1 g to 0.4 g. For the sinusoidal inputs the numbers of cycles used were 5, 10, and 15. In addition to the simplified input motions, ground motion recordings were also used for comparison.

2.2 Parametric Analysis Results

In the following sections, the results of the parametric analysis are presented and discussed. The general behavior of the levees analyzed under dynamic loading is discussed first, followed by a presentation and discussion of the computed displacements. The soil-structure interaction is then discussed for the profiles with cutoff walls. Lateral earth pressures and structural element demands are presented. Within these sections, the analyses of Profile 1 with Ricker wavelet inputs are presented in greater detail, with the remaining analyses presented in summary and compared to

Profile 1. The results of the parametric analysis are followed by a discussion of results from select analyses using ground motion recordings as inputs instead of simplified inputs and are then compared to existing recommendations for seismic design of levees. Results of supplemental analysis conducted in order to validate the assumptions made in modeling the soil-wall interface are also presented at the end of this section.

2.2.1 General Response and Failure Surface Development

The nature of the response of the levee under dynamic loading was observed to be generally similar for the various inputs, soil profiles, and cutoff wall types, with some variations for certain motion input parameters and soil properties. In this section, the general response and failure surface development of the levee is described for profiles with no wall and profiles with a cutoff wall. This is followed by a discussion of the effects of the various input parameters on the failure surface development.

For the profiles with no cutoff wall, displacements and shear strains indicate that failure surfaces begin to develop on both sides of the levee under dynamic loading. A deep failure surface that extends into the foundation develops on the landside, running from the crest to the toe. On the waterside, a shallower, more complex failure develops. The primary failure surface is a shallow circular failure running from the upper portion of the slope to the toe. There also appears to be a secondary failure surface, which is slightly deeper and runs from the crest to the toe. This failure however, is not as developed as the former waterside failure. The presence of a cutoff wall alters the response of the levee by forcing the landside failure to the landside of the levee crest. This results in an overall reduction in the size of the landside failure mass and a slightly shallower failure surface. On the waterside, the wall causes the shallow toe failure to become slightly larger,

with the entry point shifting up the waterside slope. For many of the analyses with a cutoff wall (described in more detail below) a more complex failure developed. Figure 2-3 presents the maximum shear strain contour for one of the Ricker wavelet analyses for Profile 1 with a simplified schematic of the observed general failure mechanisms. The shallow waterside failure (area A) remained consistent with the other analyses. As the landside failure mass (area C) moves towards the landside, an active failure wedge (area B) is formed on the waterside of the wall and the wall is pushed towards the landside. The only other general variation in failure surface development was observed for some of the sand profiles, where relatively small shallow toe failures developed on both sides of the levee, instead of the deeper failures.

The input motion parameters (frequency, intensity, and number of loading cycles) were all seen to have significant effects on the response of the levee system. For the Ricker wavelet loadings, both with and without a cutoff wall, the failure development consisted of circular failure surfaces on both sides of the levee, as discussed above. The failure developments for the levee with no cutoff wall were quite similar for the Ricker wavelet inputs and harmonic inputs, although the failure was much more developed (higher shear strains) for the harmonic loading. Also, the deeper, secondary waterside failure that was observed for the Ricker wavelet input was not present for the harmonic input, instead the two primary failure surfaces dominated. With the cutoff wall in place however, the dynamic response under simple harmonic loading was significantly more complex than for the Ricker wavelet, although certain elements remained similar. On the landside of the levee, the failure consisted of a single circular failure surface, but on the waterside, the combined shallow circular failure and active failure wedge were observed. It is likely the case that this is an extension of the response that was observed for the Ricker wavelet loading, but it was not fully developed for a single cycle of dynamic loading. Regardless of input type, for all analyses,

the degree to which the mechanism developed was heavily dependent upon the intensity and frequency of the input. For a given profile, as the frequency decreased and the intensity increased, the failure surfaces became more developed. It was also observed that, particularly for the sand profiles, as the input frequency decreased, the circular failure surfaces tended to deepen. It should be noted that no unique behavior was observed around the natural frequency of the profile, which was in the vicinity of 2.0 Hz for all profiles. Overall, it was observed that a decrease in input frequency was detrimental to the response of the levee, as were increases in input intensity or number of loading cycles.

The effect of soil type and properties on the failure surface developments is also of interest. In general, the behaviors of the three clay profiles (Profiles 1, 2, and 3) were quite similar to each other, although the magnitude of the strains varied. For a given input motion, there were slight differences in failure surface development between the three profiles. On the landside, Profile 2 had a slightly deeper failure surface than Profiles 1 and 3, which had very similar landside failure surfaces. On the waterside of the levee, Profiles 1 and 2 had similar shallow toe failures, but the secondary, deeper failure was slightly deeper for Profile 1 than for Profile 2. For Profile 3, only one clear failure surface developed on the waterside, running from the crest to the toe, as deep as the base of the levee.

The sand profiles (Profiles 4, 5, and 6) also exhibited similar behavior to each other, with slight variations. The shear strains were highest for Profile 6, followed by Profile 5, and Profile 4, although they were all of similar orders of magnitude for a given input motion. This may seem counterintuitive since Profile 4 is the weakest of the three, but is a result of the different dynamic site response characteristics of the profiles. Profile 4 has the lowest initial stiffness *and* was modeled with the lower bound modulus reduction curve, while Profile 5 has higher initial stiffness

and was modeled with less modulus reduction (average modulus reduction curve). These combined factors result in Profile 5 allowing for more transmission of the input energy through the foundation material to the levee, and thereby higher strains than Profile 4. The geometry of the failure surfaces was very similar for Profiles 4 and 5, but varied for Profile 6, which was a layered profile. The landside failure surface for Profile 6 was shallower than for 4 and 5, because it was constrained by the layered soil strengths. The waterside failure surface, being entirely within the levee, which was of uniform soil for each profile, had similar geometry for all three profiles. Also, for the inputs that resulted in the formation of an active failure wedge in Profile 6, the wedge differed from those observed in other analyses in that it did not run to the tip of the cutoff wall, but rather intersected the wall at a shallower depth. This is again due to the layering in soil strengths.

Differences in behavior were also observed for the two different cutoff wall types; steel sheet pile and soil cement bentonite, although the differences were not as dramatic as the differences between having a wall and not having a wall. The primary differences in behavior were observed for the lower frequency inputs (1.2 Hz and 1.9 Hz). For the levee with the soil cement bentonite wall, the failure developments were similar to those for the sheet pile wall in that there was a combined mechanism of landside and waterside circular slope failure with active wedges forming along the wall. For the soil cement bentonite wall, however, the active failure wedge was much more developed (in terms of shear strains) with circular failure surfaces extending from it at shallow and deep depths. For the sheet pile wall case the circular failures were more dominant, and the failure wedge was not as developed. This can be explained conceptually by the differences in stiffness contrast between the wall and soil for the two cases. The steel sheet pile wall is several orders of magnitude stiffer than the surrounding soil. Therefore, in the vertical direction, the surrounding soil is more likely to move relative to the wall, resulting in failure along the top of the

wall. This then intersects the developing circular failure and allows for it to develop further. The soil cement bentonite wall, on the other hand, is closer in stiffness to the surrounding soil. Therefore, in the vertical direction, the soil and wall are more likely to deform together. The soil and wall thus move downward together, similar to a wedge zone in a bearing capacity-type failure, with circular failure surfaces extending from it. The failure surface developments for the high frequency input (5.0 Hz) were essentially the same for the two different wall types.

2.2.2 Horizontal and Vertical Surface Displacements

The analysis results suggest that the extent to which the general behaviors, discussed above, develop is strongly dependent on the frequency content and intensity of the input wavelet, the soil strength and stiffness, the presence (and type) of cutoff wall, and the number of cycles of loading. The following section presents horizontal displacements across the ground surface for a selection of the analyses, in order to illustrate the effect of each of the various parameters. Following the presentation of the horizontal displacements, vertical displacements are discussed.

The analyses conducted using the varying Ricker wavelet inputs illustrate well the dependence of the response of the levee on the frequency content of the input motion. Figure 2-4 presents the horizontal displacements along the ground surface (shifted by the residual displacements in the free field on the respective side of the levee) for several Ricker wavelet inputs with a range of center frequencies, for Profile 1 with a steel sheet pile cutoff wall. It is immediately apparent that the magnitude of the displacements increases dramatically as the center frequency of the input wavelet decreases. The horizontal displacements for the remaining soil profiles exhibited similar dependence on input frequency. The dependence on frequency is partially due to the

inherent increase in energy of a Ricker wavelet associated with a decrease in frequency. However this alone does not account for the frequency dependence. This is illustrated later in section 2.2.6.

The input intensity of the ground motion also has a very strong effect on the response of the levee. Figure 2-5 shows the horizontal displacements across the ground surface for Profile 4 (loose sand) with a steel sheet pile wall and a 5-cycle sinusoidal input excitation with a frequency of 1.9 Hz. The magnitude of the displacement increases significantly as the input intensity increases.

The soil type, strength, and stiffness also had a significant impact on the levee displacements. Horizontal ground displacements for each soil profile are presented in Figure 2-6. The displacements presented are for the profiles with a sheet pile wall and a 5-cycle sinusoidal input with input intensity of 0.4 g and frequency of 1.9 Hz. The clay profiles exhibited significantly higher displacements than the sand profiles. The displacements for the stiff clay profile, Profile 2, are lower than Profile 1. On the landside of the levee, Profile 3 had similar displacements to Profile 1. However on the waterside, Profile 3 had approximately 30% lower displacements. This indicates that the landside failure surface was primarily within the levee, while the waterside failure surface was influenced more by the foundation. When comparing the displacements for the sand profiles to each other, it can be seen that Profile 4 exhibits the smallest horizontal displacements with Profile 5 exhibiting slightly greater displacements. Again, this is due to the dynamic site response of the foundation material. Profile 6 has the greatest displacements of the three sand profiles, since it combines the relatively low strength of the levee and shallow soils with the site response properties of the deep stiff foundation soils.

Of primary interest is the change in response for profiles with cutoff walls and its dependency on the type of cutoff wall. Figure 2-7 presents horizontal surface displacements for Profile 6 with no wall, a steel sheet pile wall, and a soil cement bentonite wall. The figure presents results for 5-cycle harmonic inputs with intensity of 0.4 g and frequency of 1.9 Hz. As the figure indicates, the presence of a cutoff wall reduces the computed displacements. This is due to the geometric constraints that a cutoff wall places on the failure surface developments, as described previously. This was true for all of the soil types investigated. Also, it was observed that, for the different profiles, there was no dramatic change in the relationship between the displacements with and without a cutoff wall, but rather they remained relatively constant for all profiles. In general, the steel sheet pile wall resulted in slightly lower displacements than the soil cement bentonite wall. Overall the presence of a cutoff wall is beneficial to the stability of the levee.

Finally, the number of cycles of loading had a significant impact on the response of the levee. Figure 2-8 presents the horizontal surface displacements for Profile 4 with a steel sheet pile cutoff wall subject to a harmonic input with intensity of 0.4g and frequency of 1.9 Hz, for a range of cycles. As the number of cycles increase, the displacements increase significantly on both sides of the levee, although the shape and general behavior remains constant. It does appear however that the increase in displacements from 10 to 15 cycles is somewhat smaller than the increase in displacements from 5 to 10 cycles. This is due to the fact that as ground shaking continues, the levee will eventually reach a new deformed equilibrium state.

Although only horizontal displacements have been presented to this point, the vertical displacements along the levee crest are of critical concern as well for the performance of a levee. The loss of freeboard during a seismic event is essentially the key parameter with respect to the flood control function of a levee. However, most simplified seismic slope displacement procedures

(e.g. Makdisi and Seed, 1978) estimate Newmark-type, horizontal displacements. Therefore ratios of vertical crest displacements to the maximum horizontal displacement on the waterside slope are presented in the following section and the effect of the various input parameters on that ratio is discussed.

In order to illustrate the nature of the vertical displacements and how it varies for the three different wall types, vertical displacements across the ground surface are presented in Figure 2-9. The displacements in this figure are for Profile 6 with a 5-cycle harmonic input with input frequency of 1.9 Hz and shaking intensity of 0.4 g. The profile with no cutoff wall exhibits the greatest vertical displacements whereas the sheet pile wall and soil cement bentonite walls are able to arrest some of the vertical displacements in the vicinity of the crest. Since the soil cement bentonite wall is able to deform with the surrounding soil, it results in greater vertical levee displacements than the sheet pile wall, which is stiffer relative to the surrounding soil. This trend was observed for all input motions.

Table 2-2 presents ratios of vertical crest displacements to maximum horizontal waterside slope displacements for selected analyses. The table is arranged to illustrate how this ratio tends to change for various input parameters, with each set of columns showing the influence of a different input parameter. In general, it was observed that for profiles with cutoff walls, the vertical displacements were lower than the horizontal displacements. It was also observed that as the input frequency decreased and the input intensity increased, the ratio of vertical to horizontal displacements increased. This was also true for an increase in the number of cycles of loading. The third column of table 2-2 shows how the ratio changes for different soil strengths. For the uniform soil profiles, the ratio of vertical to horizontal displacements increases as strength decreases.

However, it can be seen that for layered profiles, the ratio increases more, since the displacements and associated ground motion energy dissipation are more focused in the shallower, weaker soils.

2.2.3 Lateral Earth Pressures

For the profiles with cutoff walls, the interaction between the wall and the surrounding soil are important aspects of the response of the levee. In the following sections, the behavior of the lateral earth pressure on the steel sheet pile wall is discussed for several profiles for both Ricker wavelet and harmonic inputs. This is followed by comparison to the earth pressures observed on a soil cement bentonite wall under harmonic loading.

Figures 2-10(a) and (b) present lateral earth pressure-time histories for several points along the waterside and landside interface of the wall, respectively, for a single analysis. As seen in these figures, upon initiation of acceleration (around time = 0.65 seconds), the pressures at all nodes, and on both sides of the wall, decrease in a relatively uniform manner. All of the pressures then rebound, except for the shallow nodes along the landside of the wall. At this point, the behavior on opposite sides of the wall begins to change and the pressures at certain nodes begin to exhibit different behaviors, relative to other nodes on the same side of the wall. On the waterside of the wall, the pressures begin decreasing again after rebounding, although not in a uniform manner for all nodes. The pressures on the shallowest 5 nodes rapidly decrease, while the pressures on the deeper nodes decrease only slightly. This is essentially mirrored on the opposite side of the wall, where the shallow nodes experience a dramatic increase in pressure, while the deeper nodes only experience a slight increase in pressure. As the model returns to rest, the pressures on the shallow nodes return rapidly towards their initial values. The pressures on the deep nodes oscillate slightly and then gently increase, before reaching their final values. The residual pressures for the deep

nodes are all greater than the initial values. On the landside, the residual values are significantly greater for the shallow nodes, and on the waterside they are significantly lower.

This type of lateral earth pressure was observed, to some extent, for all of the input wavelets. For a given input intensity, as the center frequency decreased, the number of nodes that behaved like the shallow nodes (as described above) increased. For high frequency and low intensity inputs, the pressures at all depths essentially behaved in a uniform manner, relative to each other. In order to compare the lateral earth pressure behaviors for the various input wavelets, earth pressure profiles were taken at the instance when they reached their overall maximum on each interface, determined as the time at which the resultant of the lateral earth pressure distribution was greatest. These instances are marked on Figure 2-10 for each side of the wall with dashed vertical lines. From these lateral earth pressure profiles, the earth pressure coefficient, K, defined as the ratio of horizontal effective stress to vertical effective stress, was computed along the wall. Figure 2-11 present the profiles of K at the instance that the maximum earth pressure occurred on the wall for various input frequencies. The static at-rest earth pressure coefficient, K_0, and active and passive seismic earth pressure coefficients, K_{AE} and K_{PE}, computed according to Coulomb-type theory, are also plotted for reference. These figures further illustrate the two types of behavior that were observed in the wall pressures. For the higher frequency inputs, the earth pressure coefficient is relatively constant with depth, indicating monotonically increasing lateral earth pressure with depth. For the lower frequency inputs however, only the deeper nodes exhibit a constant earth pressure coefficient and the shallower nodes exhibit greater earth pressure coefficients. This indicates a bulge in the lateral earth pressure profile at shallow depths. Figure 2-12 presents the average (not including any bulge in earth pressure) and maximum seismic coefficient increments for each analysis, for the landside of the wall.

Lateral earth pressures on the steel sheet pile wall were also examined for Profiles 2 and 3, under Ricker wavelet loading. As the soil strength and stiffness change, the interaction between the wall and soil, and the structural demands placed on the cutoff wall change. When comparing these figures to the earth pressure time histories for Profile 1, it is immediately apparent that there are different behaviors for the different profiles. In general, the lateral earth pressures, both static and dynamic, are lower for the stronger profile, Profile 2. For Profile 2, the earth pressures at various points along the wall increase and decrease in a relatively uniform manner, while Profiles 1 and 3 exhibited nodes with non-uniform increase in pressure (as compared to other nodes along the wall). These were described previously as shallow nodes and were associated with a bulge in the lateral earth pressure profile. For the 0.4g input wavelet with a center frequency of 2.0 Hz (for which lateral earth pressure time histories are plotted), Profile 1 exhibited the most nodes behaving in this manner, Profile 2 exhibited essentially none, and Profile 3 exhibited some. Furthermore, for Profile 2, the earth pressures on the waterside of the wall and the landside of the wall behaved very similarly to each other throughout the dynamic loading, suggesting that the wall and soil were moving in phase with each other. For Profiles 1 and 3, the points along the wall that behaved as shallow nodes had earth pressures which were essentially mirrored on opposite sides of the wall, suggesting that the wall and soil are moving out of phase, with the wall pushing towards one side and pulling away from the other. These behaviors appear to be closely related to the development of the failure surfaces within the levee. For input wavelets that induce more developed failure surfaces, the number of nodes that behave as shallow nodes increases. This suggests that the earth pressures, and particularly the bulge in the earth pressure profile which was observed for some cases, are heavily influenced by the development of slope failures within the levee.

The earth pressure coefficients and the seismic earth pressure increments were computed for each analysis for Profiles 2 and 3, in the same manner as Profile 1, discussed above. Figure 2-13 presents the average and maximum seismic earth pressure coefficient increments. All points in Figure 2-13 were taken at the instance of maximum lateral earth pressure on the landside of the wall for input wavelets with intensity of 0.4g. The average seismic earth pressure coefficient increments were compared to existing experimental results for cross-braced walls presented by Sitar et al. (2012), in which values of earth pressure coefficient increment ranging from approximately 0.15 to 0.3 were reported for scaled ground motion recording inputs with peak intensity of 0.4g. Results from this study for input frequencies of 2.0 Hz and higher agree very well with these experimental results. Results for input frequencies of 1.0 Hz are outside of the range presented by Sitar et al. since they used scaled ground motions and 1.0 Hz is lower than the typical frequency content of an actual ground motion. Of the wall types investigated in the experiment, a cross-braced wall best reflects the physical setting of an embedded wall, such as a cutoff wall. For the results presented here, in general, as the soil becomes stronger, the average seismic earth pressure coefficient increases. This is in accordance with Coulomb theory for passive earth pressures. However, as the soil becomes weaker, and as the input frequency decreases, the likelihood of a bulge in the lateral earth pressure profile increases and the magnitude of the bulge increases. This is consistent with the observation that slope failure within the levee allows for higher passive pressures to develop along the cutoff wall.

Analyses performed for Profile 1 under sinusoidal loading indicated that the number of cycles of loading has a significant effect on the lateral earth pressures observed on the wall. For the analyses with the sinusoidal input, for the first cycle of loading, behavior similar to what was observed for the Ricker wavelet input was seen, with shallow nodes exhibiting more relative

change in pressure than deeper nodes. This may be associated with the initiation of the landside failure. However, as the loading cycles continue, different behavior becomes apparent. The pressures on the shallow nodes appear to reach a somewhat constant value, while the deeper nodes exhibit consistent change with time. Figure 2-14 presents the pressures at a shallow and deep node on both sides of the wall, to highlight the difference in these two behaviors. The lateral earth pressure at the shallower node oscillates about a constant value on both sides of the wall. The deep node oscillates about a constantly increasing value on the landside, which is matched by a decreasing value on the waterside. This suggests that, for the shallow node, the soil and wall are in phase, despite increases and decreases associated with each cycle of loading. The earth pressure on the deep node however shows that the wall is pushing towards the waterside soil and is pulling away from the landside soil. This is consistent with the failure mechanism presented in Figure 2-3, since the wall is pushed towards the landside due to the formation of the active failure wedge on the waterside. The shallow nodes do not exhibit a general change in pressure because of the landside failure, which moves away from the wall.

Lateral earth pressure profiles and associated seismic earth pressure coefficient profiles were also taken at the instance of maximum total lateral earth pressure for the harmonic input analyses. Figure 2-15 presents the seismic earth pressure coefficients on the landside of the wall with depth for Profile 1 with 0.4-g harmonic inputs of varying frequencies. When comparing this figure to the analogous figure for the Ricker wavelet inputs, it can be seen that under harmonic loading, the bulge in earth pressure at shallow depths is no longer present. However, a deeper bulge in earth pressure can be seen around a depth of 9.1 meters. Although the seismic earth pressure coefficient associated with the bulge is lower for the harmonic input, the associated earth pressure is much greater, because it occurs under greater vertical stress than for the Ricker wavelet input.

This further verifies the formation of the active failure wedge on the waterside of the cutoff wall and illustrates that the degree to which it develops increases as the input frequency decreases.

The lateral earth pressure behavior was also observed to vary for the sand profiles (Profiles 4, 5, and 6) subject to sinusoidal loading. The lateral earth pressure time histories were examined in a similar manner as described above for Profile 1, with the behavior of the pressures at each point being designated as either transient or relatively steady state. For the lower frequency inputs (1.2 Hz and 1.9 Hz) the deeper nodes tended to behave in a transient manner, with pressures increasing on the landside of the wall. The shallower nodes tended to exhibit steady-state behavior. For Profile 6, some of the deepest nodes also exhibited steady-state behavior, consistent with the observation that, when formed, the waterside active failure wedge intersected the wall above the base (rather than at the base). For some of the lower frequency inputs it was also observed that there was sometimes a region of nodes around a depth of 9.1 meters that exhibited slight increase in pressure on the landside, although surrounded by nodes that did not. For the highest frequency input (5.0 Hz) all of the pressures along the wall behaved essentially in a steady state manner, although there were very slight increases in landside pressure at some locations. These increases were minimal as compared to those observed for the lower frequency inputs. The seismic lateral earth pressure coefficients associated with the maximum lateral earth pressure profiles on the landside of the wall illustrate this behavior and are presented in Figure 2-16 for inputs intensities of 0.4 g.

Finally, the lateral earth pressure behavior was observed to vary significantly for a given soil profile with different cutoff wall types. The lateral earth pressures on the soil cement bentonite wall, for Profiles 4, 5, and 6, were tracked through the analyses and exhibited different behavior than the earth pressures on the sheet pile wall. The pressures on the sheet pile wall either reached

a steady state or changed significantly on one side of the wall, with opposite change on the other side of the wall. The pressures on the soil cement bentonite wall did not exhibit this type of behavior. Instead, for a given depth, the earth pressures were generally very similar on opposite sides of the wall. This difference in behavior can be attributed to the difference in wall/soil stiffness contrast. The soil cement bentonite wall, having a similar stiffness to the surrounding soil, is able to deform and comply with some of the displacements from the surrounding soil, while the sheet pile does not. The maximum lateral earth pressure profiles on the soil cement bentonite wall were converted to earth pressure coefficients and are also presented in Figure 2-16. Only results for analyses with 1.9-Hz input are shown since the soil cement bentonite wall results are not as frequency-dependent, relative to the steel sheet pile wall results. Because the soil cement bentonite wall is able to absorb surrounding deformations, the seismic earth pressure coefficients are significantly lower than those for the steel sheet pile wall. They all tend to exhibit a slight increase with depth, but no significant bulging as was observed for the sheet pile wall.

2.2.4 Cutoff Wall Demands

Cutoff wall bending moments were investigated for Profiles 1, 2, and 3, under Ricker wavelet loading. As with the results previously discussed, the structural demand placed on the cutoff wall was heavily dependent on the characteristics of the input wavelet. Figure 2-17 presents the maximum bending moment profiles for all Ricker wavelet analyses with an input intensity of 0.4g, for Profiles 1, 2, and 3. These moment profiles were taken during the dynamic loading at the instance when the overall maximum moment occurred at any point along the wall. The moments presented here are all within the moment capacity of the selected section (approximately 90 kN-m), although typical moment capacities for steel sheet piles used in cutoff applications may be much

lower. As seen in the figure, moments increase significantly as input frequency decreases. Moments also increased significantly as the input intensity of the wavelet increased. The largest moments occur for Profile 3, due to the fact that it has non-uniform strengths and stiffnesses along the length of the wall. This is in agreement with what has been observed for piles in layered soils, as summarized by Di Laora et al (2012). The smallest moments occur for Profile 2, which is the strongest and stiffest profile. It is also observed that the depth at which the maximum moment occurs changes for different soils. For Profile 2, it occurs in the region where the levee meets the foundation soils. For the weaker profiles, it occurs at shallower depths within the levee. This suggests that when a slope failure develops within the levee, it places the maximum demand on the cutoff wall, while when a slope failure is less developed moment demands are likely a result of differential motion between the levee and foundation.

Moments were also computed for Profiles 4, 5, and 6 under Ricker wavelet loading. The locations of the maximum bending moments were deeper than was observed for the clay profiles under Ricker wavelet loading and correspond roughly with the locations of the peaks in lateral earth pressure. For a given profile, the greatest moments occur for the lowest frequency inputs and decrease as the input frequency increases. It was also observed that the magnitude of the moment increased as the intensity of the input motion increased. As was observed with the clay profiles, as the strength of the soil increased, the maximum bending moment tended to decrease, however the moments for the non-uniform profile, Profile 6, tended to be greatest.

Analyses were also performed using sinusoidal inputs instead of Ricker wavelets. In general, it was observed that bending moments were greater for the sinusoidal inputs than the moments observed during Ricker wavelet loading and the maximum bending moment occurred at greater depth. This is due to the further development of the failure mechanisms under increased

loading cycles. Also, the deeper location of the maximum bending moment indicates that as the loading cycles increase, the deeper portions of the cutoff wall become more engaged in supporting the seismic lateral earth pressures.

Since the soil cement bentonite wall was modeled using finite different zones with a constitutive model, instead of a beam structural element, maximum shear strains are presented instead of bending moments. Figure 2-18 presents maximum shear strain profiles within the soil cement bentonite wall for Profiles 4, 5, and 6. As seen in the figure, the strains exceed the yield strain for the lower frequency inputs. However, this indicates plastic yielding and it is important to note that brittle fracture, which is likely under these strains, is not modeled here. These strains were taken from 0.4g sinusoidal inputs with 5 cycles. Again, it is seen that, for a given soil profile, as the input frequency decreases, the magnitude of maximum shear strains within the wall increases. This was also true for an increase in input motion intensity. As with the steel sheet pile wall, the greatest demand is placed on the wall for the layered soil profile, Profile 6. It should also be noted that the depths at which the maximum shear strains occur are very similar to the depths at which the maximum bending moment occurred for the corresponding profile with a sheet pile cutoff wall.

2.2.5 Recorded Ground Motion Analyses

In order to validate the trends that were observed in the analyses using Ricker wavelets and harmonic inputs, additional analyses were conducted for Profile 3 using ground motion recordings from actual earthquake events. Five ground motion recordings were selected from the PEER NGA database (PEER, 2011) and are presented in Table 2-3. The ground motions were selected based on their peak ground acceleration and mean period (as defined by Rathje et al, 1998) using the

methodology proposed by Athanasopoulos-Zekkos and Saadi (2012). Ground motions with similar peak ground accelerations and different mean periods were chosen so that the effect of frequency content on the response of the levee could be observed. In the following sections, the results of the analyses with ground motion recording inputs are presented and compared to the results obtained using Ricker wavelets and simple harmonic inputs.

In general the development of failure surfaces under ground motion recording inputs was quite similar to what was observed with the Ricker wavelet and harmonic inputs. For the analyses with a steel sheet pile cutoff wall, circular failure surface developed on both sides of the wall, with the waterside failure being shallower than the landside failure. There was very little evidence of formation of a failure wedge along the wall. For the analyses with a soil cement bentonite wall, there were again circular failure surfaces on both sides of the wall, however they were slightly deeper than was observed for the steel sheet pile wall. Also, formation of a failure wedge on the waterside of the wall was apparent. For both cutoff wall types, as the peak ground acceleration of the input motion increased, the magnitude of the shear strains mobilized increased. It was also seen that for two input motions having similar peak ground accelerations, the magnitude of shear strains mobilized was greater for the motion with the lower frequency content.

The horizontal displacement behavior of the profiles for recorded ground motions was very similar to the behavior observed for the Ricker wavelet and harmonic inputs. Figure 2-19 presents horizontal surface displacements for Profile 3 with both types of cutoff walls, subject to each recording from the ground motion suite. When comparing the displacements for the analysis with NGA 0901 with those for NGA 0963, it can be seen that the frequency content of the motion indeed has a dramatic effect on the response. The two motions have very similar peak ground accelerations, Arias Intensities, and durations, but different frequency contents. NGA 0963 has a

higher mean period and results in significantly greater displacements. The same is observed when comparing NGA 0150 and NGA 0589. This is consistent with what was observed for the Ricker wavelet and harmonic input analyses. The dependence on input intensity was also consistent, with an increase in intensity resulting in an increase in displacements. One aspect of the displacement results for the ground recording inputs that varies relative to the results for the simplified inputs is evident when comparing the displacements for the profile with a sheet pile wall to the profile with a soil cement bentonite wall. With the ground recording inputs, the horizontal displacements observed for the profile with a sheet pile wall are systematically slightly greater than those observed for the profile with a soil cement bentonite wall. With the simplified inputs, the two wall types resulted in relatively little difference in horizontal displacement.

The lateral earth pressures observed during the ground motion recording input analyses suggest that the simplified dynamic inputs provide a good indicator for the behavior of the interaction between the cutoff wall and surrounding soil. As was observed for the simplified inputs, under loading with ground motion recordings, the lateral earth pressure time histories along the steel sheet pile cutoff wall exhibited one of two distinct behaviors. Earth pressures on a given node either exhibited relatively steady state behavior with time, or transient behavior, with pressures increasing on one side of the wall, matched by a decrease on the opposite side of the wall. For the soil cement bentonite wall, the lateral earth pressure behavior was also as discussed previously for the simplified inputs, with the pressures being generally very similar on opposite sides of the wall for a given depth. For the various combinations of input parameters and soil profiles, the most direct comparison of maximum lateral earth pressure profiles can be made between the ground record input analyses for Profile 3 and the sinusoidal input analyses for Profile 1. Earth pressure coefficient profiles for these analyses are presented in Figure 2-20. As the figure shows, the

magnitudes of the maximum lateral earth pressure coefficients are very similar for the ground record input and the analogous sinusoidal input. The depth at which this occurs is different due to the fact that two separate soil profiles (1 and 3) are being compared. Despite these differences, this figure illustrates that the simplified inputs are good indicators of the soil-structure interaction for true ground record inputs.

2.2.6 Comparisons to Existing Recommendations

To provide context to the parametric analysis results, comparisons have been made to a selection of existing recommendations and guidelines for the seismic design of earthen levees. As previously mentioned, the existing guidelines are relatively limited and do not consider the effects of the presence of a cutoff wall. In the following sections, the results of this study for clay profiles are presented alongside recommendations from the International Levee Handbook, the United States Army Corps of Engineers, and the California Department of Water Resources. Comparisons to results for sand profiles are made in subsequent chapters, in which the effects of liquefaction are considered.

A review of case histories of embankment response during earthquakes by Swaisgood (2003) is presented in the International Levee Handbook as guidance for seismic design of earthen levees and provides field data to which the results of this study can compared. Seismically-induced crest settlements for approximately 70 embankment dams are presented, including earthfill dams, hydraulic fill dams, concrete faced rockfill dams and earth core rockfill dams. Regression analysis performed by Swaisgood suggests that PGA and earthquake magnitude are the primary factors that influence crest settlement, while dam type, height, ratio of crest length to dam height, slope angles, and reservoir water level were concluded to have minimal effect. A regression equation for crest

settlement (presented as percentage of embankment and foundation thickness) as a function of PGA and earthquake magnitude is proposed by Swaisgood. Figure 2-21 presents the data from this study using Ricker wavelet inputs for profiles with no wall and with a steel sheet pile wall, compared to the crest settlement data for earthfill embankments from Swaisgood. As seen in this figure, the data from this study agrees very well with the field data presented by Swaisgood. When comparing the settlements for the no wall profiles with the sheet pile wall profiles, the settlements are systematically slightly lower for the profiles with a sheet pile wall, however based upon the best fit line for these two data sets, the difference appears relatively small.

Figure 2-22 presents the same data from this study, plotted separately by input frequency, compared to the regression equation proposed by Swaisgood. In addition, ranges of values of Arias Intensity (I_a) for the input motions are plotted on the figure. When plotted separately by input frequency, it becomes more apparent that crest settlements for the profiles with sheet pile cutoff walls are indeed lower than for profiles with no cutoff wall, particularly for input motions with low frequencies. This figure also illustrates that for a single value of Arias Intensity, a decrease in frequency results in an increase in settlements. In the context of the regression equation presented by Swaisgood, the presence of a cutoff wall results in a decrease in crest settlement roughly equivalent to a decrease in earthquake magnitude of approximately 0.3.

Recently the United States Army Corps of Engineers (USACE) published a technical letter on the seismic evaluation of levees (2013). While the document is primarily focused on levees that are vulnerable to seismic activity due to liquefaction potential, certain guidelines are sometimes adopted for all levees. One of these is the general rule of thumb that seismically-induced vertical displacements should be considered on the order of 0.7 times the maximum horizontal displacement. Figure 2-23 presents the ratio of vertical displacements to maximum horizontal

slope displacement for the Ricker wavelet analyses from this study. A linear best fit line is also plotted for both the no wall and sheet pile wall data sets, to indicate a rough average of the ratio value. The ratios are roughly on the order of 0.7, although they have a relatively wide range. Furthermore, the ratios for the profiles with sheet pile walls are consistently lower than for profiles with no cutoff wall. This data suggests that a single value for the ratio of vertical to horizontal displacements may be inadequate, and should incorporate the effect of the presence of a cutoff wall.

The results of this study were also compared to guidelines put forth by the California Department of Water Resources Urban Levee Program. Shewbridge et al (2009) present a simplified relationship based on numerical modeling analyses for estimating Newmark-type displacements of earthen levees as a function of seismic yield coefficient, maximum seismic coefficient, and earthquake magnitude (similar to the results of Makdisi and Seed (1978)). Figure 2-24 presents the results of the ground motion recording analyses from this study for profiles with no cutoff wall, steel sheet pile walls, and soil cement bentonite walls, in comparison to the simplified relationship. Overall, the displacements data from this study agrees very well with the proposed simplified relationship. It is immediately apparent that the profiles with cutoff walls result in lower displacements than the profiles with no cutoff wall. However, the type of cutoff wall (i.e. sheet pile or soil cement bentonite) appears to have relatively little effect on the seismically-induced displacements. This data suggests that the proposed simplified relationship may overestimate seismic displacements for levees with cutoff walls.

2.2.7 Supplemental Analysis for Validation of Interface Modeling Assumptions

In order to investigate the implications of using glued interfaces between the cutoff wall and surrounding soil, a set of supplementary analyses was conducted, using unglued interfaces. Two analyses were performed using Ricker wavelet inputs; one with a PGA of 0.1g and one with a PGA of 0.4g. In addition to these analyses, one analysis was conducted with a true ground motion recording as input. The key results that were used to characterize the response of the levee system throughout the original parametric analysis were compared between the analyses with the glued and unglued interfaces. The results suggest that, for the purpose of this parametric analysis, modeling the connection between the cutoff wall and surrounding soil does not invalidate the parametric analysis conclusions. Presentation of these results is preceded by a discussion of the details of the glued and unglued interface modeling.

For the original parametric analyses, the interfaces were defined as glued. Under this condition, there is no slip or separation allowed at the interface, but elastic displacement is allowed. For the 'unglued' analyses, the interface was assigned Coulomb-type properties and the interface between the structural element and the soil was allowed to slip and separate if the Coulomb strength criteria were exceeded. The primary drawback of modeling an unglued interface however is that additional structural Rayleigh damping must be included to remedy numerical noise. This increased Rayleigh damping results in a dramatic decrease in the required timestep (three orders of magnitude) and thereby an increase in computational time, which becomes prohibitive for an extended parametric analysis.

For the three inputs that were investigated with the supplementary analyses, the 0.4g-PGA Ricker wavelet analysis generally results in the greatest difference between the glued and unglued cases. Therefore the results presented from the supplementary analyses are for the 0.4g input.

Figures 2-25, 2-26, and 2-27 present comparisons of shear strain contours, surface displacements, and lateral earth pressure time histories, respectively.

2.3 Conclusions of Parametric Analyses of Levees Founded on Non-liquefiable Soils

A parametric analysis was conducted using finite difference numerical modeling in order to investigate the dynamic response of earthen levees with embedded cutoff walls. A range of dynamic excitations, both simplified and actual ground motion recordings, were used to identify the key parameters of the input motion. Several soil profiles were investigated and both steel sheet pile and soil cement bentonite cutoff walls were modeled. The key findings of this portion of the study are presented below.

- Based on the results of the parametric analysis, the presence of an embedded cutoff wall does alter the dynamic response of a levee, as compared to a levee without a cutoff wall. Shear strain contours indicate that the wall results in a change in the geometry of the dynamic failure surface, by forcing the entry point of the landside failure surface to the landside of the levee crest centerline.
- Comparison of the analyses performed using simplified dynamic inputs with the analyses for actual ground motion recordings indicated that Ricker wavelet pulses and simple sinusoidal inputs are very good indicators of trends and behaviors observed for actual earthquakes.
- The ratio of vertical to horizontal slope displacement was observed to deviate significantly from the commonly assumed value of 0.7 and was observed to by systematically different for levees with and without cutoff walls. For analyses of clay profiles with Ricker wavelet

inputs, the ratio was observed to vary between 0.25 and 1.2. The ratio was consistently lower (by approximately 0.1) for levees with sheet pile cutoff walls, as opposed to levees with no cutoff wall. The average value of the ratio for levees with no cutoff wall ranged between 0.7 and 0.9 and the average value of the ratio for levees with a steel sheet pile cutoff wall ranged between 0.6 and 0.8.

- Comparison of horizontal slope displacements for ground motion recording inputs with simplified relationships for Newmark-type displacements (Shewbridge et al 2009) indicate that the simplified relationship tends to overestimate displacements for levees with cutoff walls. The overestimation was observed to be as greater as 80%. Very little difference (less than 5%) was observed in horizontal displacements between levees with steel sheet pile cutoff walls and levees with soil cement bentonite cutoff walls.

- Levee crest settlements (as percentages of combined levee height and foundation thickness) computed for analyses of clay profiles with Ricker wavelet inputs, agreed very well with case history data presented by Swaisgood (2003). For levees with steel sheet pile cutoff walls, computed crest settlements were consistently between 10% and 20% lower than for levees with no cutoff wall. When compared to the regression equation presented by Swaisgood (2003) for crest settlement as a function of PGA and earthquake magnitude, the presence of a cutoff wall results in a decrease in crest settlement roughly equivalent to the decrease in settlement due to a decrease in earthquake magnitude of approximately 0.3.

- Input frequency was observed to have a significant effect on crest settlements, with lower frequencies resulting in higher settlements. For a given input PGA a change in frequency from 5 Hz to 1 Hz resulted in an increase in crest settlement by more than 1 order of magnitude. For a given Arias Intensity, a change in frequency from 5 Hz to 1 Hz resulted

in an increase in crest settlement by approximately 1 order of magnitude (e.g 16 cm to 160 cm).

- It was observed that the earth pressures on deep portions of the cutoff wall behave similarly to what has been observed for braced retaining structures. However, at shallower locations, particularly within the levee itself, the wall pressures were strongly influenced by adjacent levee slope movements. A simple monotonically increasing lateral earth pressure profile is not adequate to characterize the dynamic wall pressures, as this was seen to under-predict lateral earth pressures at shallow locations, by as much as approximately 100%.

Table 2-1, Material properties for parametric analyses of dynamic response of levees with conventional cutoff walls

Profile	Drained φ	Elastic Modulus (kPa)	Poisson's Ratio	Dry Unit Wt. (kN/m^3)	Hysteretic Damping Model*
1	25º	2.05e5	0.3	15.7	V&D: PI=50, OCR=1 (a = 0.94, b = -0.58, x_0 = -0.65, y_0 = 0.085)
2	32º	5.55e5	0.3	15.7	V&D: PI=30, OCR=1 (a = 1.02, b = -0.64, x_0 =-1.01, y_0 = 0.035)
3	Linearly increasing w/ depth, ranging between values for Profiles 1 and 2		0.3	15.7	Decreasing with depth (V&D), PI=50, 40, 30 (a =0.96, b =-0.55, x_0 = -0.82, y_0 = 0.06) for PI = 40
4	32º	2.39e5	0.3	17.3	S&I: Lower Bound G/Gmax, Avg damping (a = 0.98, b = -0.57, x_0 = -1.7, y_0 = 0.03)
5	38º	3.36e5	0.3	18.9	S&I: Avg. G/Gmax, Avg. damping (a = 0.98, b = -0.575, x_0 = -1.45, y_0 = 0.02)
6	Three layers of equal thickness with upper layer matching Profile 4, base layer matching Profile 5, and middle layer as shown below				
	35º	2.74e5	0.3	18.1	S&I: Avg. G/Gmax, Avg. damping

Steel Sheet Pile Wall			
I (m^4)	Area (m^2)	Elastic Modulus (kPa)	Unit Wt. (kN/m^3)
4.57e-5	3.6e-3	2.1e8	75.9

Soil Cement Bentonite Wall				
Φ	Cohesion (kPa)	Elastic Modulus (kPa)	Poisson's Ratio	Dry Unit Wt. (kN/m^3)
1º	105	2.5e4	0.25	19.6

* V&D: Vucetic and Dobry (1991), S&I: Seed and Idriss (1970)

Table 2-2, Ratios of vertical crest displacement to maximum horizontal waterside slope displacements for selected simplified input analyses

Profile: 1		4		*Varies*		6		4	
Cutoff Wall: Steel Sheet Pile		Steel Sheet Pile		Steel Sheet Pile		*Varies*		Steel Sheet Pile	
Input Frequency*: Varies*		1.9 Hz		1.9 Hz		1.9 Hz		1.9 Hz	
Input Intensity: 0.4 g		*Varies*		0.4 g		0.4 g		0.4 g	
Input Type: Ricker Wavelet		Harmonic - 5 cycles		Harmonic - 5 cycles		Harmonic - 5 cycles		*Varies*	
Input Frequency (Hz)	y_{disp}/x_{disp}	Input Intensity (g)	y_{disp}/x_{disp}	Profile	y_{disp}/x_{disp}	Cutoff Wall Type	y_{disp}/x_{disp}	Input Type	y_{disp}/x_{disp}
1	0.79	0.1	0.44	1	1.35	None	1.02	Harm. 5 Cycles	0.79
2	0.75	0.2	0.58	4	0.79	Steel Sheet Pile	0.92	Harm. 10 Cycles	0.92
3	0.69	0.3	0.94	5	0.57	Soil Cem Bent	0.85	Harm. 15 Cycles	0.97
4	0.68	0.4	0.97	6	0.92				
5	0.66								

Table 2-3, Ground motion recording suite for analyses of levees with conventional cutoff walls

NGA File Number	Event Name	t_95 (seconds)	PGA (g)	PGV (cm/sec)	Arias Intensity (m/s)	Tm (seconds)	1/Tm (Hz)
0901	Big Bear – 01	14.9	0.51	34.5	3.32	0.28	3.57
0963	Northridge – 01	13.7	0.49	52.0	3.16	0.55	1.8
0150	Coyote Lake	5.3	0.41	49.2	0.77	0.67	1.49
0589	Whittier Narrows – 01	8.6	0.39	16.3	0.87	0.39	2.56
1734	Northridge – 06	4.0	0.31	10.9	0.18	0.28	3.57

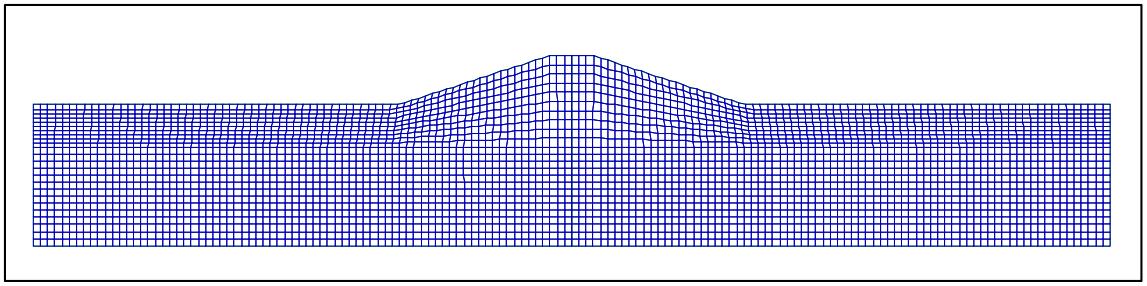

Figure 2-1, Finite difference grid used in parametric analysis

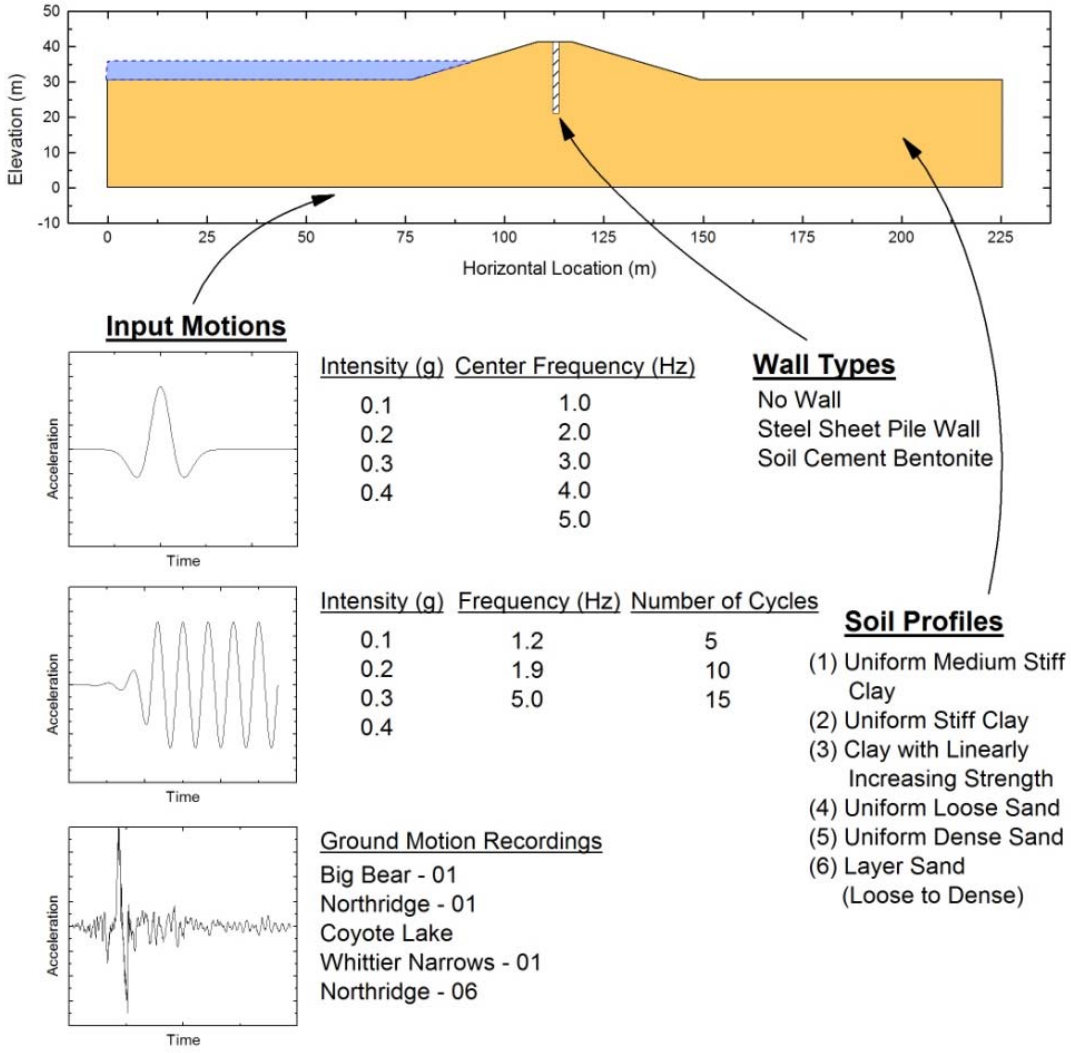

Figure 2-2, Parametric analysis combinations for dynamic response of levees with conventional cutoff walls founded on non-liquefiable soils

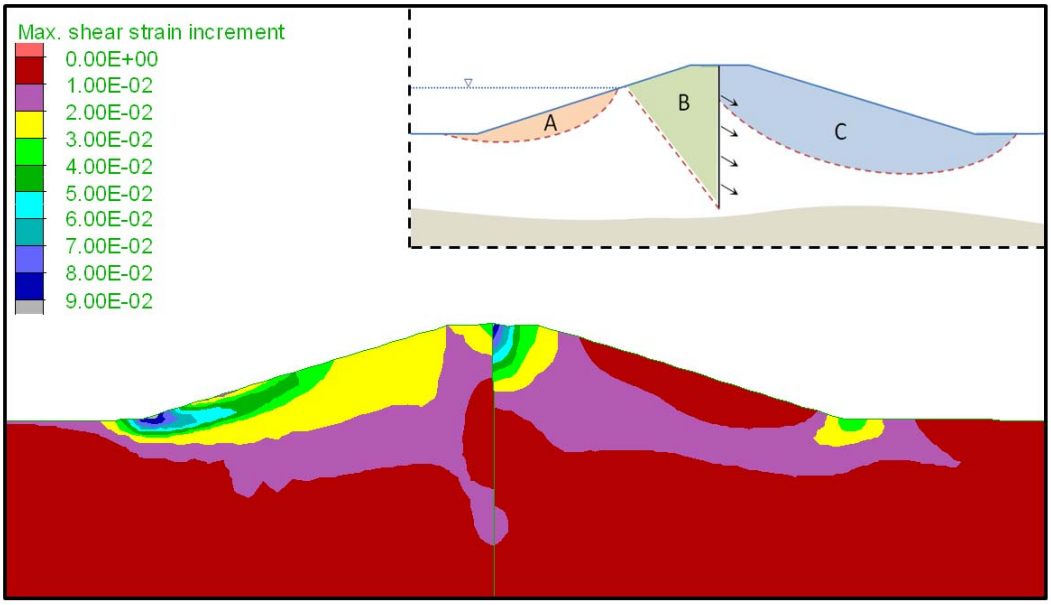

Figure 2-3, Maximum shear strain contours and schematic of observed failure mechanism (inset) for levees with conventional cutoff walls founded on non-liquefiable soils

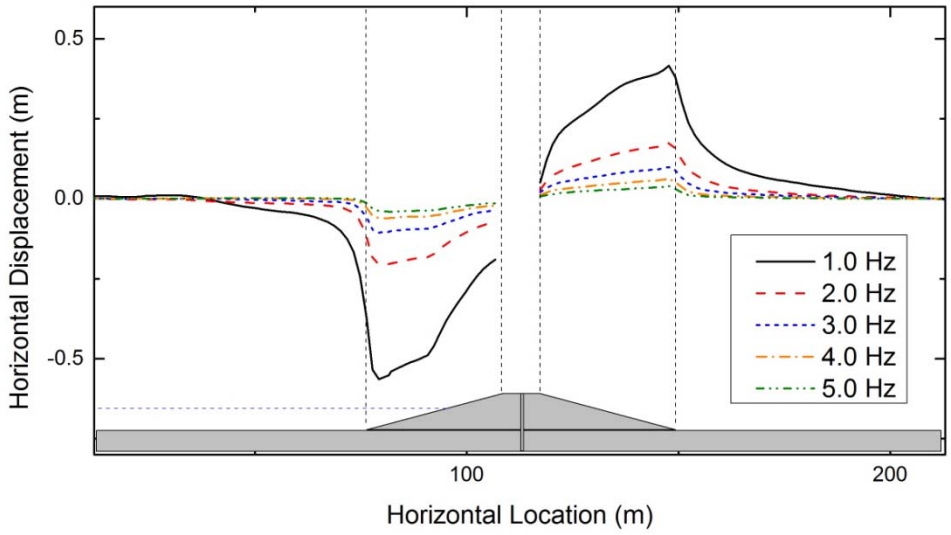

Figure 2-4, Profile 1 (with steel sheet pile wall) horizontal displacements along ground surface for PGA = 0.4g

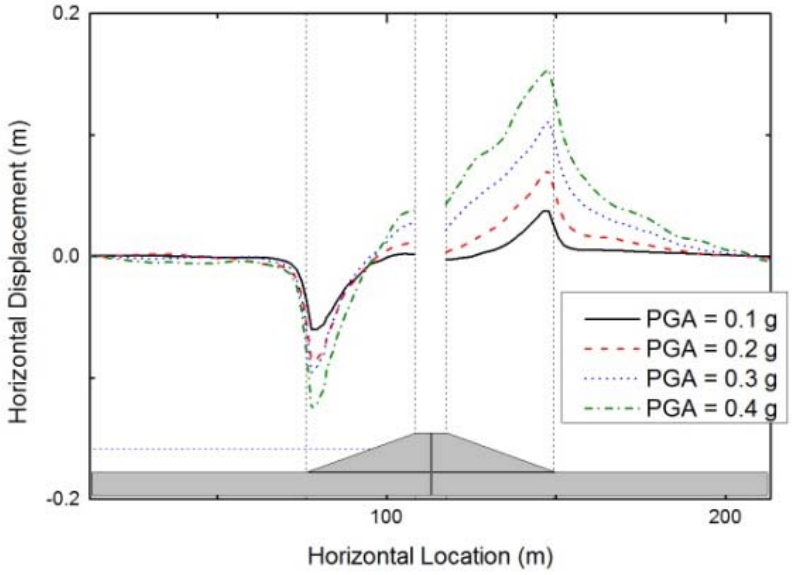

Figure 2-5, Horizontal surface displacements for Profile 4 with a steel sheet pile wall and 5-cycle sinusoidal input with frequency of 1.9 Hz

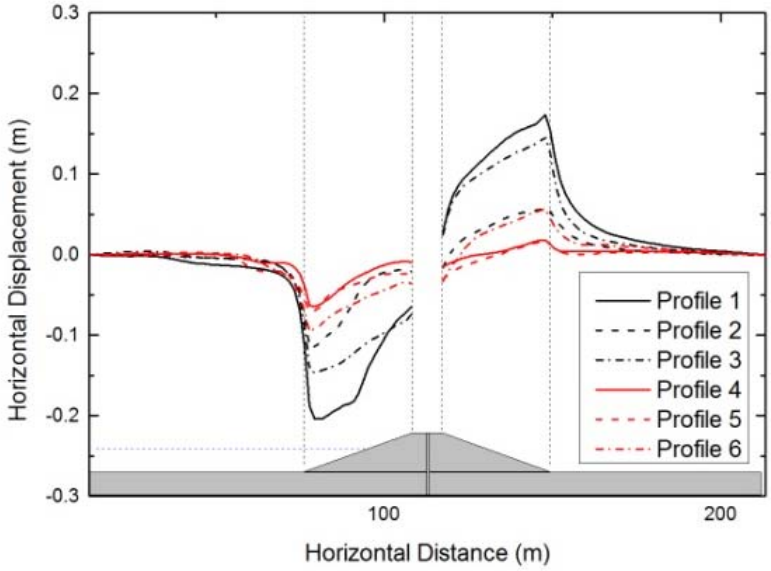

Figure 2-6, Horizontal surface displacements for various soil profiles (with steel sheet pile cutoff wall) with 5-cycle sinusoidal input with input intensity of 0.4g and input frequency of 1.9 Hz.

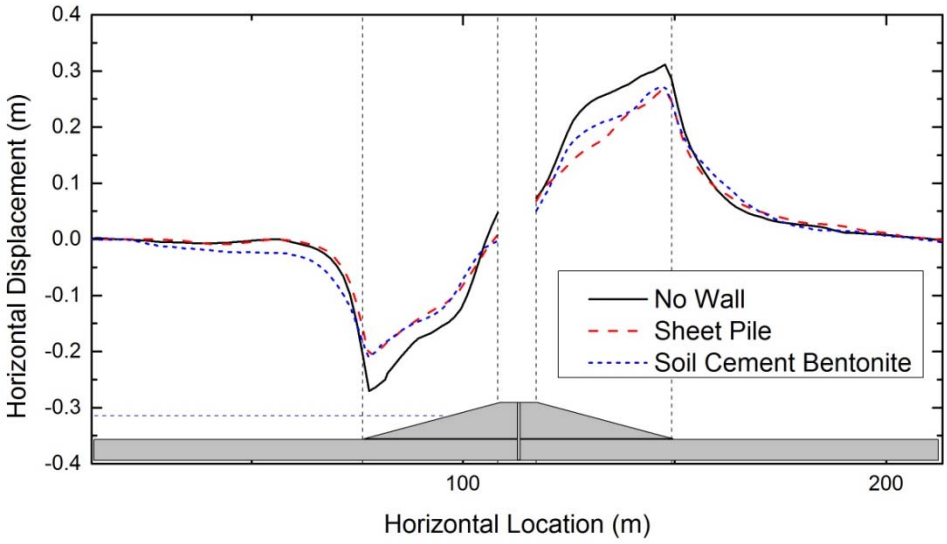

Figure 2-7, Horizontal surface displacements for Profile 6 with various cutoff walls (5-cycle harmonic input, 0.4 g intensity, and 1.9 Hz frequency)

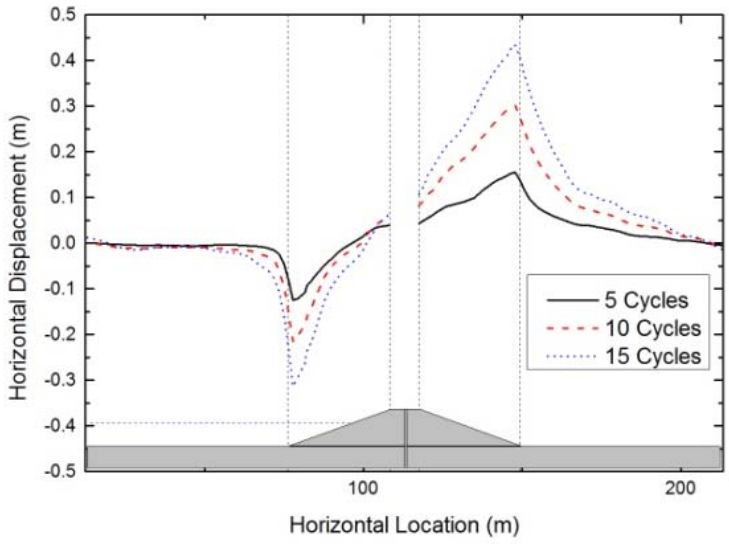

Figure 2-8, Horizontal surface displacements for Profile 4 with a steel sheet pile wall with sinusoidal input (of varying cycles), 0.4 g, 1.9 Hz

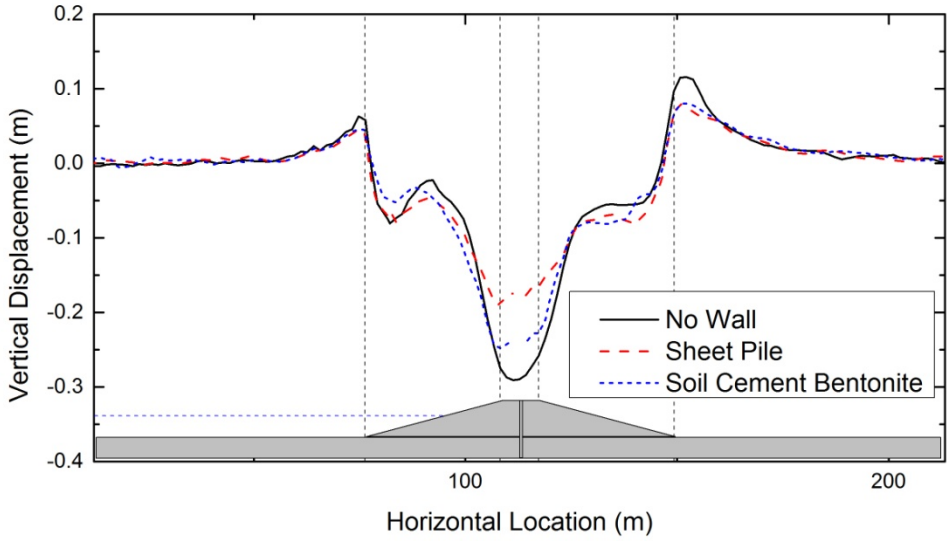

Figure 2-9, Vertical surface displacements for Profile 6 with various cutoff walls (5-cycle harmonic input, 0.4 g intensity, and 1.9 Hz frequency)

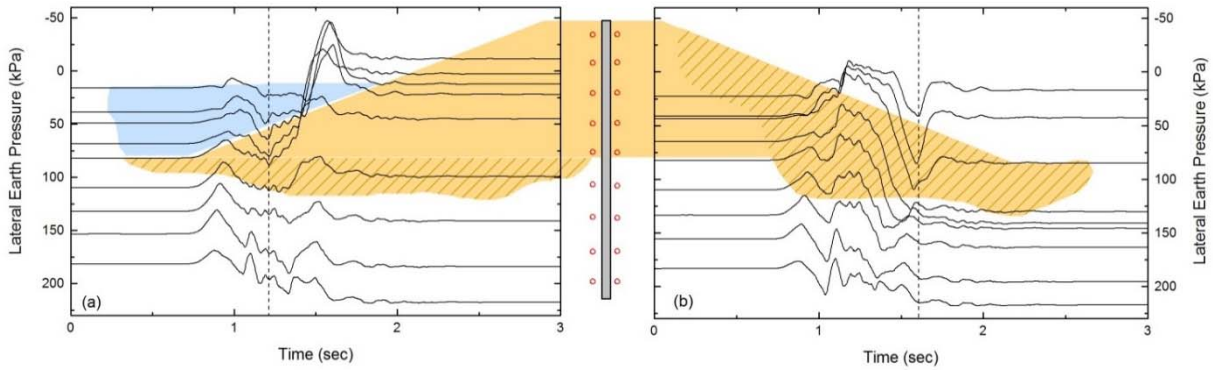

Figure 2-10, Lateral earth pressure – time histories for PGA = 0.4g, center frequency = 2.0 Hz, on (a) waterside interface and (b) landside interface

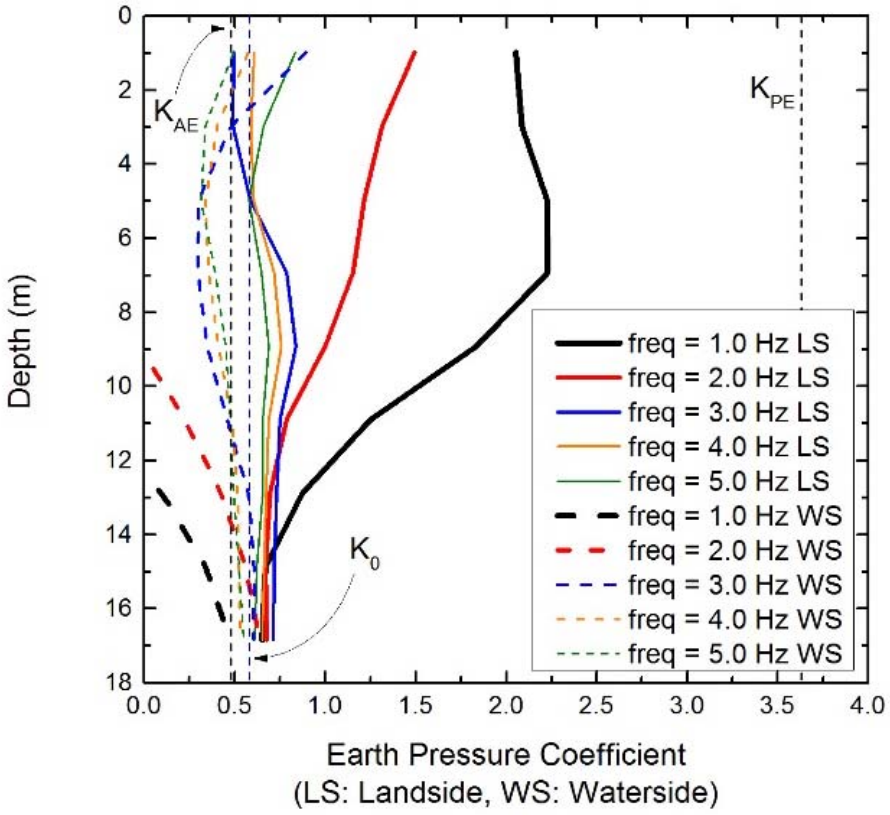

Figure 2-11, Earth pressure coefficients, at instance of maximum earth pressure on the wall for various input frequencies, with input intensity = 0.4g

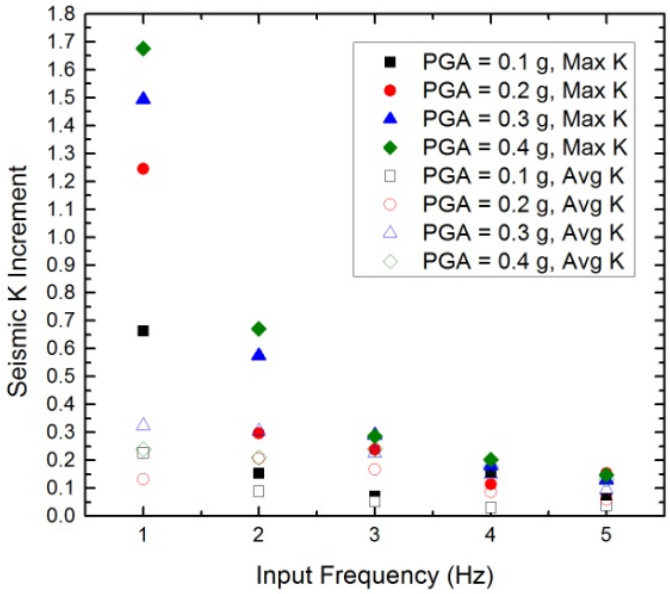

Figure 2-12, Average and maximum seismic earth pressure coefficient increment on the landside of the wall at instance of maximum lateral earth pressure

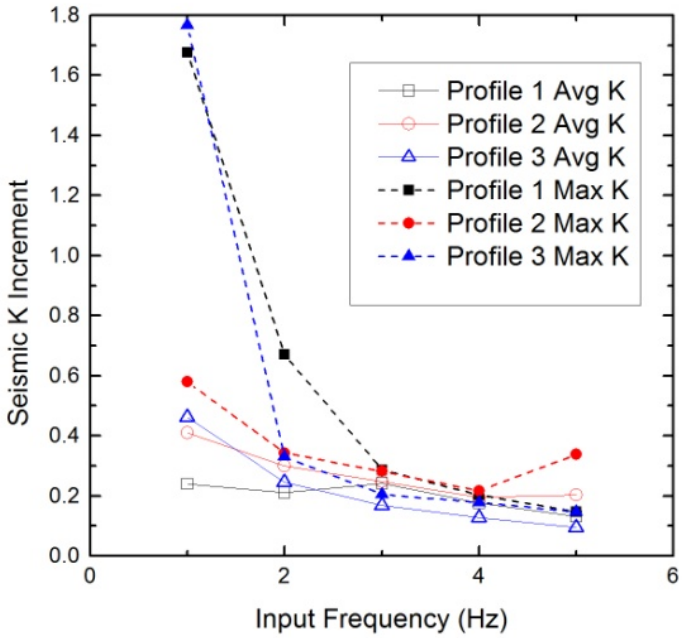

Figure 2-13, Average maximum seismic earth pressure coefficient increments for Profiles 1, 2, and 3, for input wavelets with intensity of 0.4g.

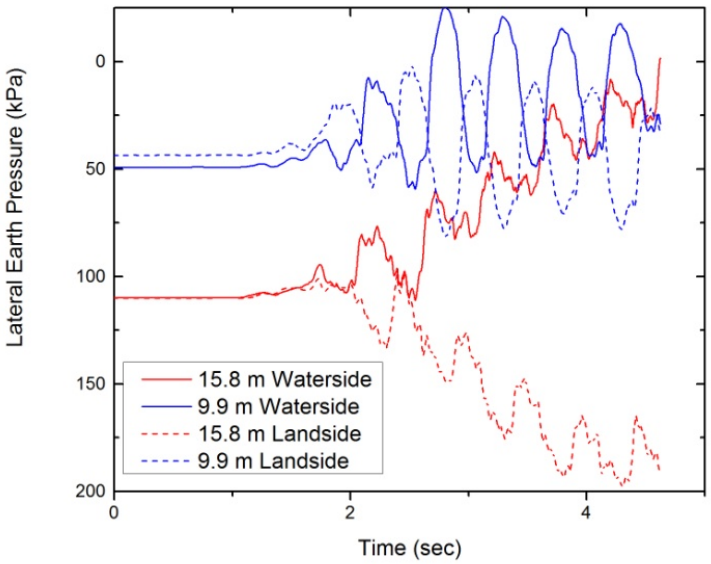

Figure 2-14, Lateral earth pressure – time histories for two nodal depths on both sides of the cutoff wall

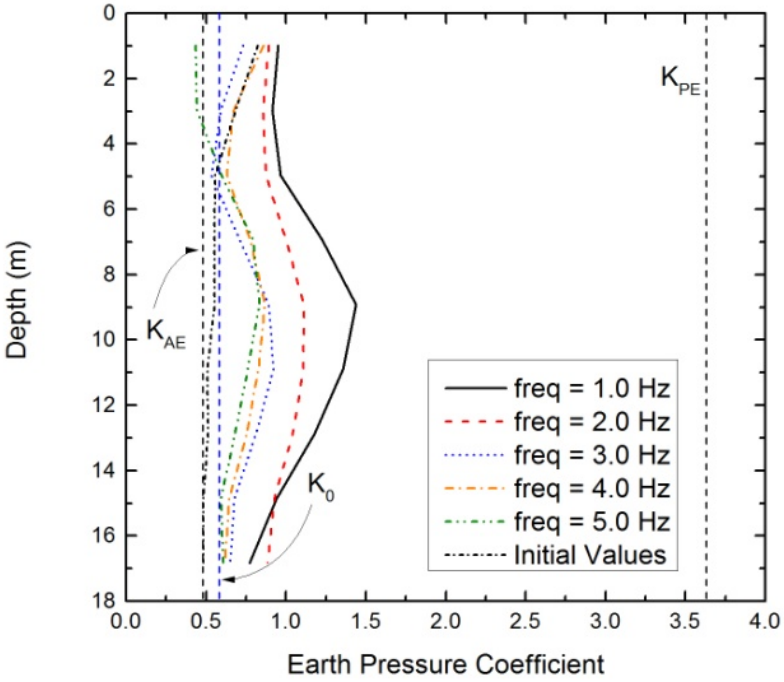

Figure 2-15, Seismic earth pressure coefficients on the landside of the wall with depth for Profile 1 with 0.4-g harmonic inputs

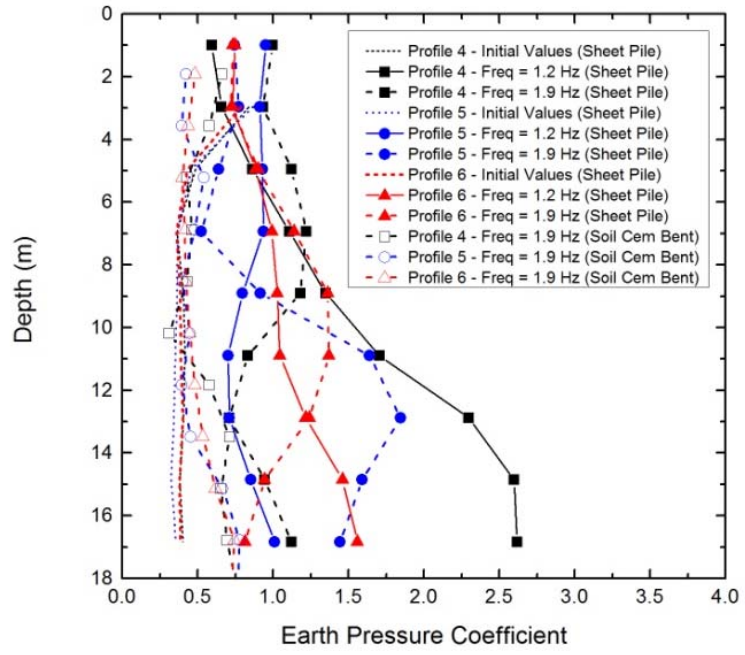

Figure 2-16, Earth pressure coefficients at instance of maximum lateral earth pressure on landside of sheet pile wall and soil cement bentonite wall for Profiles 4, 5, and 6 (All for input intensity of 0.4 g, 10 cycles)

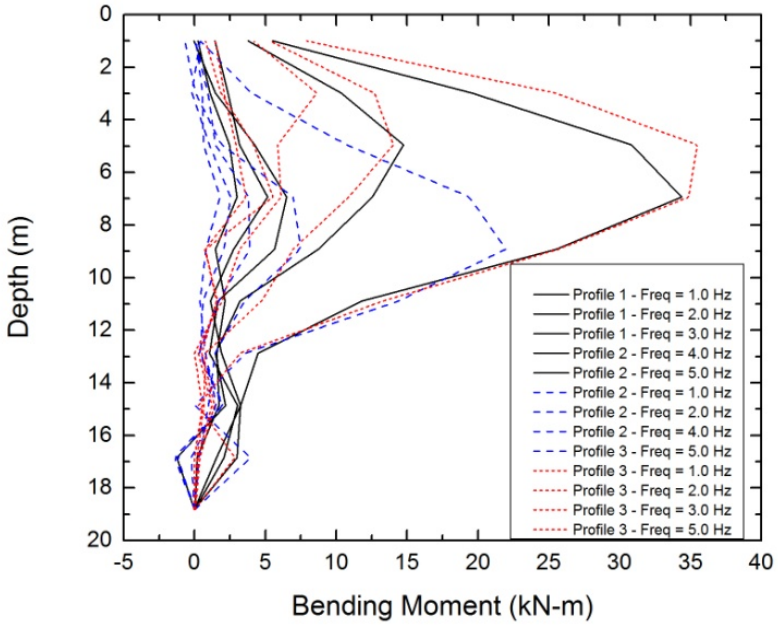

Figure 2-17, Maximum steel sheet pile wall bending moment profiles for 0.4g Ricker wavelet analyses for Profiles 1, 2, and 3

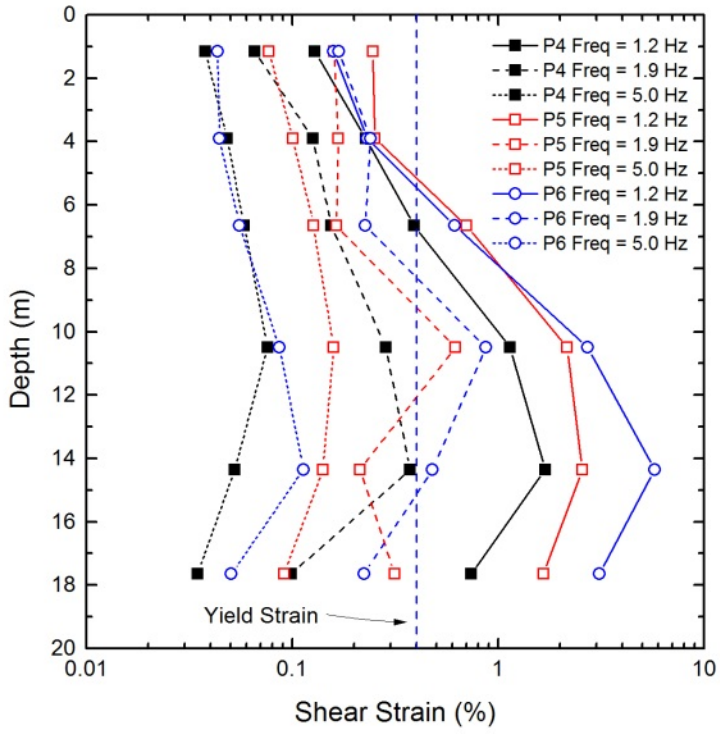

Figure 2-18, Maximum soil cement bentonite wall shear strain profiles for 0.4g, 5-cycle sinusoidal input analyses for Profiles 4, 5, and 6

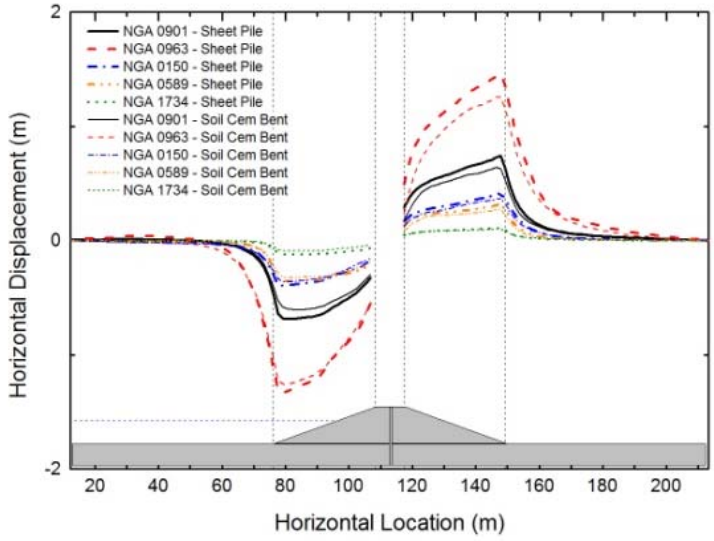

Figure 2-19, Horizontal surface displacements for Profile 3 with various ground motion recording inputs

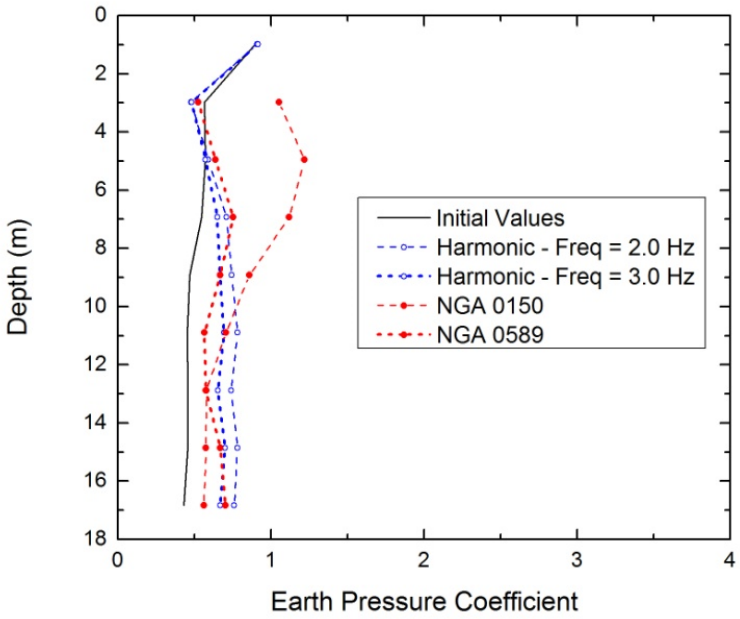

Figure 2-20, Maximum lateral earth pressure coefficient profiles for Profile 3, 5-cycle, 0.4g sinusoidal inputs and ground motion recording inputs

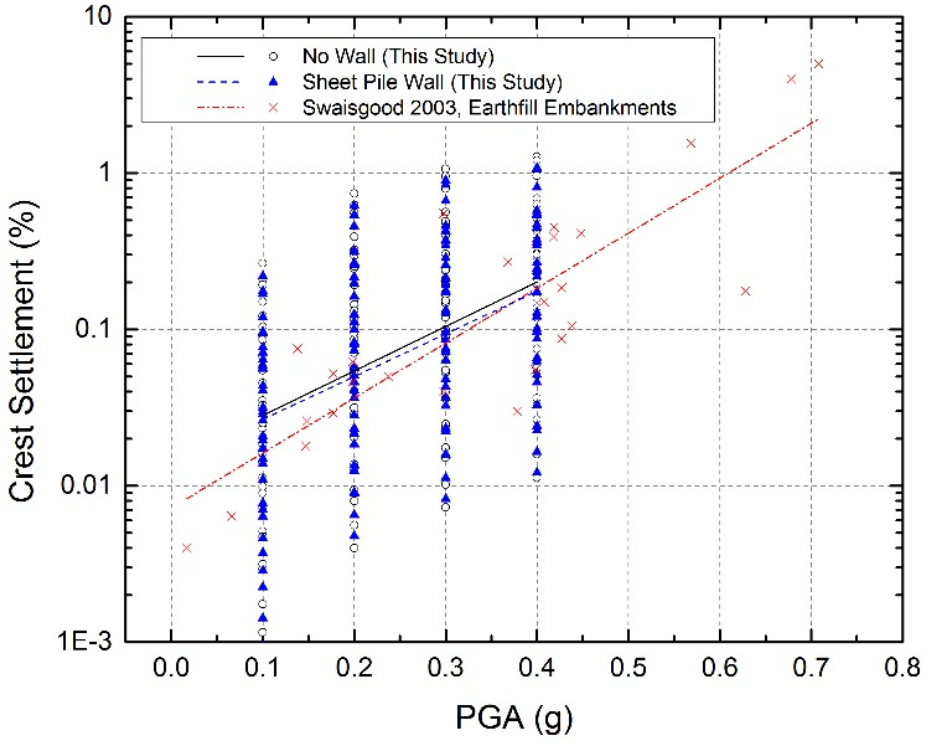

Figure 2-21, Comparison of crest settlement data for Ricker wavelet analyses with case history data presented by Swaisgood (2003)

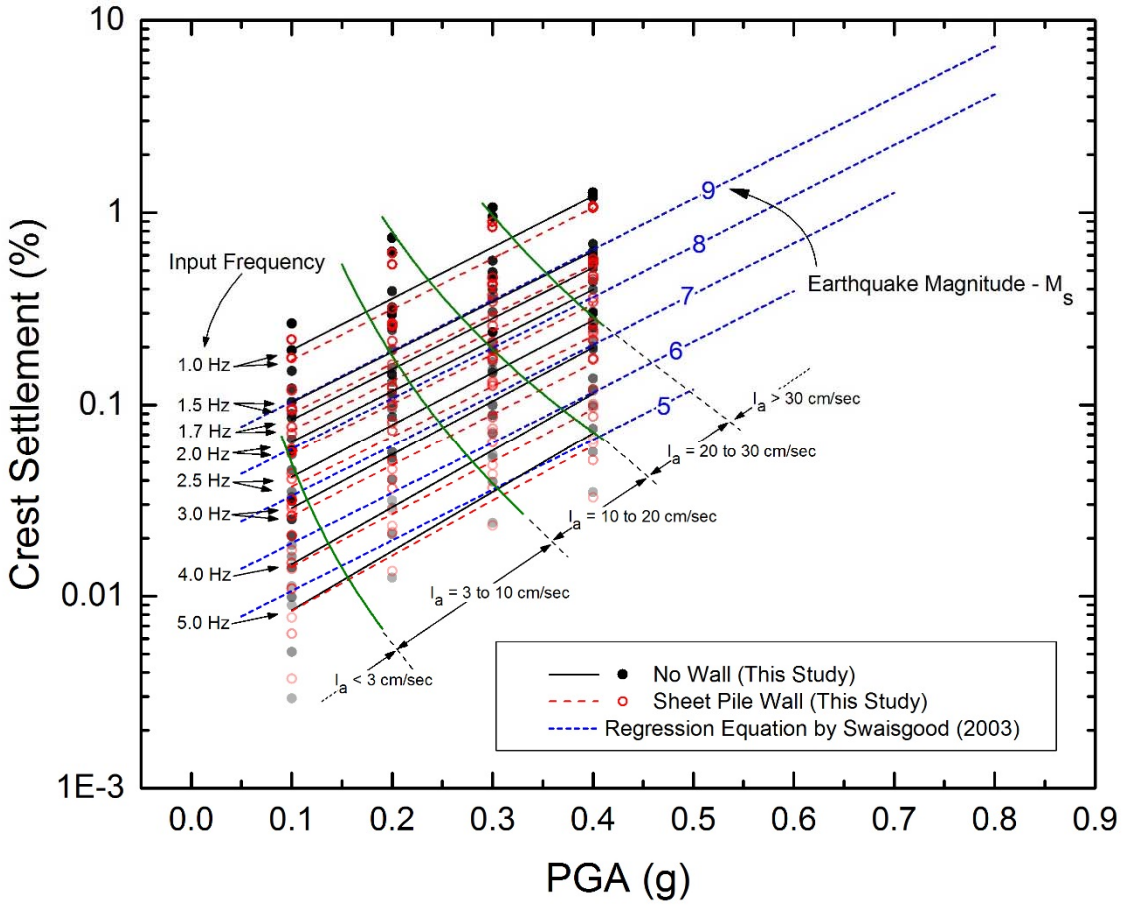

Figure 2-22, Comparison of crest settlement data for Ricker wavelet analyses by input frequency with proposed regression equation by Swaisgood (2003)

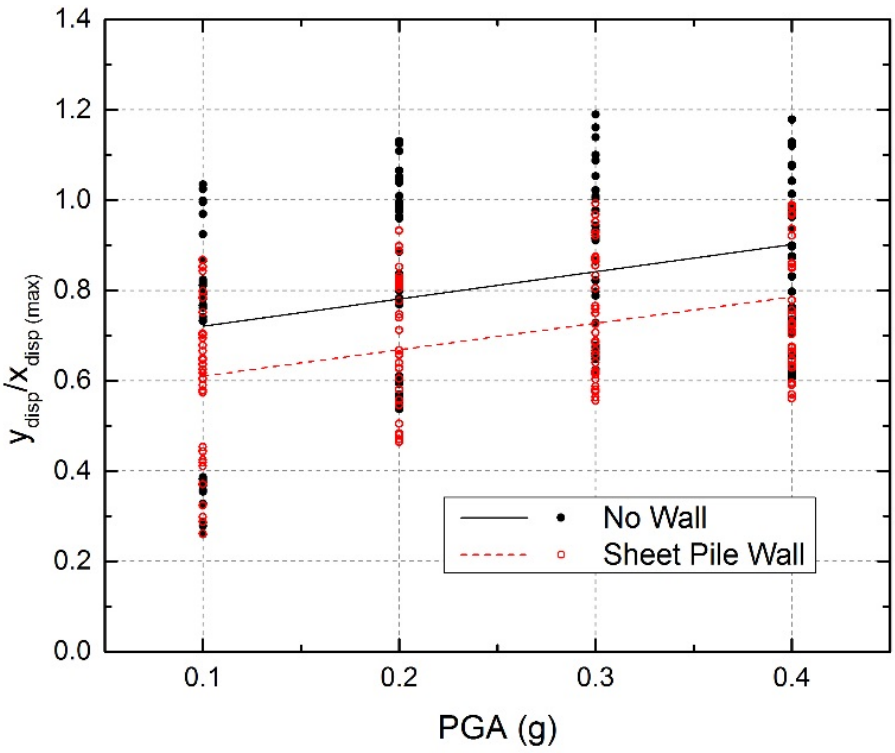

Figure 2-23, Ratio of vertical displacements to maximum horizontal slope displacements for Ricker wavelet analyses

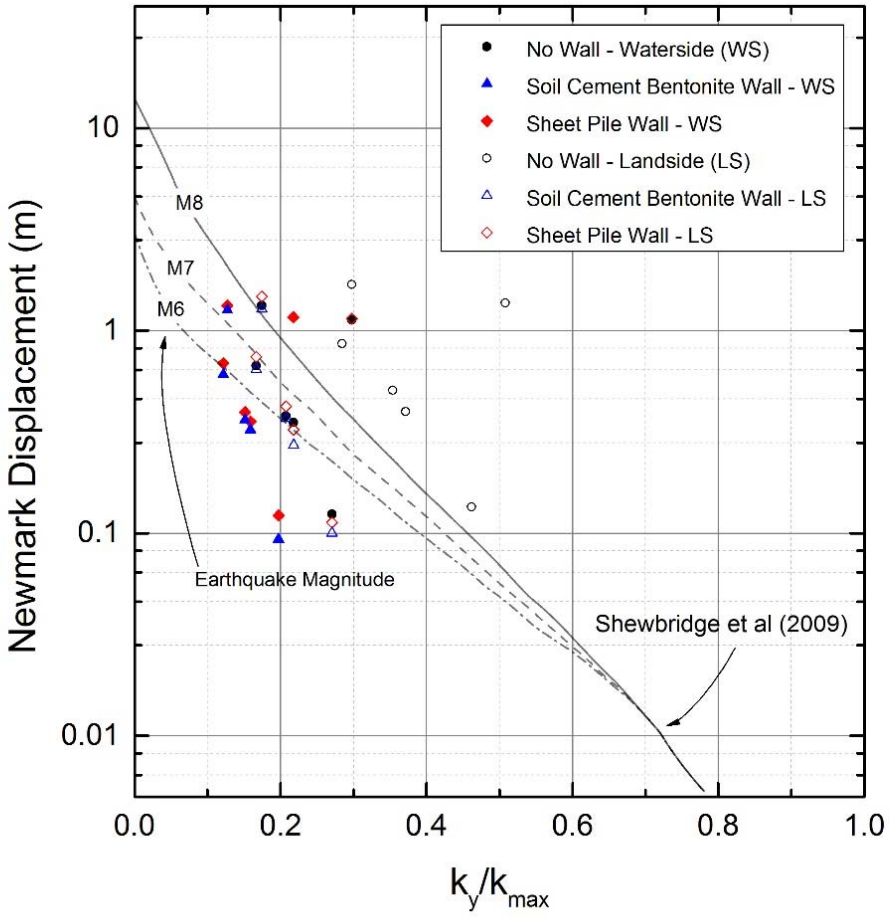

Figure 2-24, Comparison of Newmark displacements from ground motion recording analyses with simplified relationship proposed by Shewbridge et al (2009) (WS – Waterside, LS – Landside)

(a)

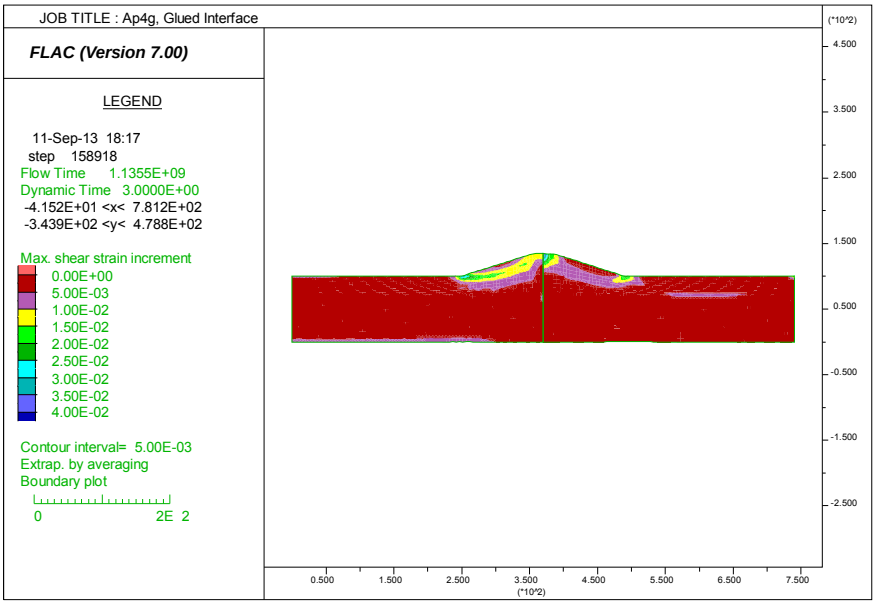

(b)

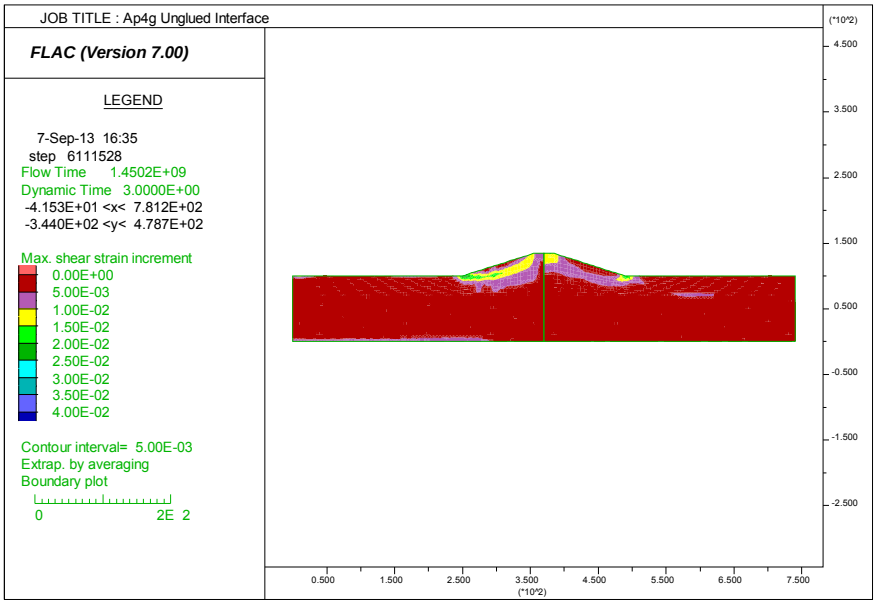

Figure 2-25, Maximum shear strain contours for (a) glued interface analysis and (b) unglued interface analysis

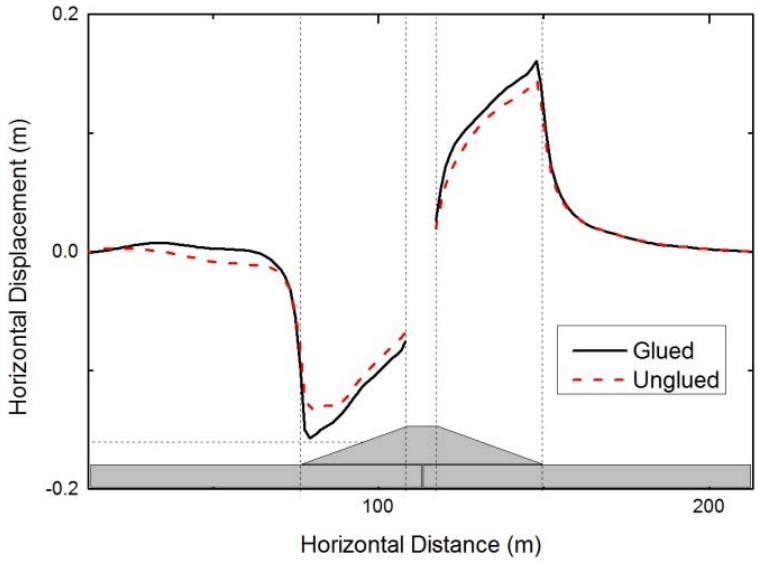

Figure 2-26, Horizontal surface displacement comparison between glued and unglued interfaces for non-liquefiable soils

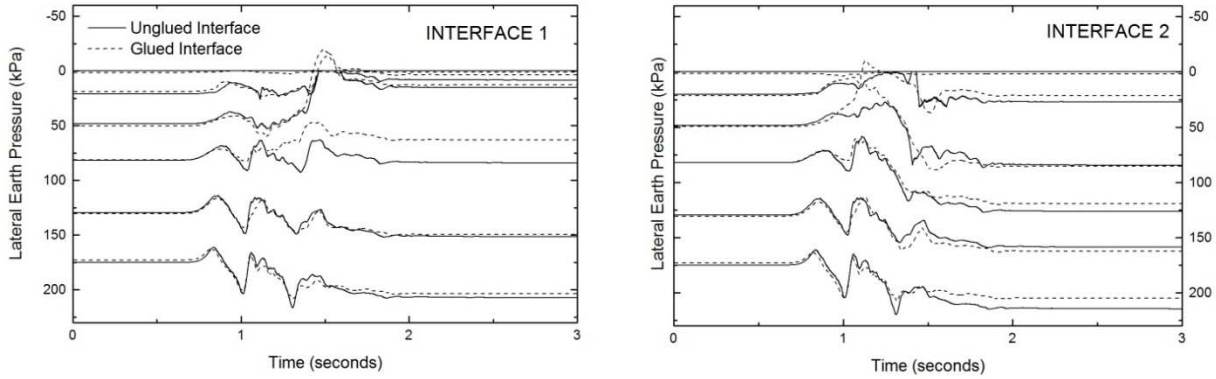

Figure 2-27, Lateral earth pressure time-history comparison between glued and unglued interfaces for non-liquefiable soils

CHAPTER 3

Dynamic Response of Levees Founded on Liquefiable Soils with Conventional Cutoff Walls

The dynamic response of earthen levees is further complicated by the presence of liquefiable soils in the underlying foundation material of many levees, as well as within the levees themselves. Since the response of levees founded on liquefiable soils may be governed by different parameters than levees with non-liquefiable soils and the failure mechanisms may be different, a separate but similar parametric analysis from the one presented in the previous chapter was conducted for levees with liquefiable soils. One of the key differences is the strong dependence of liquefaction response on the number of loading cycles. For this reason, harmonic inputs with varying numbers of cycles were primarily used as input motions. Also, due to the potential for significant reduction in shear strength during liquefaction, different failure mechanisms may result for levees founded on liquefiable soils. This in turn results in dramatically different loading conditions and demands placed on the cutoff wall element. Finally, different numerical modeling considerations were needed to capture the response of liquefiable soils as well as their interaction with the cutoff wall. This included using a state-of-the-art constitutive model to capture the pore pressure increase and subsequent strength reduction, as well as different soil-wall interface modeling considerations. A brief overview of the study of liquefaction in soils, and how it relates

to this application in particular, precedes the presentation of the input and results of this parametric analysis.

3.1 Overview of Soil Liquefaction

The broad consequences of liquefaction during earthquakes were first brought to the attention of the civil engineering community during the 1960's with the widespread liquefaction that occurred during the Niigata earthquake in Japan and the Good Friday earthquake in Alaska. Since then, soil liquefaction has received significant attention from the geotechnical engineering research community and has been the focus of a large number of studies and experiments. These have investigated a wide range of topics including the nature of the mechanism of soil liquefaction, development of methods to predict susceptibility to and triggering of liquefaction, as well as a range of simplified and advanced methods for modeling liquefaction response.

The phenomenon of soil liquefaction is typically observed in loose cohesionless soils (although it has also been observed less frequently in gravels and fine-grained soils) that experience excess pore pressure generation during undrained loading due to irrecoverable volume contraction of the soil matrix. In the context of this study, the undrained loading takes place in the form of an earthquake event, during which a rise in excess pore pressures results in a decrease in effective stress, leading to partial or complete loss of shear strength of the soil. Liquefaction is broadly categorized into two different types, 1) flow liquefaction and 2) cyclic mobility, both of which may influence the response of an earthen levee system under dynamic loading. Flow liquefaction is defined as the case in which the shear strength of the liquefied soil experiences significant reduction, such that the shear stress required for static equilibrium of an earth structure exceeds the liquefied strength. This results in dramatic instability and flow of soils. Unlike flow

liquefaction, during cyclic mobility the static shear stress may not exceed the shear strength of the liquefied soil, but the combination of cyclic and shear stresses during a dynamic event result in large deformations. Both types have the potential to influence the response of levees, but flow liquefaction is the primary mechanism of failure of slopes due to liquefaction, whereas cyclic mobility is more often associated with level-ground liquefaction and lateral spreading.

Commonly used in the geotechnical engineering design community, is the significant research that has been conducted on the determination of the susceptibility of given soils to liquefaction and the likelihood of occurrence for given earthquake events. Landmark work in this direction by Seed and Idriss (1971) proposed a simplified procedure for evaluation of the liquefaction potential of sands, based on an extensive review of case studies of the response of liquefiable soils during earthquakes. In this publication, they also identify the key factors influencing the potential for liquefaction. This laid the groundwork for many of the current tools used to estimate liquefaction susceptibility and in subsequent years there was continued study into liquefaction potential and triggering, including other effects such as sloping ground surfaces, fines content, etc. A comprehensive summary of these methods can be found in Seed et al (2003). A more recent methodology, with a focus on liquefaction triggering for earthen levees, is presented by Athanasopoulos-Zekkos and Seed (2013).

Following evaluation of liquefaction triggering, in the current state of practice, a limit-equilibrium analysis is conducted with post-liquefied residual strengths to estimate the likelihood of a flow slide. Again, a range of methods are available to estimate the residual strengths of liquefied soils. Seed and Harder (1990) proposed a relationship between residual undrained shear strength following liquefaction and SPT results, based on back-calculated strengths from liquefaction events. Stark and Mesri (1992) proposed predictions for undrained shear strength of

liquefied sand based on field case histories and laboratory tests. They presented liquefied strengths as a ratio of undrained critical strength to initial vertical effective stress versus equivalent clean sand blow count, allowing for variation of undrained strength with initial vertical effective stress. Olson and Stark (2002) proposed improved predictions for critical strength ration as functions of both SPT and CPT results, using back-calculated strengths from field case histories. In the event that the results of the analysis indicate that failure is likely, displacements are typically estimated using one of several variations of Newmark-type approaches.

These simplified methods are valuable assessment tools, but are often not adequate for special cases. In addition to the simplified assessment methods, significant advances have been made in the area of numerical modeling of liquefiable soils. There is a wide range of approaches used to incorporate soil liquefaction into numerical models. The Finn model (Martin et al 1975, Byrne 1991) is a relatively simple, empirical scheme that accounts for pore pressure increase by estimating volume contraction of the soil skeleton as a function of loading cycles. The change in pore pressure is then proportional to the estimated change in volumetric strain. UBCTOT (Beaty and Byrne 2000) is a total-stress formulation, which aims at synthesizing the commonly practiced simplified approach of liquefaction assessment. This model is also semi-empirical. UBCSAND (Byrne et al 2004) is a fully coupled, effective stress constitutive model that uses an elasto-plastic formulation with a hyperbolic relation between stress ratio and plastic shear strain. There is also a selection of fully coupled, effective stress models that are formulated based on bounding surface plasticity (e.g. Dafalias 1986, Papapdimitriou et al 2001). Each approach has its own merits and disadvantages, but together they comprise an effective toolbox of methods for numerically modeling various problems involving liquefaction. A relevant example of the use of a selection of

these advanced models is illustrated through the extensive numerical analysis of the Tuttle Creek Dam, presented by Stark et al (2012).

As has been seen with all earth structures, liquefaction poses a serious threat to earthen levees. This has been acknowledged by the engineering community relatively recently and has been addressed by guidelines put forth by various agencies. These guidelines include an approach proposed by the California Department of Water Resources (Shewbridge et al 2009), a report by the Ministry of Forests, Lands and Natural Resource Operations of British Columbia, Canada (Golder Associates 2011), an engineering technical letter by the United States Army Corp of Engineers (2013), and the International Levee Handbook (2014). These guidelines do not present any new research material, but rather synthesize existing knowledge of liquefaction and seismic slope stability, as it pertains to levees. These guidelines, and the wide body of existing work on liquefaction however, do not address the inclusion of cutoff walls in levees and the effects it may have on the triggering of liquefaction and the overall dynamic response of the levee.

3.2 Numerical Analysis Setup and Scope

A parametric analysis was conducted in order to investigate the effect of the cutoff wall on the dynamic response of an earthen levee founded on liquefiable soils. The analysis was conducted using the finite difference numerical modeling software FLAC – Fast Lagrangian Analysis of Continua (Itasca 2011). The following section describes the levees that were modeled in the analysis as well as the details of the setup and execution of the numerical model.

3.2.1 Levee Geometry and Groundwater Conditions

Two generic levee cross sections were analyzed throughout the course of this study in order to investigate how foundation soil properties affect the levee response. The dimensions of the levee were a height of 35 feet and a crest width of 15 feet, with symmetrical 3:1 (H:V) slopes. For analyses with a cutoff wall, the steel sheet pile wall was modeled at the center of the levee, extending to a depth of 65 feet below the levee crest. The foundation material was modeled to a depth of 100 feet and parameters were selected to be broadly representative of levee foundation materials typical to California. The stratigraphy and strength parameters were roughly based on the investigation data of sites that were observed to liquefy during the 1979 Imperial Valley earthquake, as documented by Youd and Bennett (1983). Two sets of strength parameters were selected for the foundation soils, a stronger set and a weaker set, with Levee A being stronger and Levee B being weaker (although both were still within the range of typically liquefiable soils). The levee and foundation soil geometry was the same for both levee sections and is shown in Figure 3-1. The ground water conditions were also the same for both levees with 15 feet of water outside of the waterside of the slope and the ground water table at the ground surface on the land side. The phreatic surface within the levee was determined using a finite-difference seepage analysis, discussed below.

3.2.2 Material Models

In order to accurately capture the behavior of the soil materials, a range of constitutive models were used in the analysis process. During the determination of the initial stress state, all materials were modeled using the Mohr-Coulomb model, which is an elastic-perfectly plastic formulation with yielding defined by the Mohr-Coulomb failure criterion. The liquefiable soils

were then assigned the UBCSAND model (Byrne et al 2004, Beaty and Byrne 1998) prior to the dynamic analysis. UBCSAND is an advanced 2-dimensional effective stress plasticity model that is able to accurately capture the generation of excess pore pressures during earthquake shaking. For the post-liquefaction portions of the analyses, soils that were determined to have liquefied during shaking were modeled using the Mohr-Coulomb model with liquefied residual strengths. Table 3-1 presents a summary of the material models and parameters used throughout the numerical analysis.

The steel sheet pile wall was modeled using beam elements with properties as shown in Table 3-1. The properties were selected to reflect an intermediate sheet pile, typical of what may be used as a levee cutoff wall. The wall elements were modeled as perfectly, linearly elastic. The wall elements were attached to the surrounding soil using unglued interfaces in order to capture potential slippage and separation.

3.2.3 Initial Stress Condition

The initial stress state of the numerical model was determined through a series of steps. Initial stresses and pore pressures were first initialized for level ground with the ground water table at the ground surface. The levee was then placed on level ground surface and the model was stepped to equilibrium with pressure applied outside of the slope to reflect the surcharge of the water on the waterside of the levee. An uncoupled fluid flow analysis was then conducted to determine the phreatic surface within the levee and pore pressure distribution throughout. Following the flow calculation, the material was then again stepped to equilibrium with effective stresses adjusted to reflect the new pore pressures.

3.2.4 Dynamic Analysis

Following the determination of the initial stress state, the dynamic analysis (a fully-coupled fluid-mechanical analysis) was performed. Material damping for the soils that were modeled using the Mohr-Coulomb model during the dynamic analysis was included with a 4-point sigmoidal hysteretic damping model, with properties to match modulus reduction and damping curves presented by Seed and Idriss (1970). In the UBCSAND model however, hysteretic damping is inherent and no additional damping was included. In addition to the hysteretic damping a small amount of stiffness-proportional Rayleigh damping was included to reduce numerical noise. Free field boundaries were applied during dynamic loading to account for the behavior at the model's lateral extents. The base of the model was modeled with absorbing boundaries and the ground motion was applied as a stress-time history along the model base, effectively modeling a vertically propagating shear wave and a compliant base (Mejia and Dawson 2006).

The UBCSAND constitutive model for this study was validated by comparing results to results from simplified liquefaction triggering analyses. These comparisons showed good agreement and are presented by Lobbestael and Athanasopoulos-Zekkos (2015).

3.2.5 Post Liquefaction Analysis

At the end of the ground motion, post-liquefaction analyses were also conducted. Rayleigh damping was increased to 5% and the model was continued in dynamic mode (with no additional motion input) in order to allow velocities to dissipate. Following the velocity dissipation period, zones modeled with the UBCSAND model that were determined to have liquefied (criteria discussed in Section 3.3, *Discussion of Analysis Results*) were switched to the Mohr-Coulomb with

liquefied residual strengths. Liquefied residual strengths were computed using the strength ratio proposed by Stark and Mesri (1992):

$$\frac{s_{u(crit)}}{\sigma'_{v_0}} = 0.0055 * (N_1)_{60-cs} \qquad \textit{Eq. (3-1)}$$

where $s_{u(crit)}$ is liquefied residual strength, σ_{vo}' is the initial vertical effective stress, and $(N_1)_{60\text{-}CS}$ is the standard blow count corrected for overburden pressure and fines content. A minimum liquefied residual strength of 250 psf was adopted based on empirical results presented by Seed and Harder (1990). The elastic shear stiffness for these zones was assigned as equal to 10 times the liquefied residual strength (following Stark et al 2012). Following assignment of the liquefied strengths, the model was allowed to continue in dynamic mode with no further motion input, until displacements stabilized, indicating a stable post-liquefied equilibrium state.

3.2.6 Ground Motion Inputs

Two types of input motions were used throughout this study: 1) uniform harmonic inputs and 2) a selection of ground motion recording inputs. For the harmonic inputs, motions with three peak ground accelerations were used (0.2g, 0.4g, and 0.6g), each with 3, 6, 9, and 12 cycles. The frequency of the harmonic motions was 1.5 Hz. This value was selected based on typical mean period values presented by Rathje et al (1998) for deep soil sites with moment magnitudes between 6.8 and 7.2 and distance between 30 and 80 km. A suite of three ground motion recordings was selected and is presented in Figure 3-2. These ground motions were selected for their ranges in peak ground acceleration and duration.

3.3 Discussion of Analysis Results

3.3.1 Liquefaction Development

Due to the potentially dramatic effects that liquefaction has on earth structures, the development and extent of liquefaction governs the response of the entire system. Accordingly, the parametric analysis results are presented beginning with observations of the liquefaction developments. In order to determine the extent of liquefaction during the dynamic analyses, excess pore pressure ratios, r_u, were computed according to equation 2,

$$r_u = \frac{u - u_0}{\sigma'_{v_0}} \qquad \textit{Eq. (3-2)}$$

where u is the instantaneous pore pressure, u_0 is the initial pore pressure, and σ'_{v0} is the initial vertical effective stress. Theoretically, liquefaction occurs when the excess pore pressure ratio is equal to 1.0. However, UBCSAND elements in which the excess pore pressure ratio exceed 0.7 were considered to have liquefied in accordance with recommendations by the developers of the constitutive model. Using this criterion, contours of maximum excess pore pressure ratios equal to 0.7 were plotted at the end of shaking for each analysis, to observe the extent of liquefaction. Figures 3-3 and 3-4 present the liquefaction extents at the end of shaking for the harmonic input analyses for Levee A and Levee B, respectively. Figure 3-5 presents the liquefaction extents for the ground motion input analyses for both Levee A and Levee B.

In observing the liquefaction results, one should note that all of the input motion/wall/soil property combinations investigated here result in at least partial liquefaction of the uppermost liquefiable layer, and range up to widespread liquefaction of all three liquefiable layers. This should be kept in mind when considering the range of scenarios to which these analysis results are applicable.

Several observations can be made by studying the figures showing the liquefaction extent for the analyzed levee profiles (Figure 3-3 to 3-5). These results are also in agreement with trends observed in previous field, laboratory, and numerical studies (e.g. Seed et al 2003), providing confidence that the model is accurately capturing the liquefaction behavior of soils. For example, as the number of cycles of loading and motion intensity increase, the extent of liquefaction increases. Also, Levee B, the looser of the two profiles, has significantly greater liquefaction extent than Levee A. In addition, the effects of overburden pressure and static shear stress (due to the presence of sloping ground) that have been previously observed are evident in these results. The soils beneath the levee are much less likely to liquefy than the soils in the free field due to the additional liquefaction resistance provided by overburden pressure. The soils beneath the levee slopes also exhibit behavior in agreement with published recommendations for K_α values (Harder and Boulanger 2007), which is a multiplier for accounting for static horizontal shear stress when estimating liquefaction resistance. For example, when observing the extent of liquefaction for Levee B for the ground motion input analyses (Figure 3-5), it can be seen that, beneath the levee slopes, only the soil in the uppermost liquefiable layer liquefies, while the deeper soils do not. For the static horizontal shear stresses in this locations, soils with strength similar to the upper layer have K_α values less than 1.0 (on the order of 0.5), while soils with strength similar to the deeper layers have K_α values close to or greater than 1.0 (suggesting more liquefaction resistance).

In addition to the verification of established trends, the contours of excess pore pressure ratios reveal valuable information about the effect of cutoff wall presence on the response of the levee. In general, it can be seen that the levees with a sheet pile wall experience more extensive liquefaction than the levees with no cutoff wall. For the ground motion recording analyses for Levee A, the results for input motion NGA0150 show very little difference between the cutoff wall

and no wall cases, but the results for Levee B (weaker levee) suggest otherwise. For Levee B, with no cutoff wall the liquefaction in the uppermost layer does not extend all the way across the levee, but with a cutoff wall, there is a zone of liquefied material below the center of the levee. For input motion NGA0728 with Levee A, liquefaction extends slightly farther under the levee with the wall in place, as well as slightly deeper in the free field. For Levee B, the same input motion results in full liquefaction of the free field soils for analyses with and without a cutoff wall, however under the levee the extend if liquefaction is deeper for the case with a cutoff wall than for the case with no wall. For Levee A with input motion NGA0901, liquefaction extends slightly further beneath the levee with a cutoff wall than without and there is also evidence of initiation of liquefaction directly adjacent to the cutoff wall on the waterside of the wall. For Levee B with the same input motion, there is widespread liquefaction in the free field and beneath the levee, although the liquefaction extends deeper under the levee for the profile with a cutoff wall.

In order to further investigate the difference in liquefaction behavior when a cutoff wall is present, it is valuable to compare how liquefaction evolves with time for the two cases (with and without a cutoff wall). Figure 3-6 presents time histories of the percentage of liquefied zones for the ground motion input analyses. The percentage of liquefied zones was computed as the number of zones at a given time with an excess pore pressure ratio greater than 0.7, normalized by the total number of potentially liquefiable zones (zones modeled using the UBCSAND model). For Levee A with input motion NGA0150 there is very little difference in the number of liquefied zones through the duration of shaking. For input motions NGA0901 and NGA0728 the difference in the percentage of liquefied zones between the analyses with and without cutoff walls appears to grow steadily through the intense shaking portions of the motions, arriving at the final liquefaction extents discussed above. These time histories suggest that there is not a specific characteristic of

the input motion that results in the difference in liquefaction extents. Also, they show that the analyses with cutoff walls have more extensive liquefaction throughout the duration of the motion.

The potential reasons for the differences in liquefaction behavior resulting from the presence of a cutoff wall can be broadly categorized into one of two types of classes: 1) differences in forces resisting liquefaction or 2) differences in forces driving liquefaction. The presence of a cutoff wall alters the initial stress state of the levee and foundation soil prior to ground shaking, which can thereby change the resistance to liquefaction. The presence of a cutoff wall results in different static horizontal shear stresses relative to a levee with no cutoff wall, since the wall forces the potential landside failure plane to the landside of the levee crest. This results in variations in the previously discussed K_α value between the two cases. With a wall in place the static horizontal shear stresses under the landside of the levee are increased, which, according to the recommended values of K_α, results in an increase in liquefaction resistance for denser soils and a decrease in liquefaction resistance for looser soils. The wall also alters the pore water pressure distribution within the levee. On the waterside of the cutoff wall, the phreatic surface is higher than for a levee with no cutoff wall, and on the waterside it is lower. On the waterside of the cutoff wall, the higher static pore pressures result in lower initial effective stresses, thereby decreasing liquefaction resistance. It also may be the case, that during shaking, the presence of the cutoff wall hinders dissipation of excess pore water pressure and accordingly furthers the development of liquefaction. Some combination of these factors may result in more liquefaction for levees with cutoff walls, relative to levees with no cutoff walls.

Apart from differences in liquefaction resistance, differences may also be a result of differences in liquefaction driving forces between the levees with and without cutoff walls. In

order to investigate this, profiles of maximum equivalent cyclic stress ratios, CSR_{eq} were plotted at several locations within the levee, where CSR_{eq} is defined as:

$$CSR_{eq} = 0.65 * \frac{\tau_{max}}{\sigma'_{v_0}} \qquad \textit{Eq. (3-3)}$$

where τ_{max} is the maximum shear stress and σ'_{v0} is the initial vertical effective stress. Vertical profiles of CSR_{eq} were investigated at the following locations: 1) waterside free field, 2) waterside levee toe, 3) center of levee, 4) landside levee toe, and 5) landside free field. Comparison between the profiles for levees with cutoff walls and levees without cutoff walls showed very little difference in equivalent cyclic stress ratio between the two cases. This is illustrated in Figure 3-7, which presents the maximum equivalent cyclic stress ratio profiles for Levee B with ground motion recording inputs. This suggests that the difference in liquefaction development observed for levees with cutoff walls is not due to differences in driving forces, although the wall presence may locally result in variations in ground motion propagation and reflection. Based on these results, the difference in liquefaction development behavior appears to be a result of differences in liquefaction resistance that arise due to the different initial stress states.

3.3.2 General Failure Development

As previously mentioned, the occurrence of liquefaction in the foundation soils dramatically affects the overall response of the levee system. The general response of the system is well illustrated by shear strain contours at the end of the ground motion. Figure 3-8 presents the shear strain contours for Levee A with input motion NGA0150 for analyses both with and without a cutoff wall. The shear strain contours indicate the development of circular failure surfaces on both sides of the levee that enter at the levee crest and extend into the upper layer of liquefiable

soil. The failure surface exit beyond the levee toes, as well as continue along the liquefied soil layer. Comparison of the shear strains for the two wall cases shows that the presence of the cutoff shifts the entry point of the landside failure to the landside of the crest center. The wall also causes the waterside failure to become more developed than for the analyses with no wall, particularly within the levee. Similar behavior was also observed for the two other ground motion inputs, as well as for the Levee B analyses. For Levee B however, the failure with no cutoff wall was more symmetric than for Levee A, resulting in a less pronounced difference between the no wall and cutoff wall cases.

3.3.3 Surface Displacements

The surface displacements that a levee experiences due to an earthquake are the key parameter with regard to the levee's performance as a flood control structure, and are presented and discussed in the following section. Figures 3-9 and 3-10 present the horizontal and vertical displacements at the end of shaking along the ground surface for the ground motion input analyses for Levee A and Levee B, respectively. When observing the displacements for Levee A, there is not a clear trend as to whether the presence of a cutoff wall results in higher or lower displacements. For the input motion NGA0150 there is very little difference between the two cases, aside from slightly higher vertical waterside displacements with the wall in place (due to the further development of the waterside failure surface, discussed previously). For the input motion NGA0728 the inclusion of a cutoff wall results in lower displacements (both horizontal and vertical) on the landside, but greater displacements on the waterside. For the input motion NGA0901 the analysis with a cutoff wall results in higher displacements (both vertical and horizontal) on the landside, but only slightly higher vertical displacements on the waterside. This

lack of a clear trend is likely due to the competing effects of the cutoff wall presence. As discussed above, the inclusion of a cutoff wall appears to increase liquefaction development, but previous studies (Lobbestael and Athanasopoulos-Zekkos 2014) have shown that the presence of a cutoff wall decreases displacements for levees without liquefaction.

The vertical surface displacements for Levee B adopt a different behavior than is observed for Levee A. The relatively symmetric vertical displacements (about the levee center) and their large magnitude are a result of the very widespread liquefaction of the foundation soils and essential destruction of the levee. For all three ground motion inputs the wall results in slightly lower vertical displacements, but in light of the magnitude, the wall presence becomes essentially negligible (for both vertical and horizontal displacements).

It is also important to consider the displacements that occur after the end of shaking, once the liquefied residual strengths have been assigned. However, of the analyses conducted here, only a select few ground motion/soil property combinations resulted in significant post-liquefaction movement. For Levee A only input motion NGA0901 exhibited significant increase in displacements after the end of shaking and for Levee B this was only observed for input motion NGA0150. For the remaining analyses, essentially no post-liquefaction movement was observed. It may be the case that the two analyses that exhibited significant post-liquefaction instability lie between two extremes, with the remainder of the Levee B analyses experiencing enough liquefaction to reach a stable deformed state during shaking and the remained of the Levee A analyses not experiencing enough liquefaction to result in post-liquefaction movement.

Given the controlled nature of the input motions, the results from the harmonic input analyses provide more information regarding displacement trends. Figures 3-11 and 3-12 present the maximum horizontal displacements on both sides of the levee and the maximum vertical

displacement on the levee crest for Levee A and Levee B, respectively. Also included on these figures for reference, and discussed later, is the data from the ground motion input analyses. For Levee A, there is relatively little difference in displacements between the analyses with and without cutoff walls, although the greatest difference is seen for high intensity, high cycle inputs, for which the wall presence results in lower vertical displacements. The results do however illustrate that the displacements depend more heavily on the number of cycles of loading than on the intensity of loading and presence of cutoff wall. For Levee B there is a more significant difference in both horizontal and vertical displacements between the cases with and without cutoff walls with the inclusion of a cutoff wall resulting in significantly lower displacements, except for inputs with a low number of cycles. The difference in the effect to wall presence for the two levees is also illustrated in Figures 3-13 and 3-14, which present the percent difference in displacements between levees with and without cutoff walls. Based on the results for both of the levees, the wall presence only appears to result in lower displacements for instances in which liquefaction is very extensive. Otherwise, the difference is negligible.

Ratios of vertical to horizontal displacements were also computed for each of the harmonic input analyses and are presented in Figure 3-15, as a function of number of cycles of loading. It can be seen that there is no consistent difference in the ratio between levees with and without cutoff walls. However, the value of the ratio varies with the number of cycles of loading. For Levee A, the ratio was seen to range between 0.45 and 0.7 and increased as the number of cycles of loading increased. For Levee B, the ratio ranged between 0.65 and 1.0 and decreased as the number of cycles of loading increased.

It is also valuable to compare the displacement results of the ground motion input analyses with the harmonic input analyses in order to observe to what degree harmonic inputs are able to

predict displacements for analogous ground motion recording inputs. In order to compare results of laboratory test data with uniform stress cycles to data results from ground response analyses, Seed et al (1975) proposed a relationship between earthquake magnitude and the equivalent number of uniform cycles at 0.65 times the maximum shear stress. Based on this relationship, an equivalent number of cycles was estimated for each of the ground motion input analyses used in this study and the resulting displacements were plotted with the results of the harmonic input analyses. When comparing these results, the difference in input intensity must be considered, since the number of equivalent uniform cycles is taken at a reduced intensity (multiplied by 0.65). Therefore, in order to directly compare the ground motion recording input results with the harmonic input results, the harmonic input results should be considered as having an intensity of 1.53 times (the reciprocal of 0.65) the reported intensity (i.e. the 0.2g intensity harmonic inputs should be considered as having an intensity of approximately 0.31g for comparison purposes). When comparing the Levee A displacements resulting from the harmonic input analyses with the results from the ground motion input analyses it is seen that the harmonic input horizontal displacements are in reasonable agreement with the ground motion input displacements and the harmonic input vertical displacements agree well. Also, the harmonic input displacements appear to suggest the same effect of wall presence. For Levee B however, the harmonic input horizontal displacements tend to be lower than observed for ground motion inputs. The vertical displacements for analyses with no cutoff wall agree well for the two input types, but for the analyses with a cutoff wall, the harmonic input analyses suggest a significant reduction in vertical displacement with a wall, that is not observed for the ground motion input analyses. However, overall the harmonic input analyses are able to reasonably predict displacements, at least within an order of magnitude.

3.3.4 Cutoff Wall Demands

Finally, for the analyses with a cutoff wall, it is of interest to observe the demands that a seismic event places on the wall. This is observed in terms of bending moments and associated lateral earth pressures. Figures 3-16 and 3-17 present bending moment time histories (including shaking and post-liquefaction portion of analyses) for the harmonic input analyses for Levee A and Levee B, respectively. For each analysis, these figures present histories at the two points along the wall for which the maximum positive and negative bending moments occurred.

The bending moment time histories for Levee A show moments undulating about an increasing value as the number of cycles increase. This is due to the increase in liquefaction extent and subsequent increase in displacements. There is essentially no change in bending moment throughout the post-liquefaction portion of the analyses, since Levee A exhibited relatively small post-liquefaction movement. For Levee B, similar behavior is seen, although for the 9- and 12-cycle analyses the moments increase with time, but then start to decrease. This is due to the very extensive liquefaction that was observed for these analyses. When all the soil around the end of the wall is liquefied, the surrounding soil is not able to transfer as much load to the wall. Also for Levee B, the 3- and 6-cycle analyses indicate a dramatic increase in bending moments during the post liquefaction period. These are the greatest bending moments observed for all of the harmonic input analyses and suggest that the greatest demands are placed on the cutoff wall when there is significant liquefaction followed by post-liquefaction movement, as opposed to very widespread liquefaction, for which little post-liquefaction movement was observed.

Bending moment time histories for the ground motion analyses for Levee A and Levee B are presented in Figures 3-18 and 3-19, respectively. For Levee A, similar behavior to the harmonic

input analyses is observe with the maximum bending moment undulating (although not uniformly) about a gently increasing value during shaking. Also, there is not significant increase in moment during the post-liquefaction portions of the analyses, although some post-liquefaction displacement was observed for input motion NGA0901. This suggests that post liquefaction displacements only influence post liquefaction wall demands when the liquefaction extends into the area around the cutoff wall. For Levee B, dramatically greater overall moments are observed as well as dramatic increases in moment during the post liquefaction portions of the analyses. The higher overall magnitude of moments for Levee B is a result of the liquefaction that extends under the levee, unlike Levee A, where only free field soils liquefied. The greatest post liquefaction increase in moment for Levee B is observed for input motion NGA0150, for which only the uppermost liquefiable layer liquefied in the vicinity of the wall. For the other two input motions however, the deeper layers also liquefied near the wall. This illustrates the significant demand imposed by partial liquefaction, as opposed to very widespread liquefaction. It is also important to note that the bending moment for some of these analyses exceeds the yield moment of the selected sheet pile section (45,000 ft-lb), although the wall was modeled as perfectly elastic.

Figures 3-20 and 3-21 present the lateral earth pressure profiles on either side of the cutoff wall, taken at the instance at which the greatest moment occurred, for Levee A and Levee B, respectively. For Levee A, relatively symmetric profiles on either side of the cutoff wall are observed at depth, however within the levee, there is significant asymmetry. This suggests that, for this profile, the wall pressures and subsequent bending moments are governed by the slope failures within the levee. This type of loading was also observed for the dynamic response of levees with cutoff walls without liquefiable soils (Lobbestael and Athanasopoulos-Zekkos 2014). However, in this case, the levee slope failures are perpetuated by the liquefaction of the free field

soils. For Levee B, where significantly higher bending moments were observed, the earth pressure profiles are not symmetric for the entire length of the wall. Instead, they essentially are significantly lower on one side of the wall. This is likely due to the liquefaction in the vicinity of the wall (in the foundation material), combined with the levee slope failures influencing the upper portion of the wall.

3.4 Conclusions of Parametric Analysis of Levees Founded on Liquefiable Soils

A parametric analysis was conducted using finite difference numerical modeling in order to investigate the dynamic response of earthen levees with cutoff walls, founded on liquefiable soils. The liquefaction behavior was captured using the advanced UBCSAND constitutive model. A levee with two sets of soil strength parameters was analyzed both with and without a steel sheet pile cutoff wall, with a range of uniform harmonic input motions, as well as recorded ground motion inputs. The key findings of this parametric analysis are summarized below.

- The effect of the presence of a cutoff wall on the dynamic displacements of a levee was seen to vary, depending on the foundation soils. For Levee A (the denser of the two levees), no systematic difference was observed in horizontal displacements between levees with and without cutoff walls. The difference in horizontal displacements (normalized by displacements for a levee with no wall) between the two cases ranged from -10% to 10% and averaged approximately 0%. For Levee B, the presence of a wall was seen to result in a reduction in horizontal displacements by 15% on average, but as high as 32%.
- Similar behavior was observed for vertical crest displacements. For Levee A, there was little difference between levees with and with cutoff walls. The difference ranged from -8%

to 11%, with an average of approximately 2%. For Levee B, however, the presence of a cutoff wall resulted in a reduction of vertical displacements of 15%, on average.

- No consistent difference was observed for the ratio of vertical to horizontal displacements for levees with and without cutoff walls. However, the value of the ratio was observed to range between 0.45 and 1.0 and varied for different numbers of cycles of loading, although it converged to 0.7 for input motions with greater than 9 cycles of loading. For Levee A, the ratio was seen to range between 0.45 and 0.7 and increased as the number of cycles of loading increased. For Levee B, the ratio ranged between 0.65 and 1.0 and decreased as the number of cycles of loading increased.
- The results of the analyses conducted in this study indicate that the presence of a cutoff wall does affect the triggering of liquefaction in the soils beneath the levee, resulting in more liquefaction than for levees with no cutoff walls. The portion of liquefiable soil that experienced liquefaction (as indicated by values of excess pore pressure ratio) was seen to increase by as much as 35% upon inclusion of a cutoff wall. The increase in liquefaction due to the presence of a cutoff wall was more prominent for Levee A (denser) than for Levee B. This increase in liquefaction is likely the result of two factors: 1) the presence of the cutoff wall results in a change in the initial static stress state within the levee, which results in a reduction in cyclic resistance, and 2) the presence of the cutoff wall may hinder dissipation of excess pore pressures generated during shaking.
- With regard to the structural demands placed on the cutoff wall during and after shaking, it was observed that the worst-case scenario occurs for cased of intermediate liquefaction (in the context of this study). The greatest cutoff wall demands were observed when only

portions of the soil beneath the levee liquefied, as opposed to cases with very widespread liquefaction beneath the levee.

Table 3-1, Material model parameters used throughout analyses

	Levee A						Levee B*					
Soil Layer **	1	2	3	4	5	6	1	2	3	4	5	6
Mohr Coulomb Material Model												
Friction Angle, φ (°)	35	33	36	38	39	40		28	32	36		
Cohesion, c (psf)	100	0	0	0	0	0		0	0	0		
Elastic Modulus, E (psf)	5.72E+06	4.99E+06	5.72E+06	5.72E+06	7.01E+06	7.01E+06		4.99E+06	5.72E+06	5.72E+06		
Poisson's Ratio, ν	0.3	0.3	0.3	0.3	0.3	0.3		0.3	0.3	0.3		
Dry Unit Weight, γ_d (pcf)	110	110	110	110	115	115		110	110	110		
Fluid Flow Model Properties												
Porosity, n	0.29	0.35	0.29	0.29	0.28	0.28		*Fluid flow model properties are identical for Levees A and B*				
Permeability, k (ft/s)	1.00E-04	5.00E-04	3.00E-04	3.00E-04	7.50E-05	7.50E-05						
UBCSAND Material Model* **												
m_n160, relative density index		15	26	31				5	15	25		
m_pa, atmospheric pressure (psf)		2116.2	2116.2	2116.2				2116.2	2116.2	2116.2		
m_kge, G_max/m_pa at mean effective pressure = 1 atm		1069	1284	1362				742	1069	1268		
m_ne, power for shear stiffness stress dependence		0.5	0.5	0.5				0.5	0.5	0.5		
m_kb, value of B/m_pa at mean effective stress = 1 atm		748.6	899	953.3				519.2	748.6	887.4		
m_me, power for bulk modulus stress dependence		0.5	0.5	0.5				0.5	0.5	0.5		
m_kgp, plastic shear modulus number		822	2705	4026				156	822	2477		
m_np, power for plastic shear stiffness stress dependence		0.4	0.4	0.4				0.4	0.4	0.4		
m_rf, hyperbolic fitting coefficient		0.73	0.67	0.66				0.86	0.73	0.68		
m_phicv, c.v. friction angle		33	36	38				28	32	36		
m_phif, maximum friction angle that can be mobilized		34.5	40.8	44.3				28.5	33.5	40.5		

Steel Sheet Pile Wall			
Moment of Inertia, I (ft^4)	Area, A (ft^2)	Elastic Modulus, E (psf)	Density, ρ (slug/ft^3)
2.50E-02	2.01E-03	4.40E+09	15

** M-C material properties for layers 1,2, and 6 are identical for Levees A and B*
*** Refer to Figure 3-1 for levee geometry and soil layer numbers*
**** UBCSAND layers were modeled using the generic input parameters for UBCSAND 904aR, based on relative density index*

Figure 3-1, Geometry of levees modeled in analyses

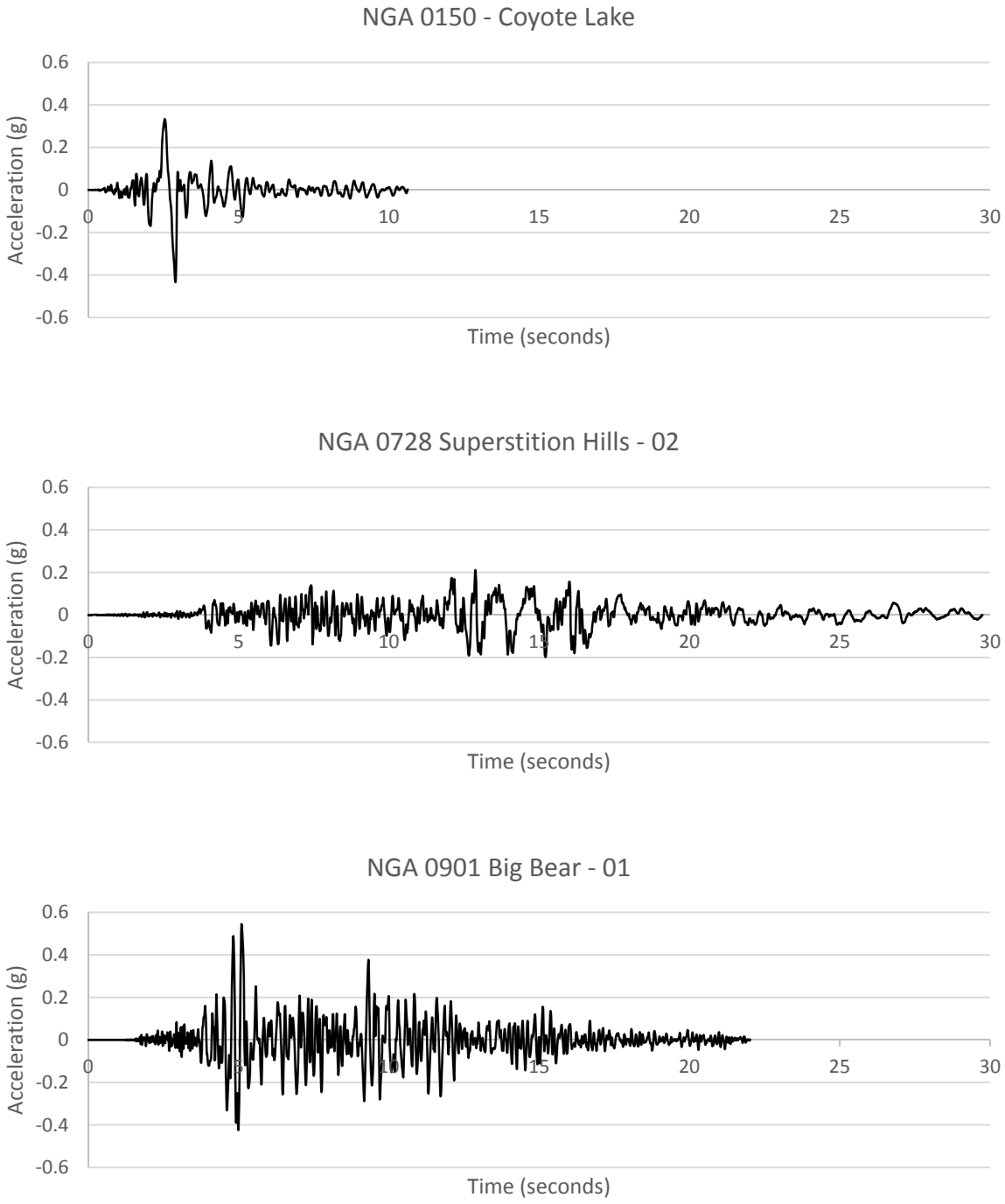

Figure 3-2, Acceleration time histories of ground motion recording inputs

(a)

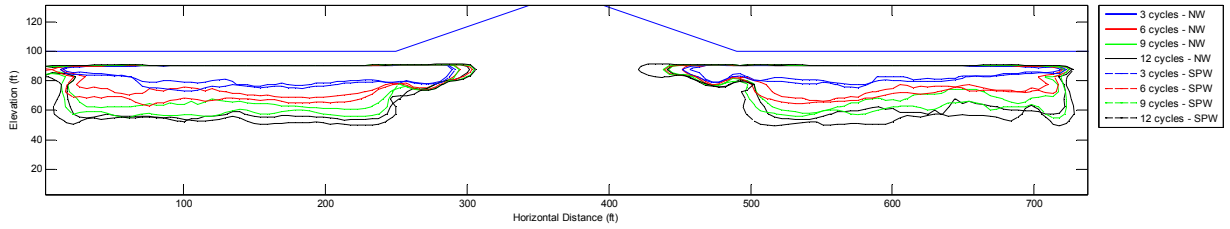

(b)

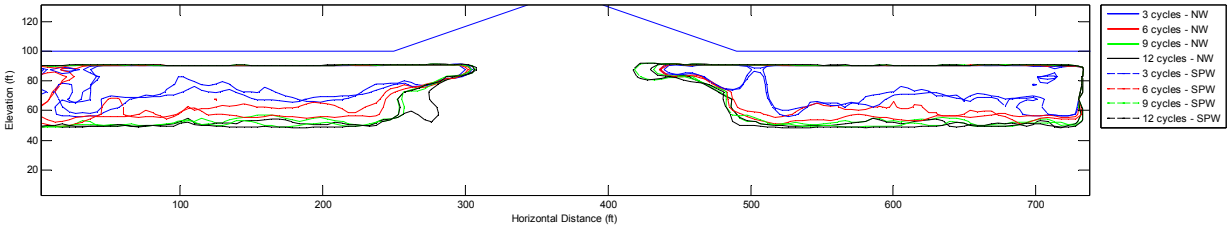

(c)

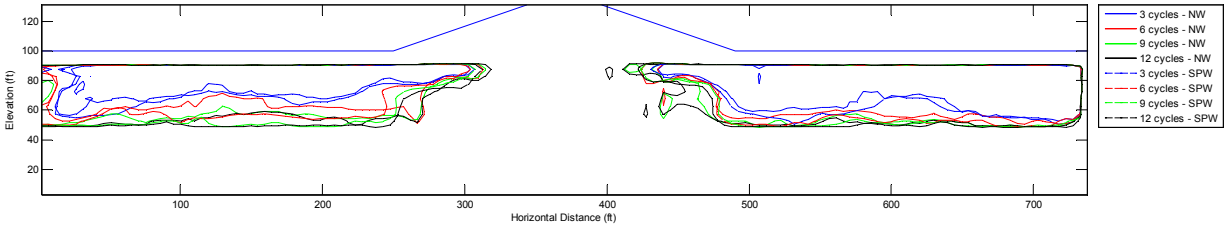

Figure 3-3, Liquefaction extents at the end of shaking for harmonic input analyses for Levee A with (a) 0.2g inputs, (b) 0.4g inputs, and (c) 0.6g inputs (NW – No Wall, SPW – Sheet Pile Wall)

(a)

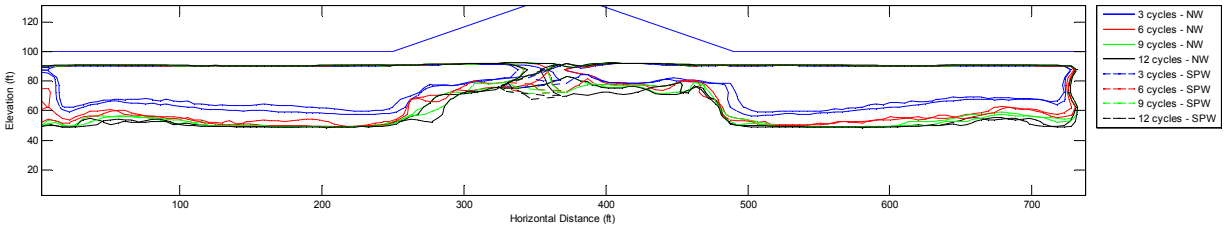

(b)

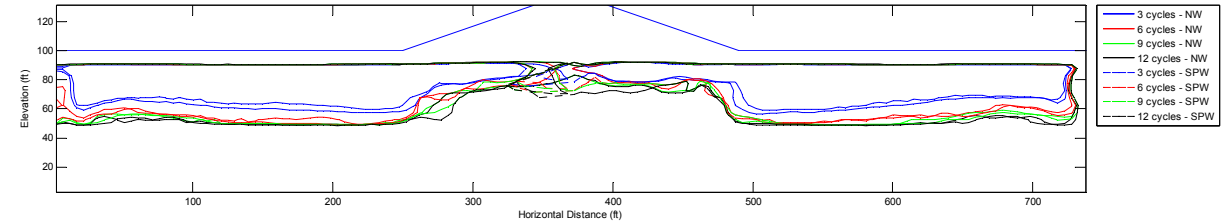

(c)

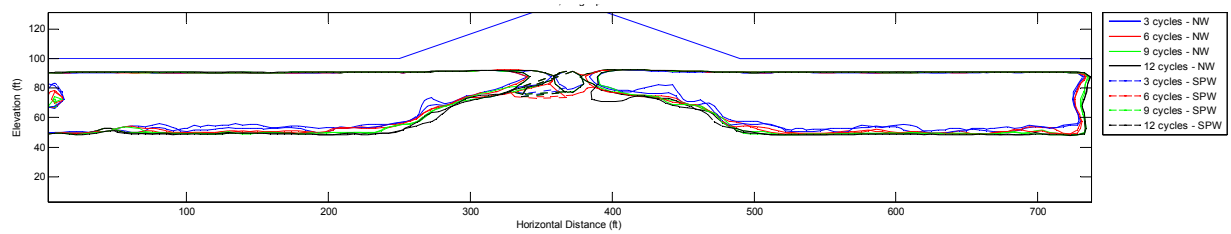

Figure 3-4, Liquefaction extents at the end of shaking for harmonic input analyses for Levee B with (a) 0.2g inputs, (b) 0.4g inputs, and (c) 0.6g inputs (NW – No Wall, SPW – Sheet Pile Wall)

(a)

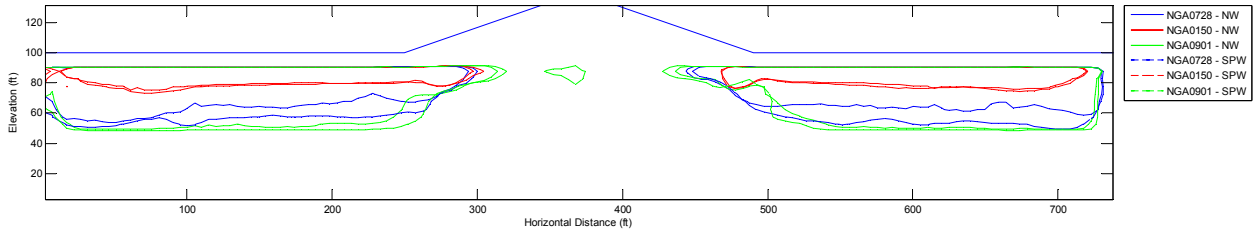

(b)

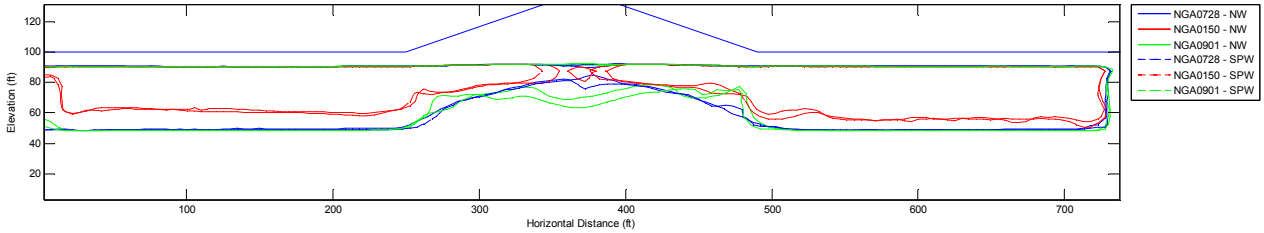

Figure 3-5, Liquefaction extents at the end of shaking for ground motion recording analyses for (a) Levee A and (b) Levee B (NW – No Wall, SPW – Sheet Pile Wall)

(a)

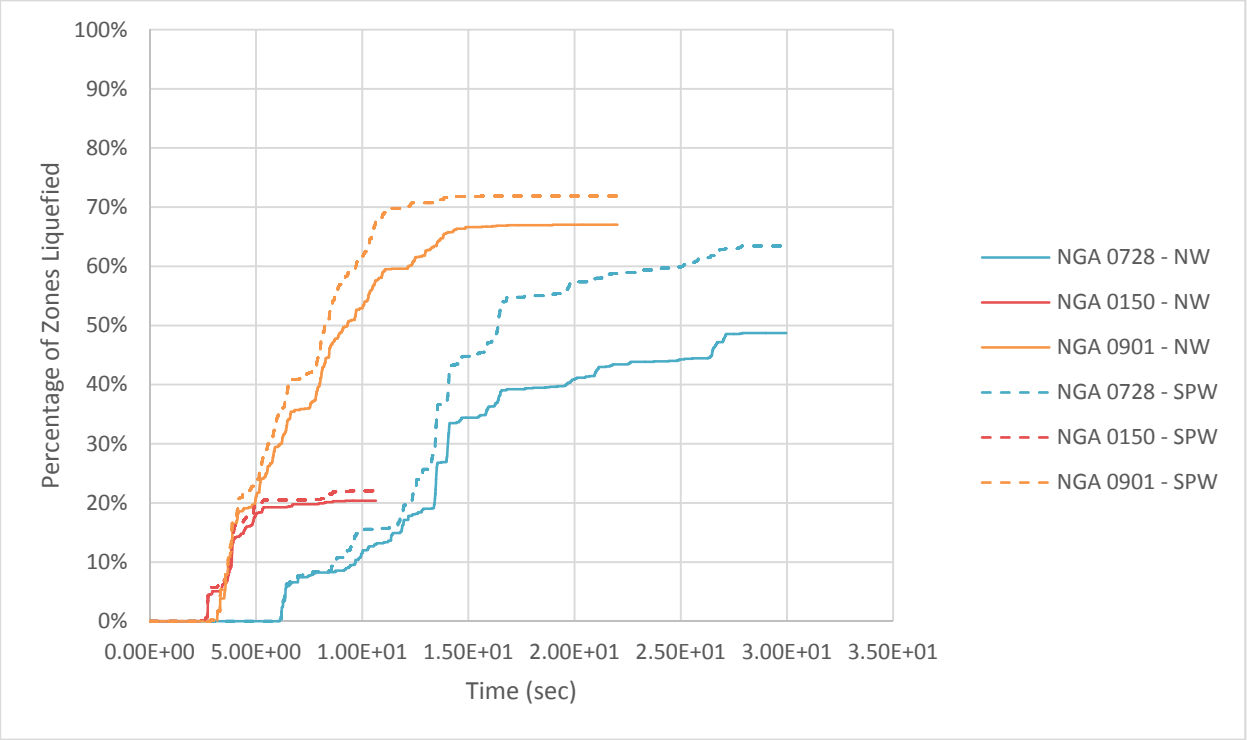

(b)

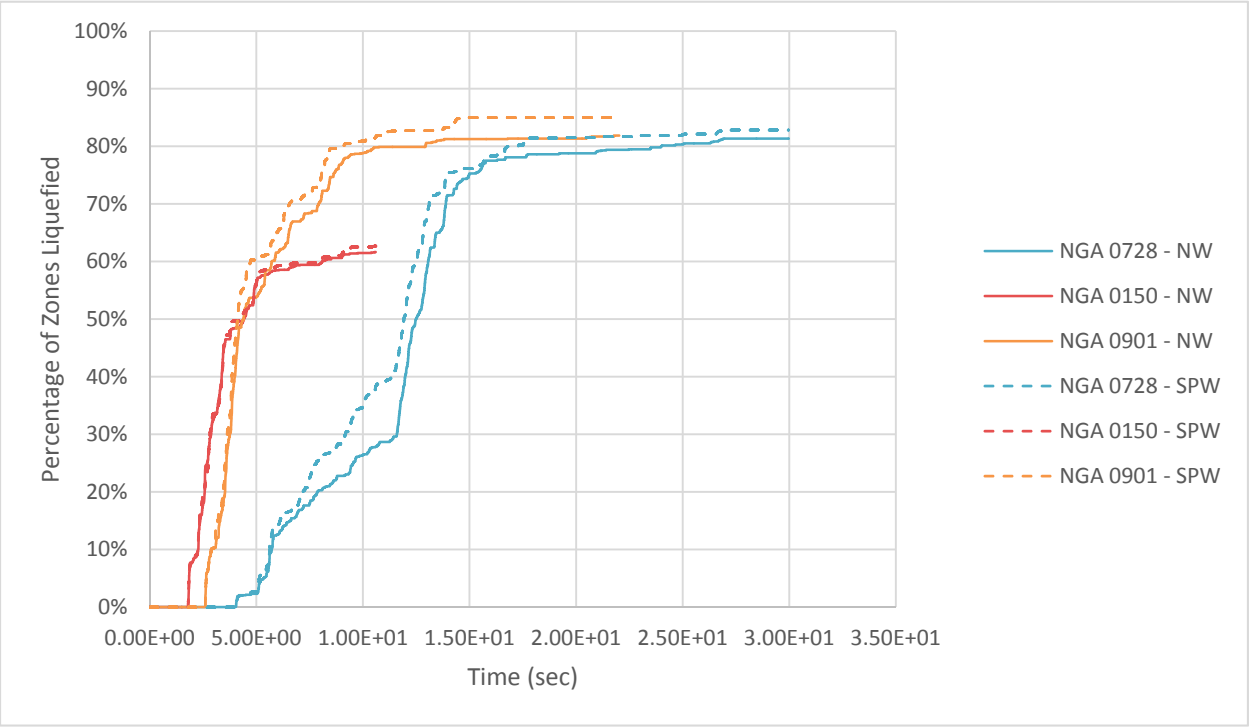

Figure 3-6, Time histories of percentage of liquefied zones for ground motion recording analyses for (a) Levee A and (b) Levee B (NW – No Wall, SPW – Sheet Pile Wall)

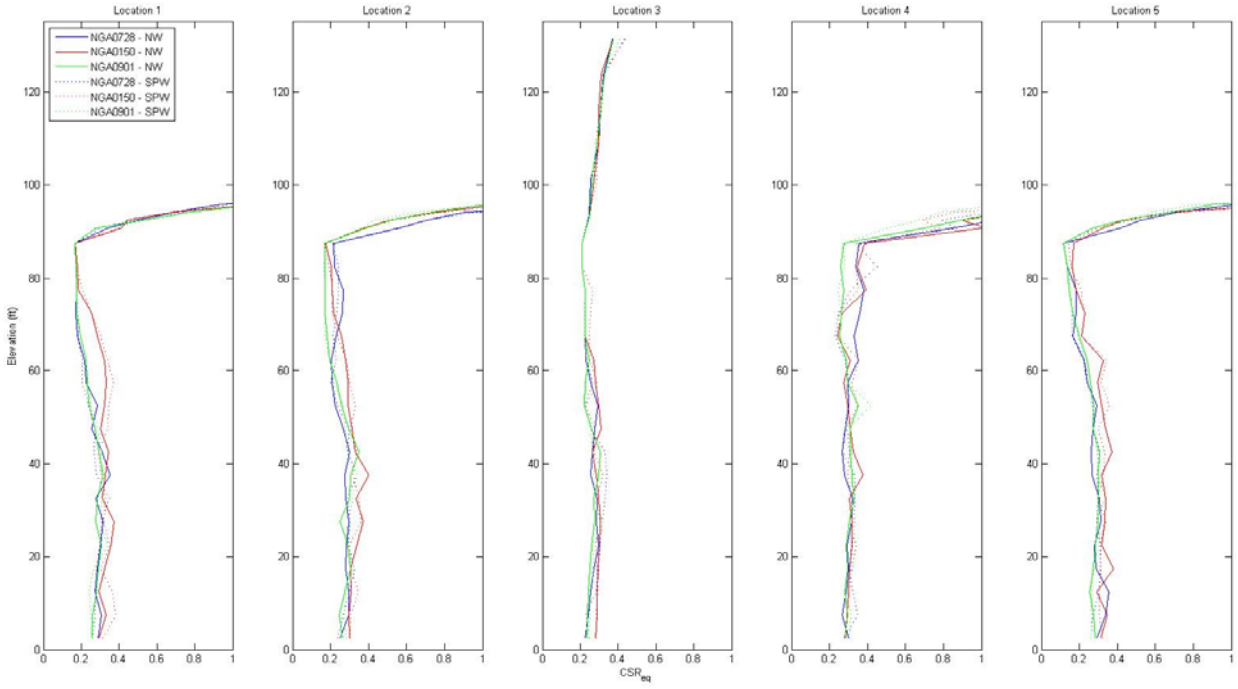

Figure 3-7, Profiles of maximum equivalent cyclic stress ratio at five locations for Levee B analyses with ground motion recording inputs (NW – No Wall, SPW – Sheet Pile Wall)

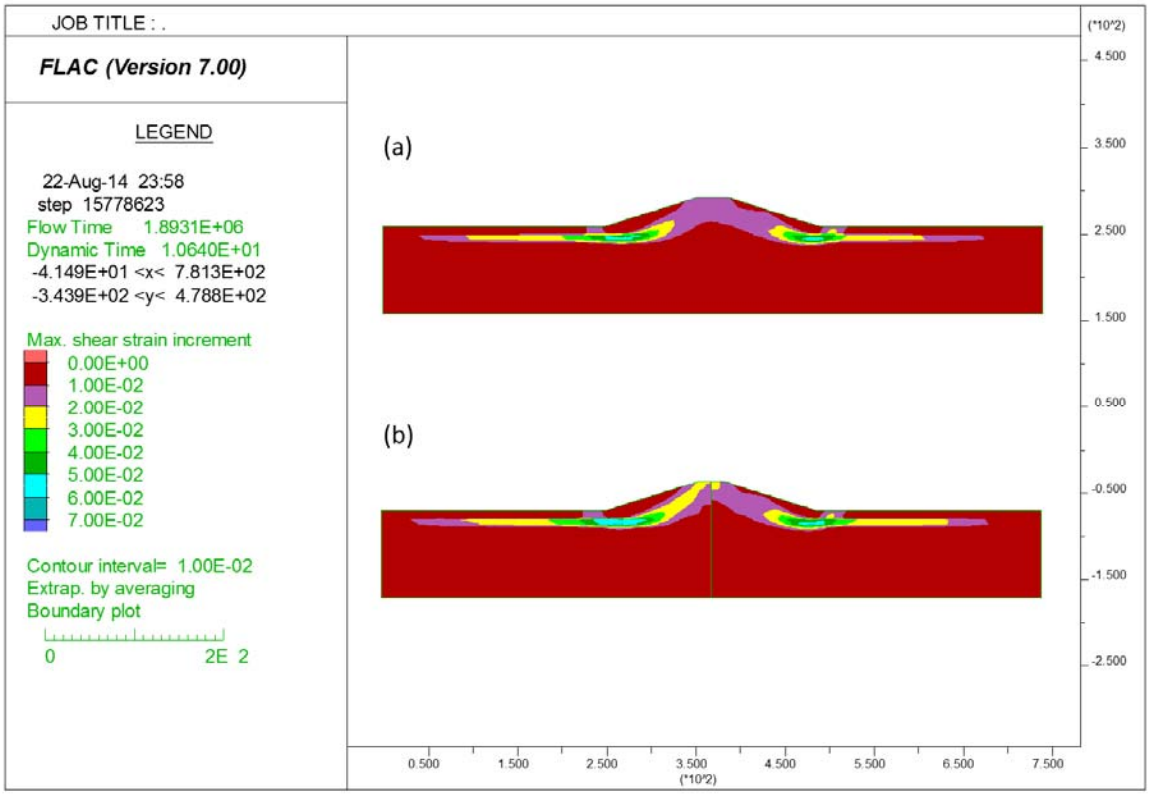

Figure 3-8, Shear strain contours at the end of shaking for Levee A with input motion NGA0150 (a) with no cutoff wall and (b) with a sheet pile cutoff wall

(a)

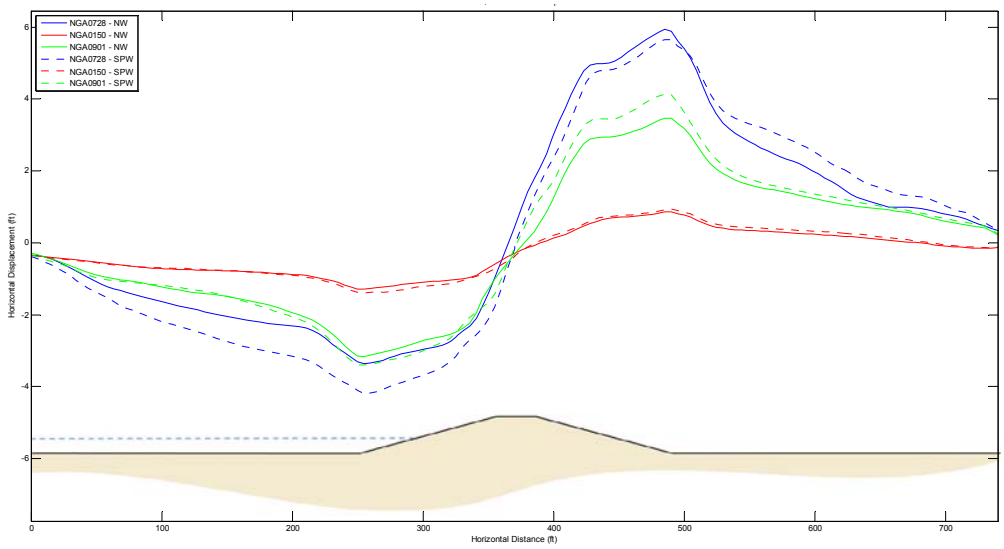

(b)

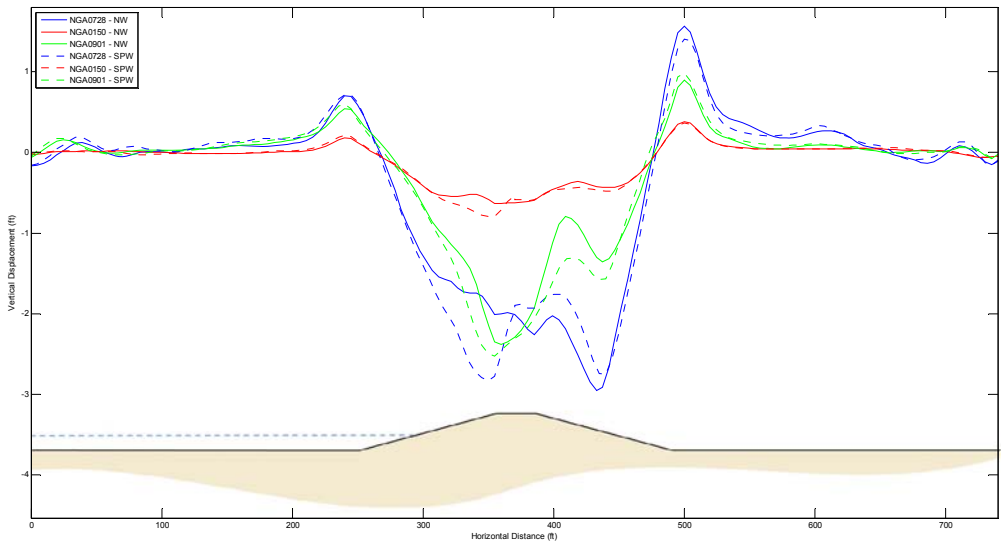

Figure 3-9, Horizontal (a) and vertical (b) displacements at the end of ground shaking for Levee A ground motion input analyses (NW – No Wall, SPW – Sheet Pile Wall)

(a)

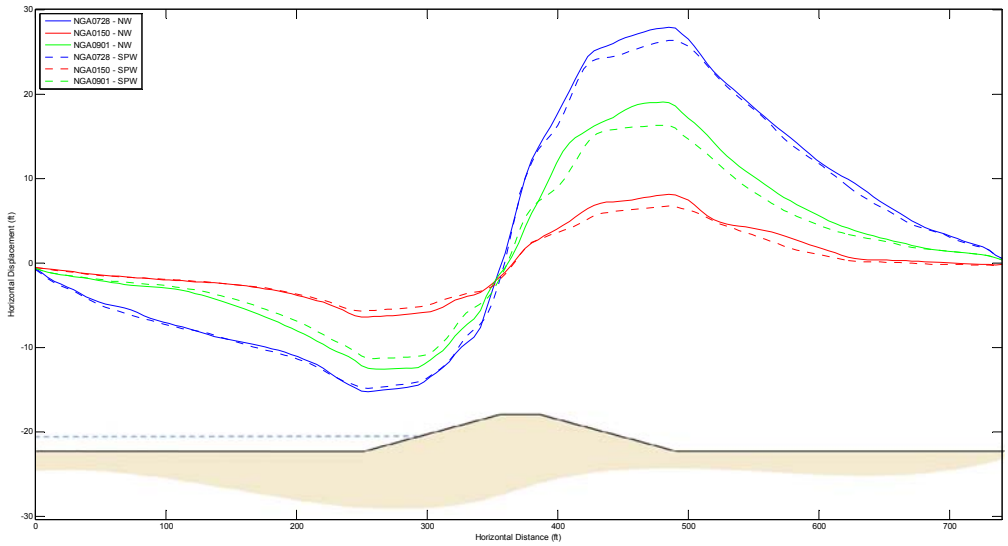

(b)

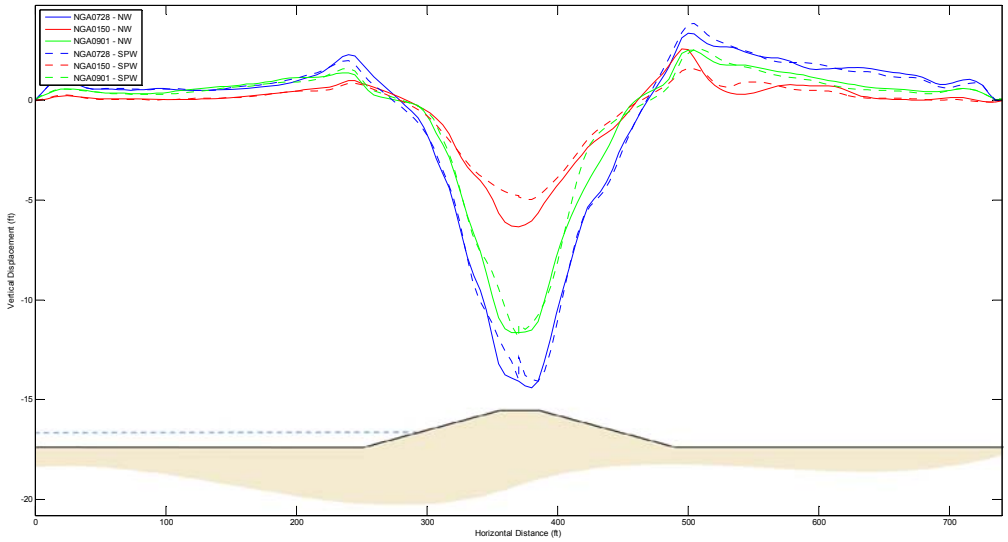

Figure 3-10, Horizontal (a) and vertical (b) displacements at the end of ground shaking for Levee A ground motion input analyses (NW – No Wall, SPW – Sheet Pile Wall)

(a)

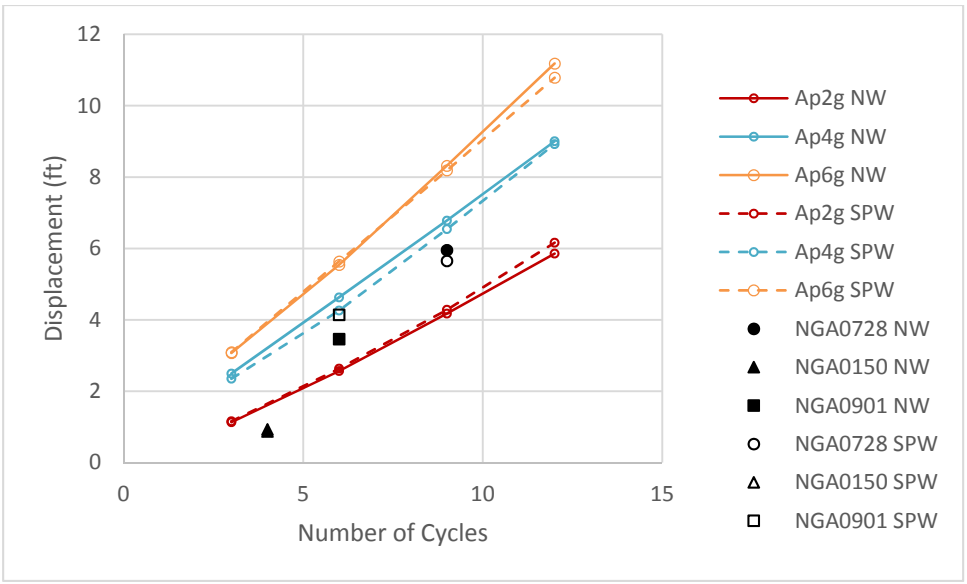
Displacement (ft)
Number of Cycles
0
2
4
6
8
10
12
0
5
10
15
Ap2g NW
Ap4g NW
Ap6g NW
Ap2g SPW
Ap4g SPW
Ap6g SPW
NGA0728 NW
NGA0150 NW
NGA0901 NW
NGA0728 SPW
NGA0150 SPW
NGA0901 SPW

(b)

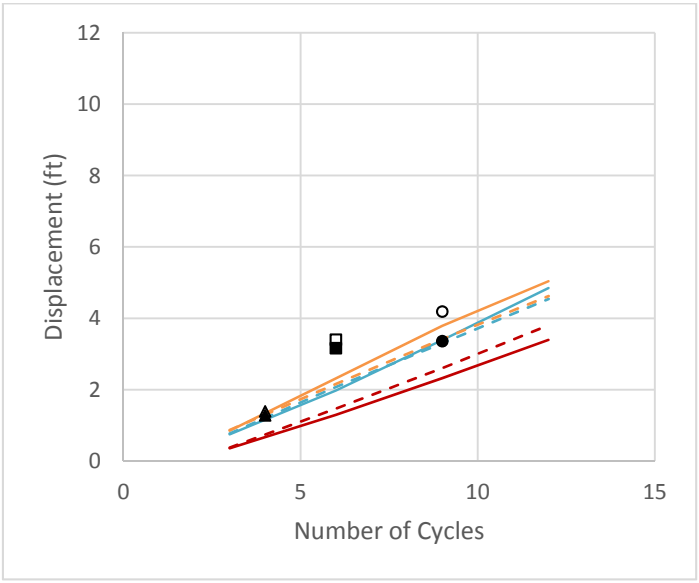
Displacement (ft)
Number of Cycles
0
2
4
6
8
10
12
0
5
10
15

(c)

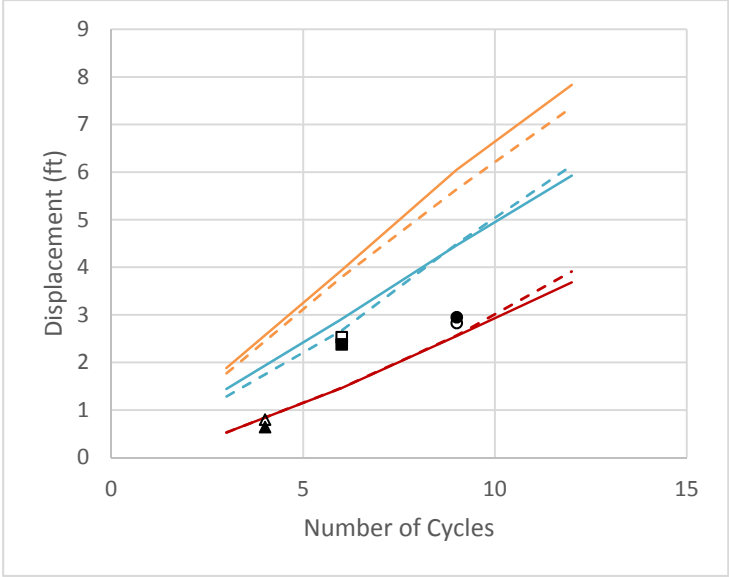

Figure 3-11, Maximum horizontal displacements on (a) the landside and (b) the waterside and (c) maximum vertical displacements at the end of ground shaking for Levee A harmonic input analyses (NW – No Wall, SPW – Sheet Pile Wall)

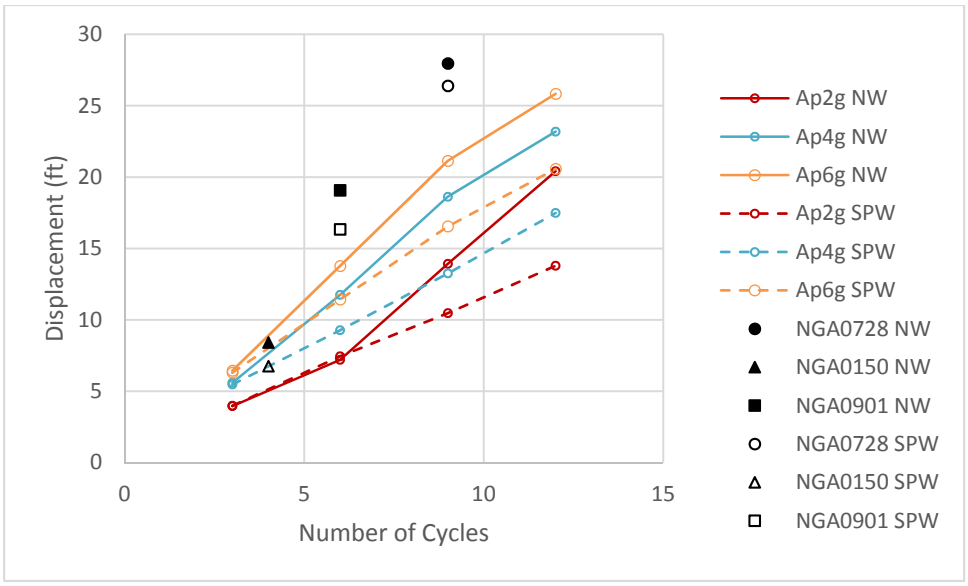
Displacement (ft)
Number of Cycles
0
5
10
15
20
25
30
Ap2g NW
Ap4g NW
Ap6g NW
Ap2g SPW
Ap4g SPW
Ap6g SPW
NGA0728 NW
NGA0150 NW
NGA0901 NW
NGA0728 SPW
NGA0150 SPW
NGA0901 SPW

(a)

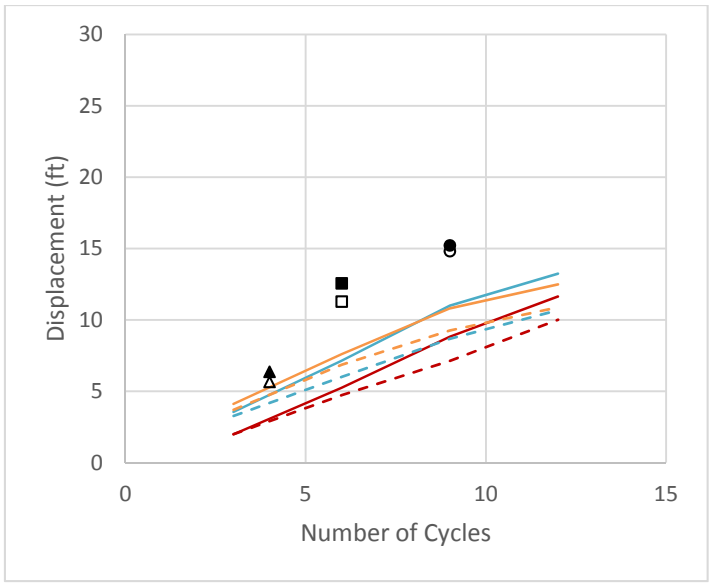
Displacement (ft)
Number of Cycles
0
5
10
15
20
25
30

(b)

(c)

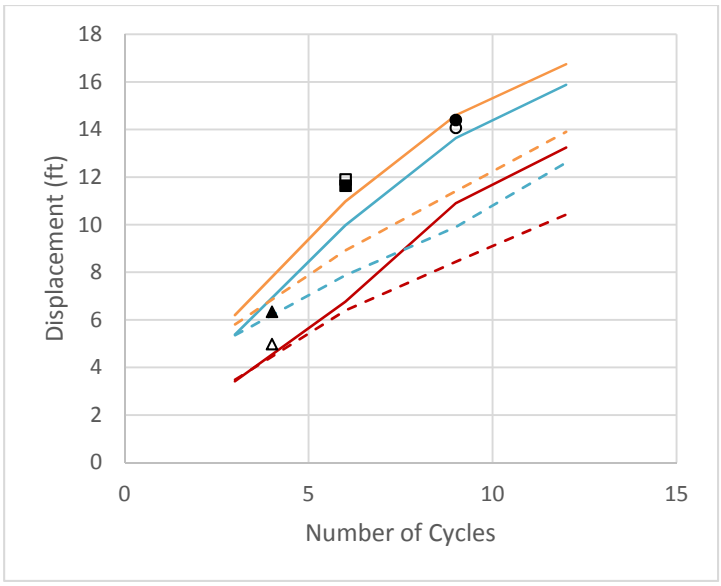

Figure 3-12, Maximum horizontal displacements on (a) the landside and (b) the waterside and (c) maximum vertical displacements at the end of ground shaking for Levee A harmonic input analyses (NW – No Wall, SPW – Sheet Pile Wall)

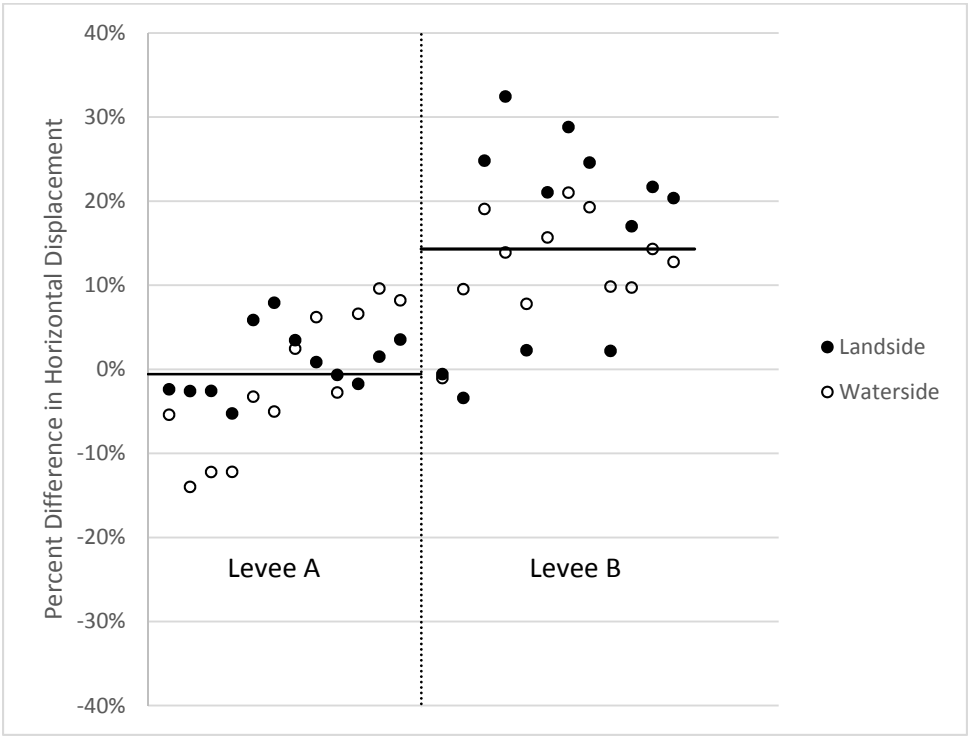

Figure 3-13, Percent differences in maximum horizontal displacements between levees with and without cutoff walls for harmonic input analyses (Normalized by displacement with no wall)

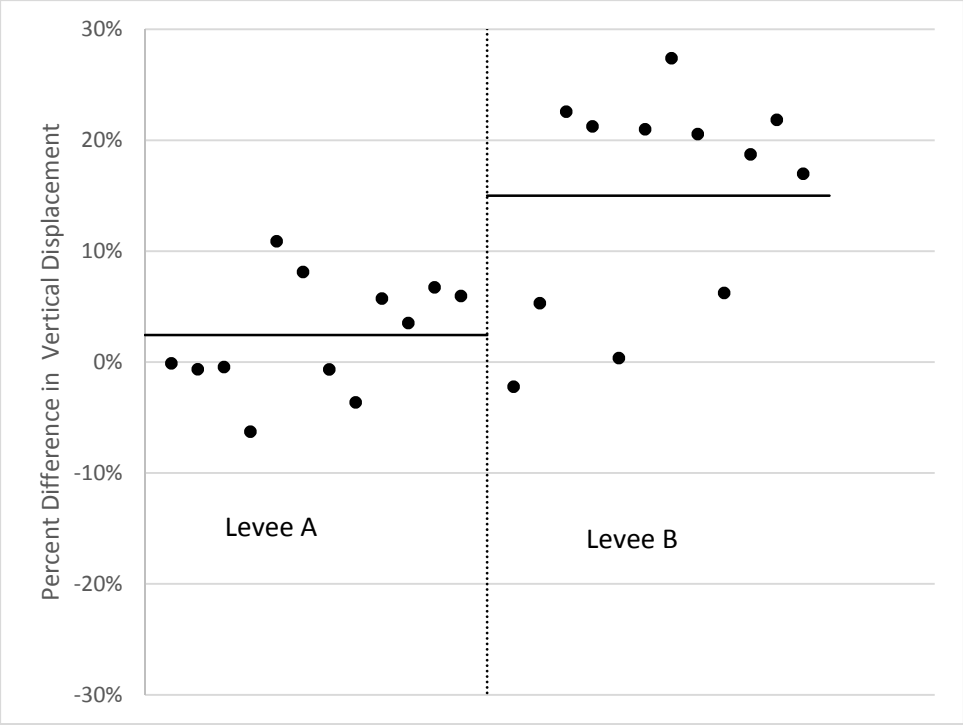

Figure 3-14, Percent differences in maximum vertical displacements between levees with and without cutoff walls for harmonic input analyses (Normalized by displacement with no wall)

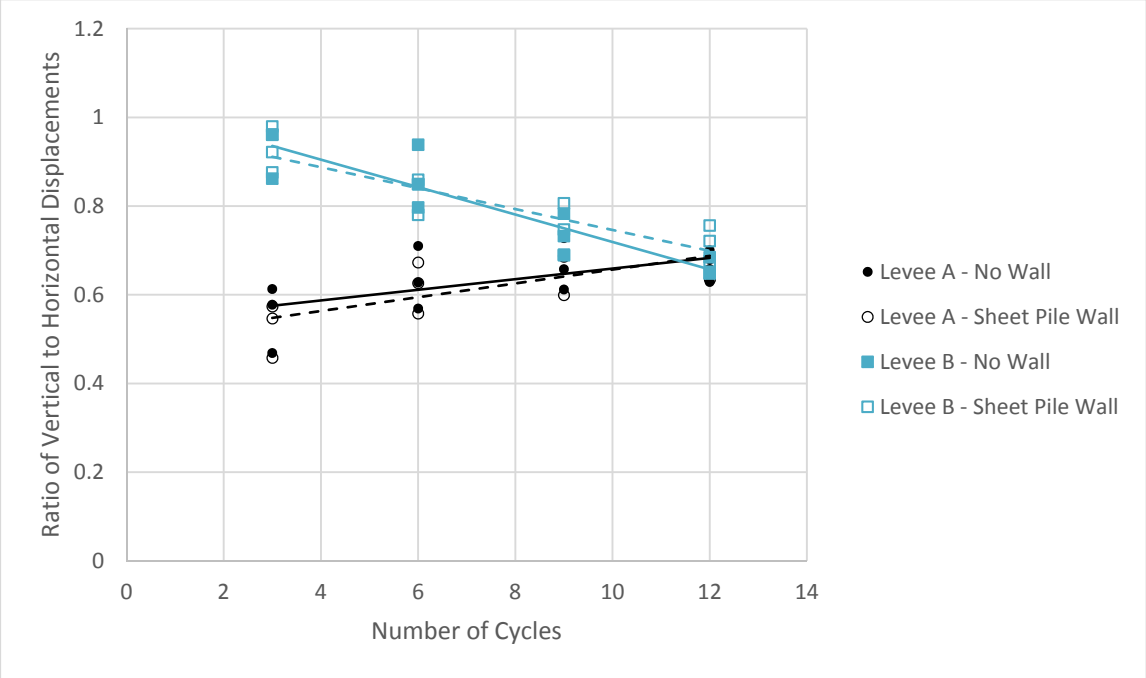

Figure 3-15, Ratios of vertical displacements to maximum horizontal displacements for harmonic input analyses

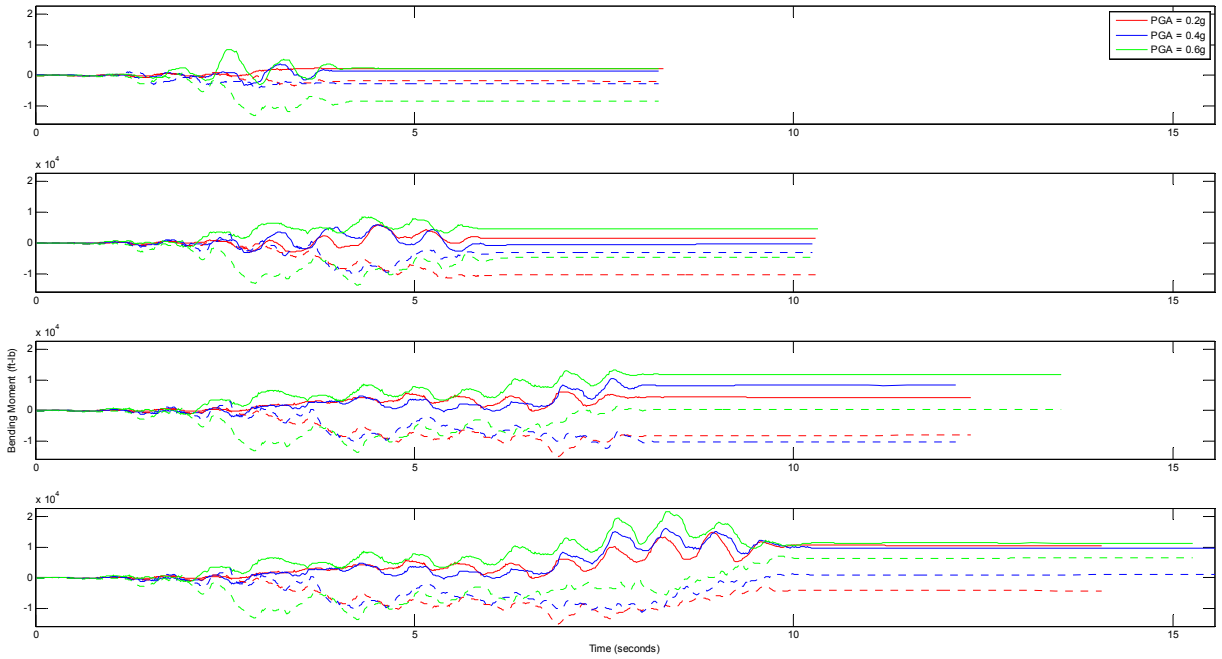

Figure 3-16, Bending moment time histories for Levee A harmonic input analyses (a) 3 cycles, (b) 6 cycles, (c) 9 cycles, and (d) 12 cycles

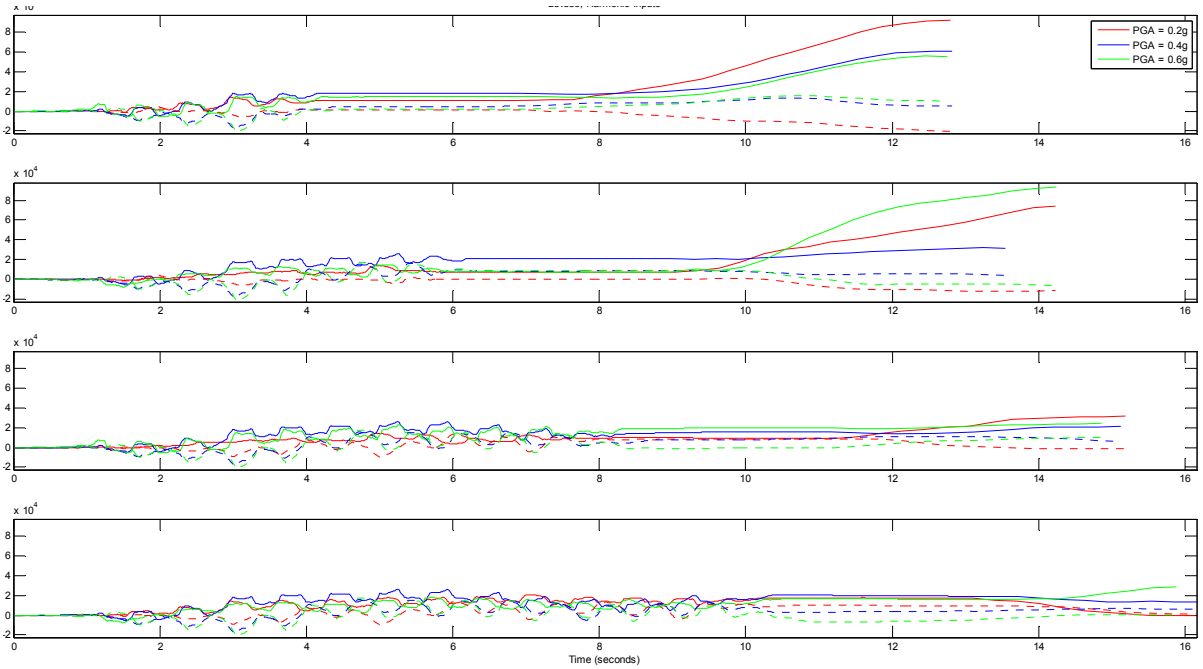

Figure 3-17, Bending moment time histories for Levee B harmonic input analyses (a) 3 cycles, (b) 6 cycles, (c) 9 cycles, and (d) 12 cycles

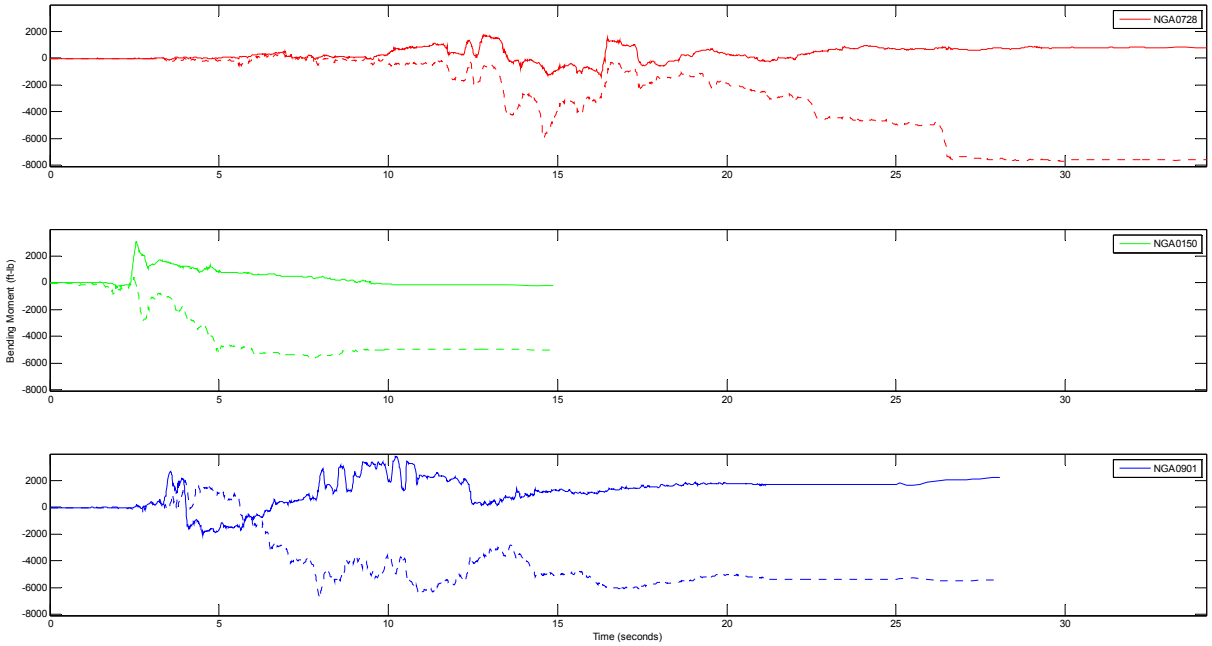

Figure 3-18, Bending moment time histories for Levee A ground motion input analyses

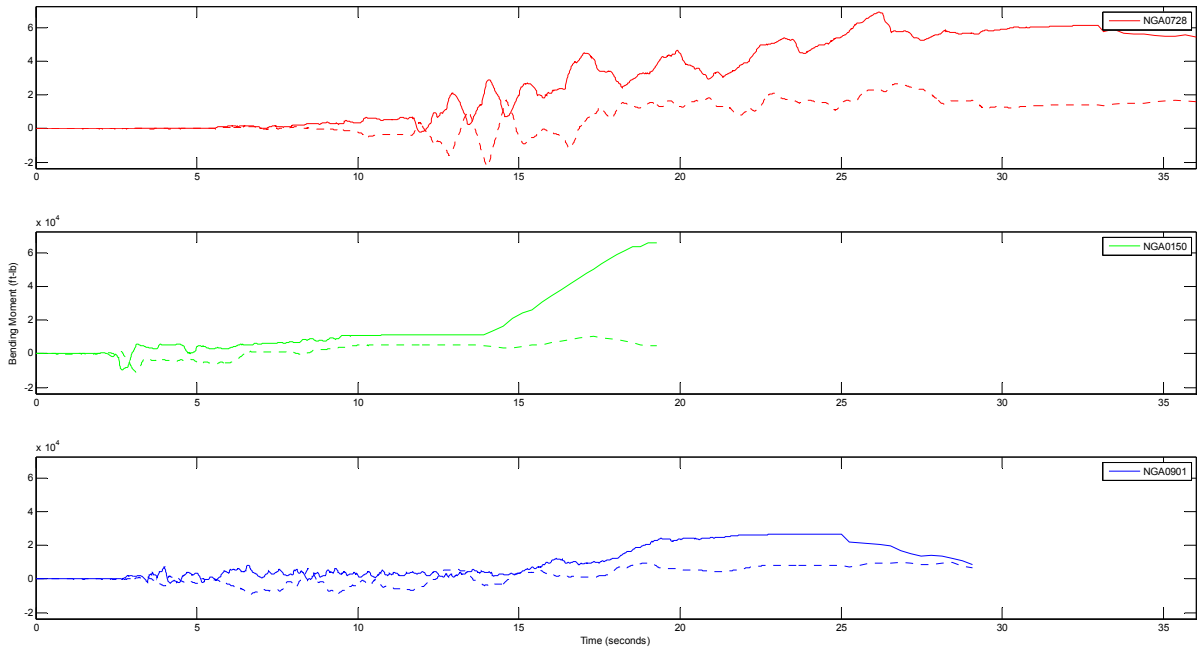

Figure 3-19, Bending moment time histories for Levee B ground motion input analyses

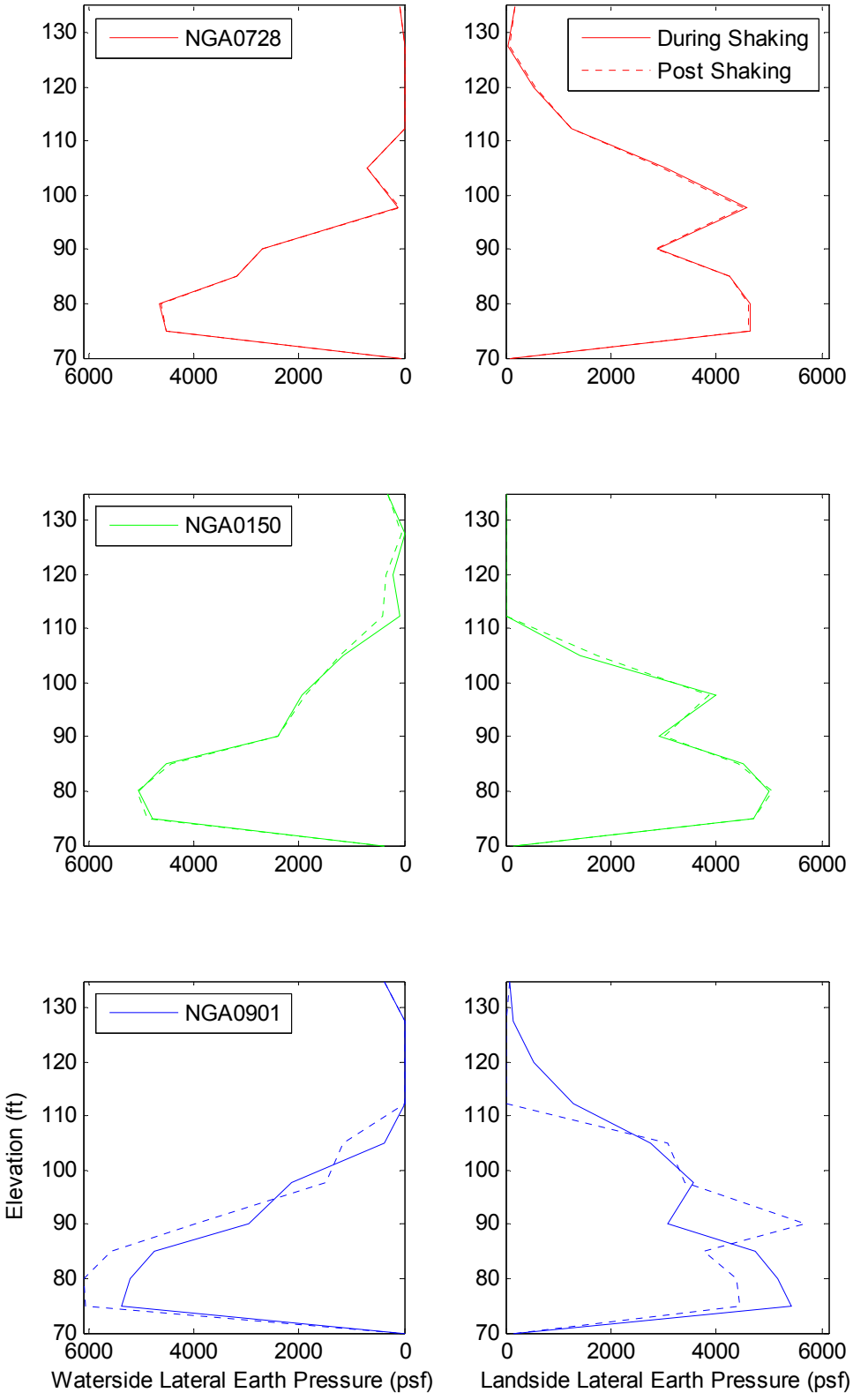

Figure 3-20, Lateral earth pressure profiles at the instance of maximum cutoff wall bending moment for Levee A ground motion input analyses

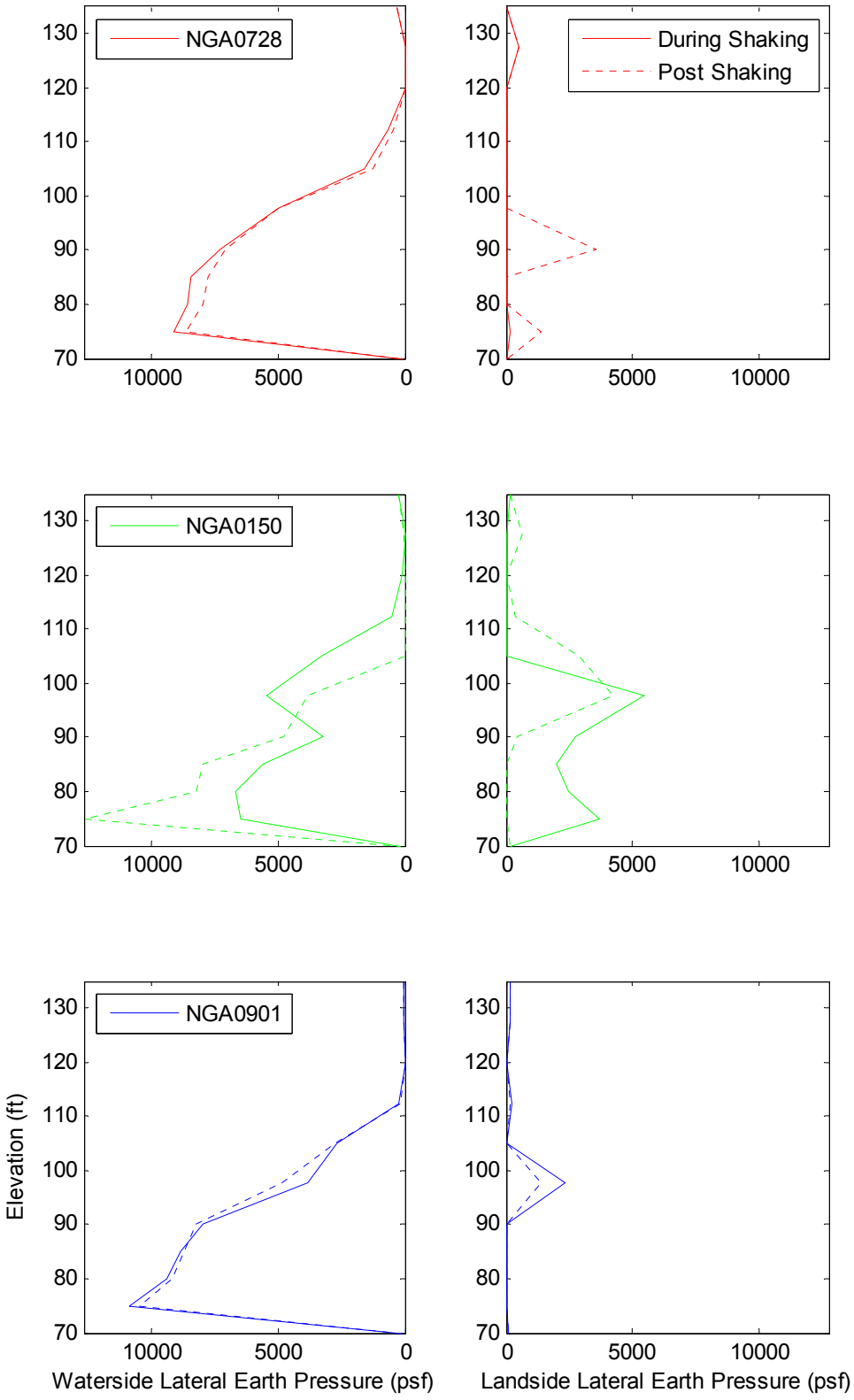

Figure 3-21, Lateral earth pressure profiles at the instance of maximum cutoff wall bending moment for Levee A ground motion input analyses

CHAPTER 4

Tailoring, Testing, and Modeling of ECC

The unique characteristics of the family of materials of engineered cementitious composites (ECC) make ECC an ideal candidate for a material for levee cutoff walls in seismic regions. Implementation of ECC in a subsurface component of a levee system presents a new set of challenges for the material including, but not limited to, new construction considerations and unique economic and environmental considerations that arise due to the extensive nature of such systems. Therefore a new version of ECC has been tailored and its feasibility for this application is investigated using a numerical modeling approach. This chapter presents a background on the ECC family of materials, a summary of the material tailoring process, and a discussion of the constitutive modeling used to capture the unique behavior of this material in a numerical simulation.

4.1 Background on Engineered Cementitious Composites

The development of ECC has been the result of a large body of research in the fields of composite materials and fracture mechanics. Early research by Aveston et al (1971 and 1973) and by Marshall and Cox (1988) joined these two fields, proposing theories regarding the behavior of composite materials consisting of brittle matrices reinforced with elastic fibers and the conditions

necessary for the development of multiple cracking. Work in this direction continued in subsequent years to include the behavior of brittle matrix composites with discontinuous, randomly oriented fibers, including the development of ECC.

ECC is characterized by a delicate balance of component material properties that result in steady-state and multiple cracking, which produce the global pseudo strain-hardening of the composite. The steady-state or flat crack propagation requires that the total available crack driving energy (complementary energy of fiber-bridging) must be greater than the resistance of the composite to crack propagation (crack tip toughness). This mode of crack propagation contrasts with the oval shaped Griffith crack observed in tension-softening fiber-reinforced concretes. Following the initiation of the first steady state crack, the fibers that bridge the crack are able to transfer the load across the crack as their collective bridging capacity is greater than the matrix cracking strength for the first crack. This process continues and an array of parallel cracks is formed, in what is called multiple cracking, shown in Figure 4-1. The micromechanics conditions necessary for combined steady state and multiple cracking are explained in detail by Li and Leung (1992). The result of the proper combination of these two behaviors is pseudo strain-hardening of the composite under tensile loading, with the possibility of dramatically increased tensile strain capacities, as compared to conventional concretes. Figure 4-2 illustrates the stress-strain behavior of such high-performance fiber reinforced composites in comparison with conventional concrete and standard fiber-reinforced composites. Unlike most fiber reinforced composites, in which fiber pullout leads to tensile softening immediately after crack initiation, ECC exhibits significant strain-hardening. The conditions that govern this behavior are presented by Li and Wu (1992) and were capitalized upon during the material tailoring process to ultimately develop ECC in the early 1990's. Variations of the material have been advanced and revised over the subsequent decades

and it has been used in a wide range of structural applications including skyscrapers, bridges, and dams. For a more thorough history of the development of ECC, the community that developed it, and early research and applications of the material, the reader is referred to Li (2003).

As research on high performance fiber reinforced composites (HPFRC's) and ECC has continued, a number of characteristics of the material have been both tailored and observed that, when combined, make ECC an ideal material for the application at hand; cutoff walls for earthen levees in seismic regions. As previously discussed, ECC exhibits tensile strain capacities that are much greater than those of traditional concretes. This ductile behavior makes ECC an ideal candidate for use in cutoff walls in seismic regions, since as shown in previous chapters, seismic events (particularly when liquefaction occurs) have the ability to result in large tensile strains in cutoff wall elements. A material that can withstand these demands without being significantly compromised is essential. Since its early development, research on ECC has led to refinement of the mix design which has resulted in higher strain capacities. For example, the use of polyvinyl alcohol fibers, as opposed to polyethylene fibers, was shown to increase the tensile strain capacity from approximately 1% to values in excess of 4% (Li et al 2001).

A high tensile strain capacity alone, however is not sufficient to meet the demands placed on a cutoff wall during a seismic event. Due to the cyclic nature of earthquake loading, the cutoff wall must be able to sustain repeated and fully reversed loading. Previous research has been conducted to investigate the response of HPFRC's to fully reversed cyclic loading and has indicated that such materials can withstand such loading. It has also been shown that this type of loading does not limit the tensile strain capacity of the material, as long as the compressive limits of the material are not reached (Kesner et al 2003). Furthermore, the cyclic loading response of these materials has been tested in experimental simulations of structural components, such as

cyclically loaded cantilever beams (Fischer and Li, 2002) and has shown favorable results. This further reinforces the hypothesis that ECC would be a strong material candidate for levee cutoff walls.

In addition to the ductile characteristics that result from the formation of microcrack arrays under tensile strain, this behavior results in permeability characteristics that are desirable for this application. For a levee cutoff wall in seismic regions, the material must be able to withstand the strains imposed by an earthquake event, without compromising its primary function as a seepage barrier. Water permeability testing conducted on ECC specimens at various levels of tensile strain indicate that the material is capable of meeting this requirement (Lepech and Li, 2009). Figure 4-3 presents the results of this testing in the form of coefficient of permeability versus tensile strain of the specimen. Even at 3% tensile strain, the permeability of the cracked specimen remained below $1X10^{-7}$ cm/sec. For reference, this is within the range of permeability of a typical clay, as well as below the maximum permeability of a compacted clay liner for a Subtitle D landfill according to the Resource Conservation and Recovery Act (RCRA).

Another unique characteristic that results from the microcracking behavior of ECC is the potential for autogenous healing of cracked portions of the material. Due to the very narrow crack width of ECC in the post-elastic stage, left over unhydrated material that is exposed to moisture during and after cracking is able to cure and essentially heal the cracks. This behavior was investigated by Yang et al (2009) and it was shown that specimens that were loaded to 3% tensile strain were able to recover nearly all of their tensile strain capacity after self-healing. This healing effect, illustrated in Figure 4-4, lends itself very well to the application of cutoff walls. A cutoff wall that is damaged by an earthquake event could potentially heal over time, since it is exposed to the moisture within the soil. This would restore the function of the wall as a seepage barrier over

time before the next major flood event, although, as previously mentioned, the permeability of a cracked specimen is still relatively low.

Apart from these characteristics, which are essential to making ECC a valuable material for use in levee cutoff walls, there are also other properties that enhance its desirability. One of these is the potential for self-sensing in conjunction with structural health monitoring systems. Hou and Lynch (2009) conducted preliminary studies on ECC as a self-sensing material and investigated the use of electrical impedance tomography for locating cracks in damaged ECC specimens. The results indicated that this approach does indeed work with ECC, which could be very valuable for levee systems, since they are such extensive structures. Structural health monitoring systems that use this self-sensing ability of ECC could potentially be very useful in triaging the repair of levees following an earthquake event. This would allow the repair process to be prioritized to the most damaged section first, and then continue to the less critical areas later, since the repair process can take several years for such large systems. When combined, the ductility, permeability, self-healing, and self-sensing capabilities, make ECC a very appealing choice for use in constructing cutoff walls for levees in seismic regions.

4.2 Tailoring of ECC for Use as a Cutoff Wall Material

Building upon the previous work that has been done on Engineered Cementitious Composites (ECC), in combination with the unique demands of this application, a preliminary ECC material specifically for use in levee cutoff walls was developed. Materials science researchers at the Advanced Civil Engineering Materials Research Laboratory (ACE-MRL) at the University of Michigan (under the supervision of Professor Victor Li) conducted an iterative material tailoring process and provided mix design recommendations accordingly. Postdoctoral

researcher Bangyong Lee worked on the development of the material from 2010 to 2011 and graduate student Lena Soler Ayoroa continued the work from 2012 until early 2014. Over the course of the material development, we held regular meetings to share information regarding target values and test results for use in numerical modeling. The material tailoring process and resulting recommendations are summarized in this section.

At the outset of this study, preliminary target values for the performance parameters of an ECC cutoff wall material were established, based on preliminary analyses and performance requirements of systems with similar objectives. Based on preliminary numerical modeling conducted prior to this study, the required tensile ductility of the material was estimated to be on the order of 2 to 3%, with the understanding that this value would likely be revised through the course of the study, as the results of more advanced numerical modeling became available. The required compressive strength of the material was set as 1 MPa, although this value is not expected to be exceeded for this application. The required maximum permeability of the material was set at $1X10^{-7}$ cm/sec, based on the requirements and performance of typical slurry wall systems. Since it is intended that this material would be implemented as a slurry-type wall, target fresh concrete properties were also established. In accordance with recommendations for placement of soil-bentonite slurry walls (Evans 1991 and Millet et al 1992), the target slump was set as approximately 100 to 150 mm. Finally, in order to be economically feasible, a target cost per square foot of cutoff wall of $16 to $25 was selected, based on the typical range of costs for steel sheet pile walls.

The tailoring of the ECC material for levee cutoff walls started by selecting an existing ECC mix design from a previous application, with properties closest to those desired. The mix that was selected was an ECC made with polypropylene (PP) fibers, developed by Yang (2008). This

version of ECC exhibited high tensile ductility and small crack width and benefited from the use of PP fibers from an economic standpoint. Also, it was designed with relatively high fly ash content, making it more sustainable than other mix designs. This PP-ECC was recreated by the ACE-MRL researchers and used as a starting point for the cutoff wall ECC. The mix was then iteratively altered to enhance certain characteristics and investigate the influence of certain components on the behavior of the material. The early portion of the tailoring process conducted by ACE-MRL is documented in a report by Lee (2011) and is summarized in the following paragraphs.

Over the course of the early portion of the tailoring process, three families of mix designs were produced, with various iterations within each family. The mix proportions of these iterations are presented in Table 4-1. The first mix family, Mix 1, started based on the previously mentioned PP-ECC. The first design, Mix 1-1, was a duplication of that mix design, although a different superplasticizer was used in order to make the fresh properties more amenable to the slurry wall construction technique. This mix exhibited significant variation in tensile strain capacity, which was followed by Mix 1-2, which included polystyrene beads (as artificial flaws) in an effort to reduce the variation. Mix 1-3 was the same as the previous mix, although a smaller amount of polystyrene beads was used to further investigate the effect of their inclusion.

The first series of mixes however exhibited a wide distribution of air bubbles, which were of concern due to their potential effect on the permeability of the material. In order to remedy this, Mix 2-1 was created with the inclusion of an anti-foaming agent (D175A by Schlumberger Tech. Co., USA). The first iteration of this mix series was created with no polystyrene beads, while the second iteration, Mix 2-2, included them to enhance the low tensile strain capacity observed in Mix 2-1.

The second series of mixes met most of the initial target criteria for the material, although further revisions were made to enhance the fresh properties. The third series of mixes was created with a higher water to cement ratio to investigate this as a way to increase the slump flow of the fresh material. Mix 3-1 and Mix 3-2 were identical, apart from the amount of polystyrene beads that were included. It was observed that the Mix 3-2 (with a smaller portion of polystyrene beads) exhibited a significant drop in 28-day tensile strain capacity over 14-day tensile strain capacity, while Mix 3-1 exhibited a slight increase. Figure 4-5 presents the tensile strain capacities at 14 and 28 days of each of the mix designs up to this point. From these mix designs, Mix 3-1 was selected as the most ideal mix and was adopted as the tailoring process continued. Mix 3-1 met all of the preliminary target strength properties as well as target cost (as shown in Table 4-1).

Following the initial stages of the material mix tailoring process, in which Mix 3-1 was selected to carry forward, further revisions were made to the mix design to achieve targets beyond the strength properties of the material (i.e. tensile strain capacity). First, revisions to the mix were made to investigate how the material could be designed in a more environmentally sustainable way. Also, since the previous mix specimens had all been cast on a vibrating table (for consolidation) efforts were made to alter the fresh properties of the materials in order to create a mix that would not require consolidation in the field. During the initial stages of the mix design, no testing was conducted to verify that the permeability of the material met the target value. Tests were conducted on the revised mix designs (in the later stages of tailoring) to investigate the hydraulic conductivity behavior of the mixes at various tensile strains. All of these revisions were made while trying not to compromise the mechanical properties of Mix 3-1.

First, efforts were made to decrease the environmental impact of the mix design, while maintaining the mechanical properties. This was approached by two components of the mix design,

the artificial flaws and the fly ash content. The polystyrene beads that were previously included as artificial flaws were replaced with Poraver® beads, which are made by extruding 100% recycled glass. This modification however resulted in a significant increase in crack size variation, and was not adopted. This increase in variation was likely due to the range in sizes of Poraver® beads that were used and replacement of the polystyrene beads with a uniformly sized Poraver® bead should still be investigated. Variations in the fly ash content of the mix were also experimented with. By increasing the fraction of fly ash, the environmental impact of the mix can be decreased and it was determined that the flash ash to cement ratio could be increased from 2.8 to 4.6, while still maintaining the previous properties.

In order to improve the fresh properties of the mix, further variations in water to cement ratio were investigated. Ultimately, a new water to cement ratio of 1.4 (increased from 0.95) was selected, to increase the slump flow of the fresh material, making it more amenable to the slurry wall construction technique.

Permeability tests were conducted on specimens made according to the new mix design, at various levels of tensile strain. Figure 4-6 presents the resulting coefficient of permeability as a function of tensile strain. As seen in the figure, the permeability of the specimens is greater than desired once the specimen is strained to 1%. This shortcoming in the mix design still needs to be addressed, however previous work on ECC materials (e.g. Lepech and Li 2008) provide confidence that the desired permeability can be met with further alterations to the mix design. Furthermore, these results to do not account for the potentially beneficial effects of autogenous healing. The current state of the mix design for the levee cutoff wall ECC material is presented in Table 4-2.

4.3 Numerical Modeling of ECC

Using the parameters for the new ECC material which were determined through laboratory testing, the unique behavior of this material had to be incorporated into the numerical model of the levee system, in order to further investigate its feasibility. Previous work done on the cyclic response of high performance fiber reinforced cementitious composites, in terms of both physical and numerical experimentation, was reviewed to select an appropriate constitutive model for the new ECC material. The following section presents a summary of the previous research conducted on modeling of HPFRCC's and a background on the model that was selected to capture the response of the ECC in the levee system analyses.

As mentioned previously, researchers have investigated the cyclic response of high performance fiber reinforced cementitious composites (HPFRCC's) like ECC, and further research has been conducted to capture their cyclic behavior in numerical models. The experimental results presented by Kesner et al (2003) were used to develop a constitutive model for nonlinear cyclic finite element analyses of structural components. The development of this constitutive model is presented by Han et al (2002) and Han et al (2003) and an overview of the model is presented below.

The constitutive model developed by Han et al was based on the co-axial total strain concept proposed by Feenstra and Rots et al (1998). This smeared crack type model is particularly convenient because it allows for the uncoupled evaluation of principle strain components, which are assumed to be aligned with the direction of cracking, as shown in Figure 4-7. In the finite element formulation, strains are updated at the beginning of each iteration in the global (*x, y*) coordinate system:

$$\varepsilon_{xy} = \varepsilon_{xy} + \Delta\varepsilon_{xy} \qquad \textit{Eq. (4-1)}$$

The strain vector is then transformed to the principal (*n, s*) coordinate system using the transformation matrix *T*:

$$\varepsilon_{ns} = T(\varphi)\varepsilon_{xy} \qquad \textit{Eq. (4-2)}$$

This strain vector is then used in the stress function *F* to compute the stresses in principal direction, which are then converted back to the global coordinate system using the transformation matrix:

$$\sigma_{ns} = F(\varepsilon_{ns}) \qquad \textit{Eq. (4-3)}$$

$$\sigma_{xy} = T^T(\varphi)\sigma_{ns} \qquad \textit{Eq. (4-4)}$$

Based on the observed cyclic behavior of HPFRCC's, the principal stresses are described as a function of the principal strain *and* the internal state variable, α, which incorporates the loading and unloading history into the model. Equation 4-3 thus becomes:

$$\sigma_{ns} = F(\varepsilon_{ns}, \alpha_{ns}) \qquad \textit{Eq. (4-5)}$$

In order to account for the Poisson's effect within the material model, the concept of equivalent strain is incorporated into this implementation. The equivalent strain, $\tilde{\varepsilon}_{ns}$, is defined as:

$$\tilde{\varepsilon}_{ns} = P\varepsilon_{ns} \qquad \textit{Eq. (4-6)}$$

where $$P = \begin{bmatrix} \frac{1}{1-v^2} & \frac{v}{1-v^2} & 0 \\ \frac{v}{1-v^2} & \frac{1}{1-v^2} & 0 \\ 0 & 0 & 1 \end{bmatrix} \qquad \textit{Eq. (4-7)}$$

The principal stress components can now be evaluated in an uncoupled manner:

$$\sigma_{n,s} = \begin{cases} \sigma_{nn} = F(\tilde{\varepsilon}_{nn}, \alpha_{nn}) \\ \sigma_{ss} = F(\tilde{\varepsilon}_{ss}, \alpha_{ss}) \\ \sigma_{ns} = 0 \end{cases} \qquad \textit{Eq. (4-8)}$$

Using the cyclic behavior of HPFRCC's observed in experiments performed by Kesner et al (2003), Han et al (2003) proposed idealized failure envelopes and loading, unloading, and

reloading relationships to model the behavior. Figure 4-8 presents an example of the experimental results of the fully reversed cyclic loading tests and Figure 4-9 presents the idealized material behavior adopted in the constitutive model. This model was able to successfully reproduce the response of a cyclically loaded cantilever type beam. The reader is referred to Han et al (2003) for the equations describing the proposed unloading and reloading behavior of the material.

In order to most accurately replicate this type of behavior within the numerical analyses of levees with ECC cutoff walls, the *Strain-Hardening/Softening Model*¸ available in FLAC, was selected to model the new ECC material. This model is an extension of the Mohr-Coulomb model that allows for the model strength parameters (cohesion, friction, dilation, and tensile strength) to be defined as functions of plastic strain (Itasca 2011). In this manner, the model can capture either hardening or softening behavior, which are both necessary to model HPFRCC's due to their tensile hardening and subsequent softening. Using this constitutive model, the new ECC material was modeled as a cohesive material by defining plastic strain-dependent functions for cohesion and tension. (Dilation and friction angles were set to zero.) Figure 4-10 presents the functions that were used to define the cohesion and tension. These functions are only used once the model experiences plastic yielding and the elastic behavior is defined by single values of the traditional Mohr-Coulomb model parameters.

In order to verify that the built-in strain-hardening/softening model was appropriate to model the ECC single element numerical tests were performed. A single element was modeled in FLAC with the constitutive model and was subject to a range of cyclic loads. The loading was arranged in such a way that made it possible to ensure that the model accurately captured several different scenarios. These included tensile loading and unloading in the elastic range, tensile loading to the strain hardening region followed by partial unloading and reloading, and tensile

loading to the softening region, followed by partial unloading. Figure 4-11 presents a stress-strain curve from a single-element test with tensile hardening, unloading and reloading. For reference, the stress-strain curve for the same loading scenario, based on the Han et al constitutive model is also shown on the figure. The strain-hardening/softening model is able to accurately capture the failure envelope, as modeled by the HPFRCC constitutive model, although it does not duplicate the unloading and reloading behavior. The strain-hardening/softening model is considered adequate for the feasibility analyses conducted in this study. Furthermore, the parameters necessary to define the unloading and reloading behavior for the new ECC material are unknown, as cyclic testing of physical specimens of this ECC mix has not yet been conducted.

Table 4-1, Mix proportions and material costs of select versions of ECC for cutoff wall applications

Component	Mix 1-1	Mix 1-2	Mix 1-3	Mix 2-1	Mix 2-2	Mix 3-1	Mix 3-2
Cement	1	1	1	1	1	1	1
Fly Ash	2.8	2.8	2.8	2.8	2.8	2.8	2.8
Polystyrene Bead	0	0.092	0.046	0	0.092	0.092	0.046
Water	0.88	0.88	0.88	0.88	0.88	0.95	0.95
Super-plasticizer	0.016	0.016	0.016	0.018	0.018	0.014	0.013
Antifoaming Agent	0	0	0	0.0076	0.0076	0.0076	0.0076
PP Fiber (by volume)	0.02	0.02	0.02	0.02	0.02	0.02	0.02
Cost per Sq. Foot*	$ 6.36	$ 9.54	$ 7.99	$ 7.04	$ 10.20	$ 9.70	$ 8.20

** Assuming a cutoff wall width of 1.5 feet*

Table 4-2, Mix proportions of most recent iteration of levee cutoff wall ECC

Component	Cement	Fly Ash	Polystyrene Bead	Water	PP Fiber (by volume)	HRWRA*
	1	4.6	0.115	1.4	2.00	0.039

**High Range Water Reducing Admixture*

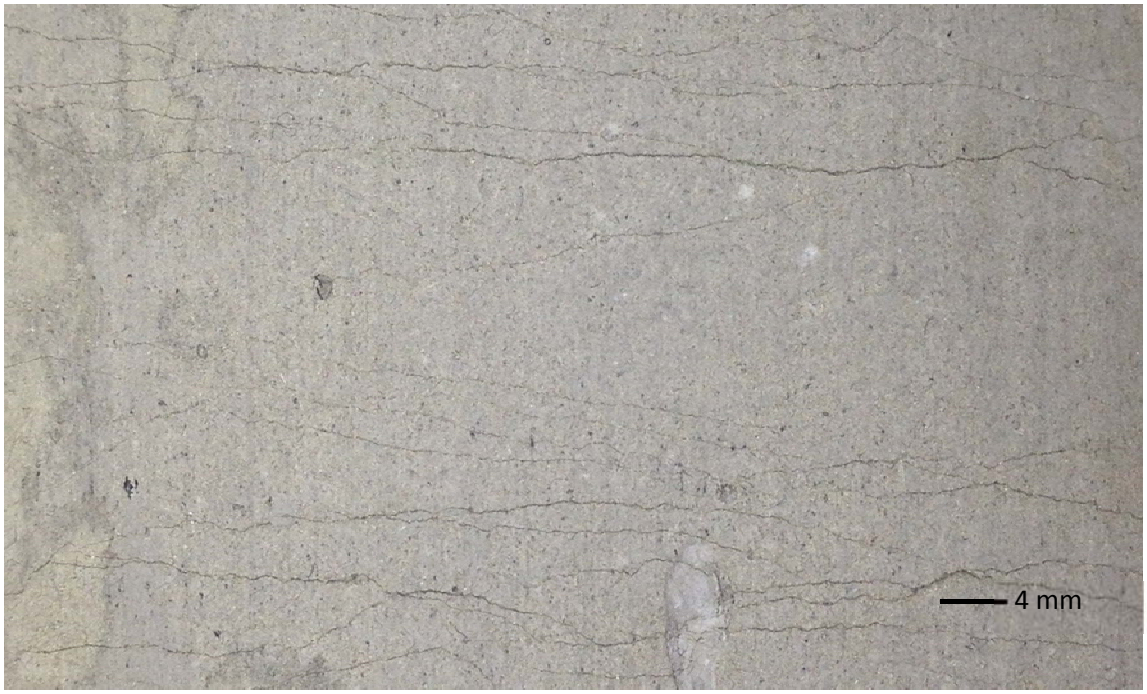

Figure 4-1, Figure of strained ECC specimen, showing multiple cracking

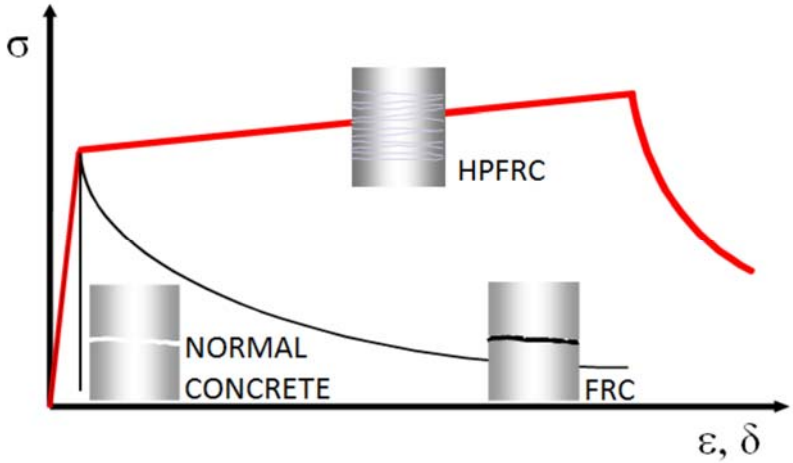

Figure 4-2, Stress-strain behavior of normal concrete, fiber reinforced concrete, and high-performance fiber reinforced concretes (Li, 2008)

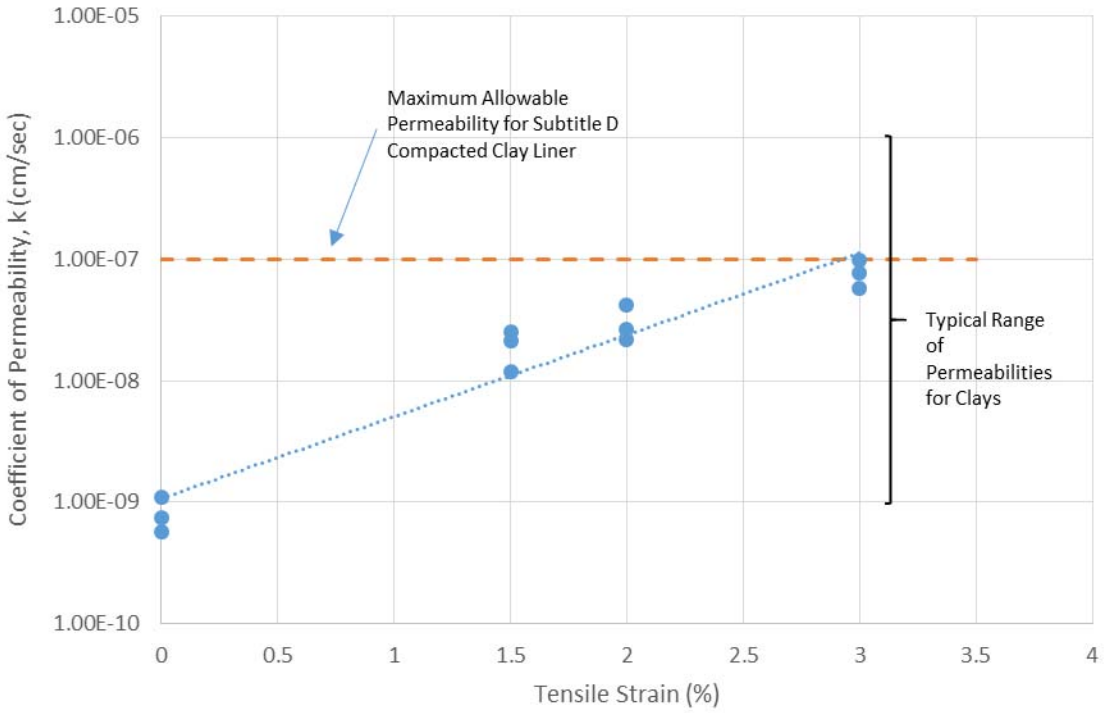

Figure 4-3, Permeability of ECC versus level of tensile strain (reproduced from Lepech and Li, 2009)

(before)

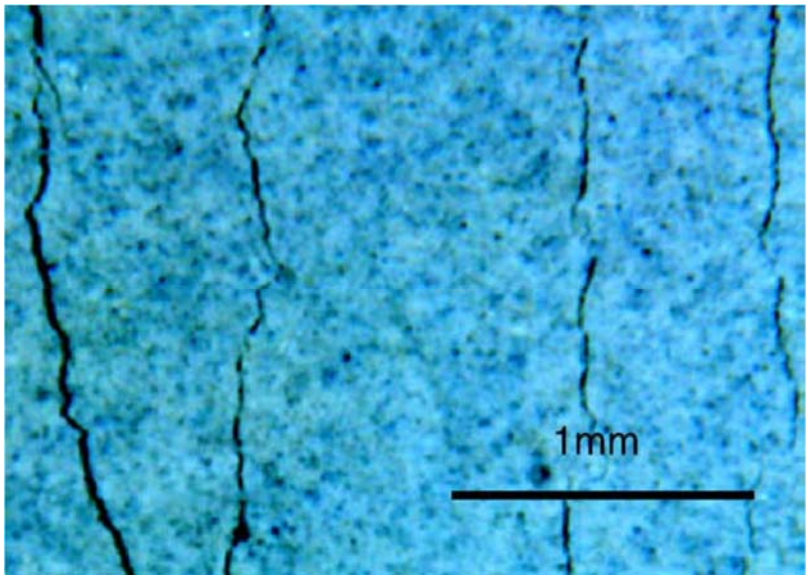

(after)

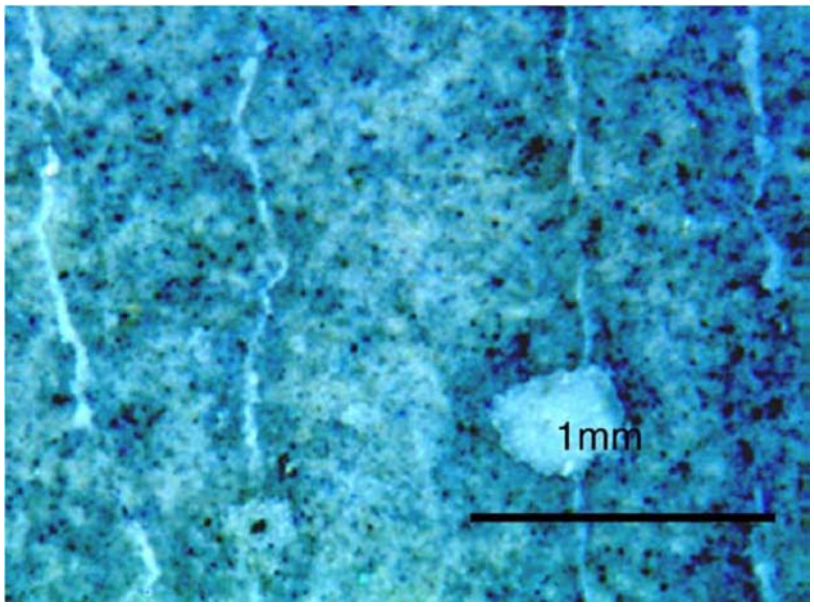

Figure 4-4, Images of ECC specimens before and after self-healing (from Yang et al 2009)

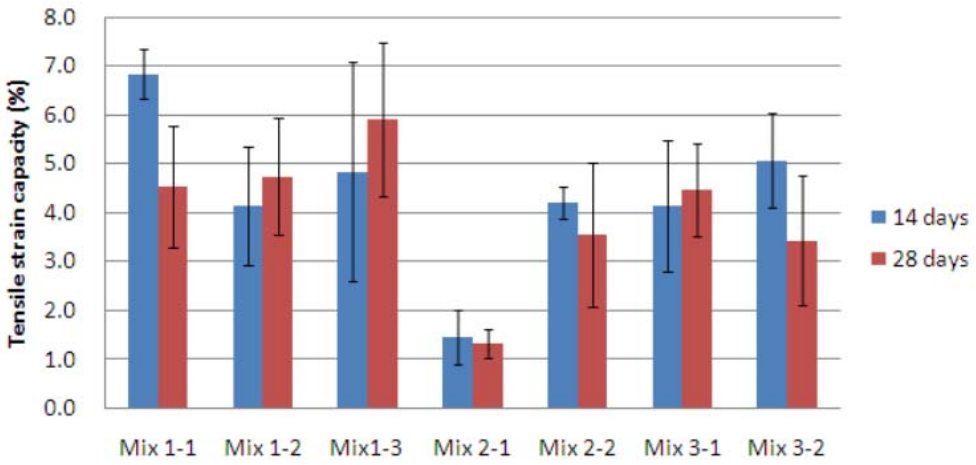

Figure 4-5, Tensile strain capacities of early cutoff wall ECC mix designs (from Lee 2011)

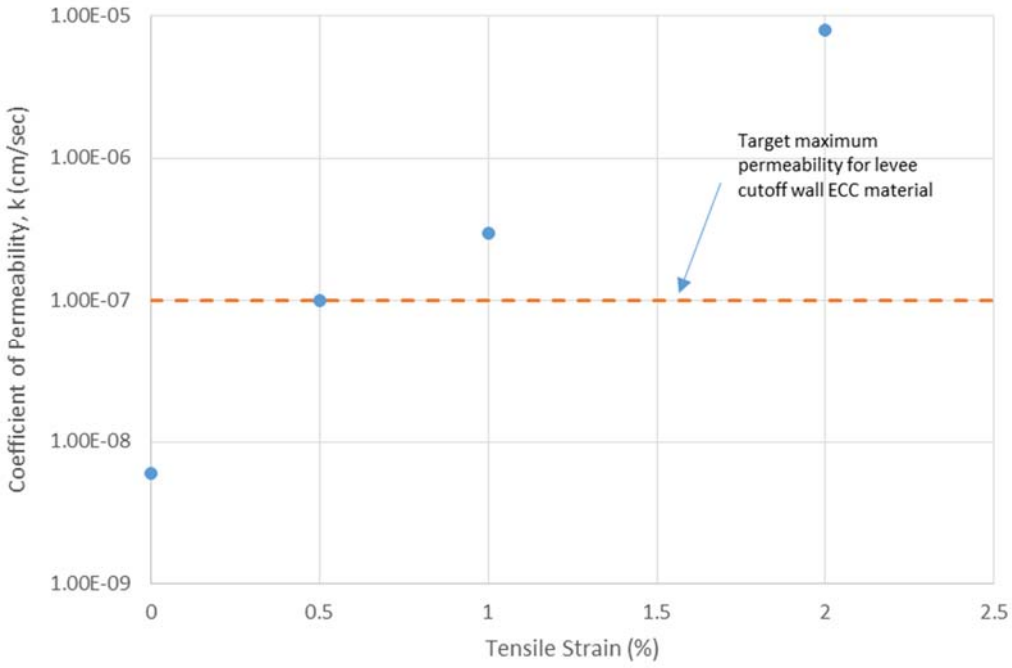

Figure 4-6, Permeability of levee cutoff wall ECC at various tensile strains

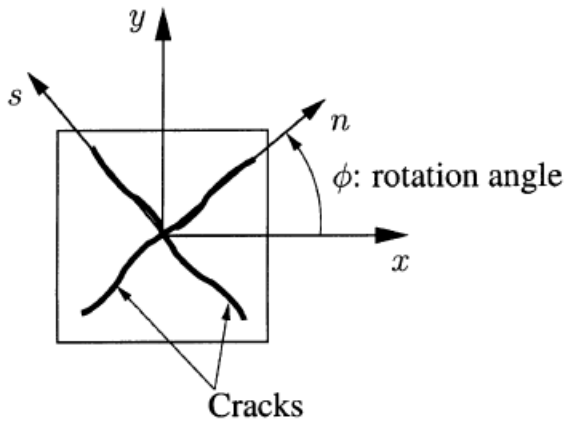

Figure 4-7, Coordinate transformation used in user defined constitutive model for ECC (from Han et al 2003)

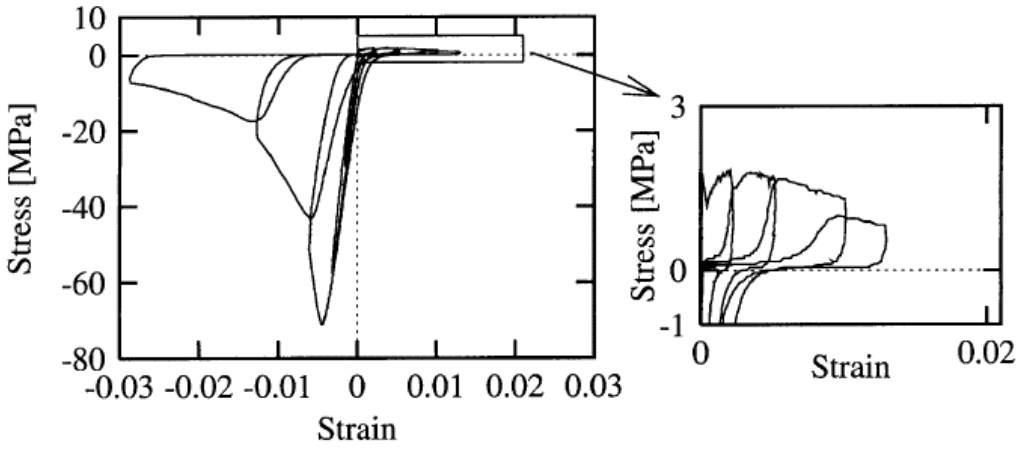

Figure 4-8, Example of fully reversed cyclic testing results for HPFRCC material (from Kesner et al 2003)

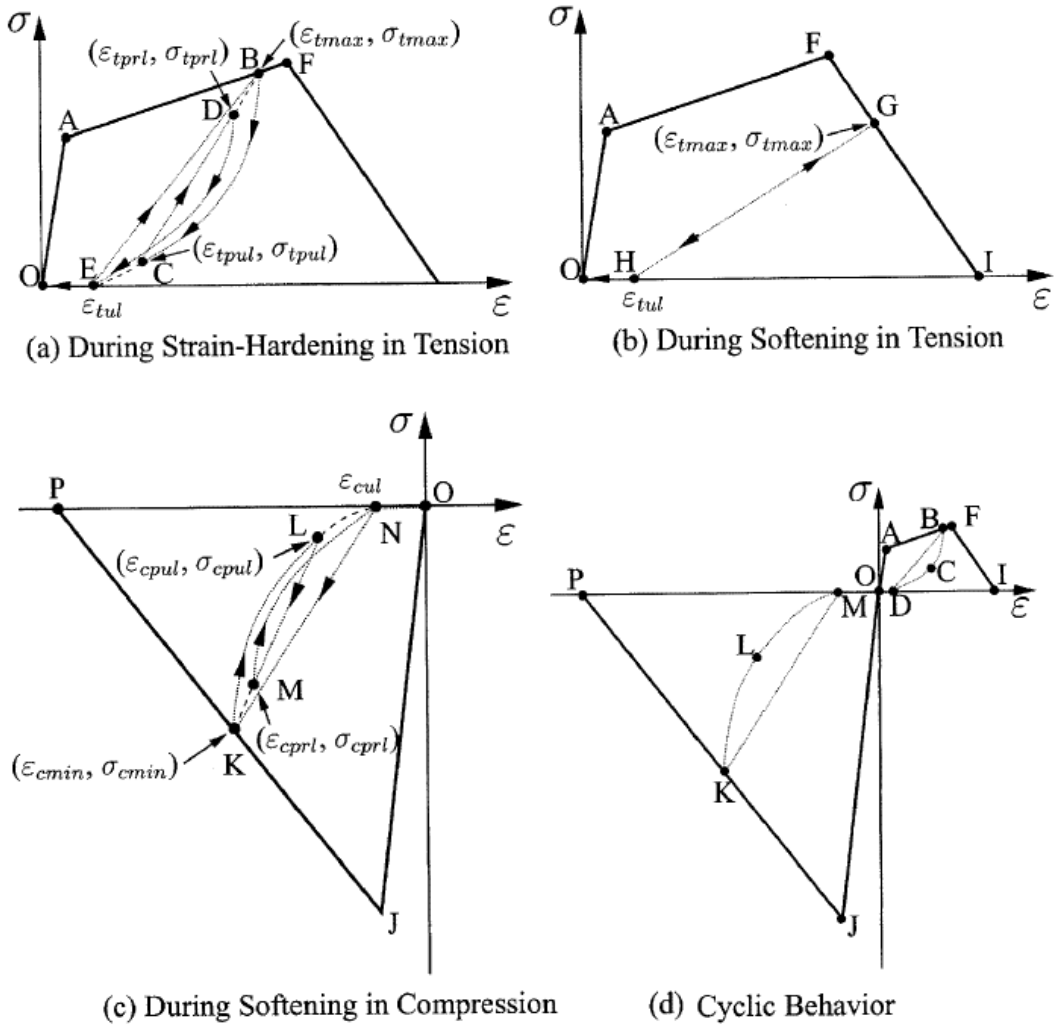

Figure 4-9, Idealized HPFRCC material behavior used in constitutive model (from Han et al 2003)

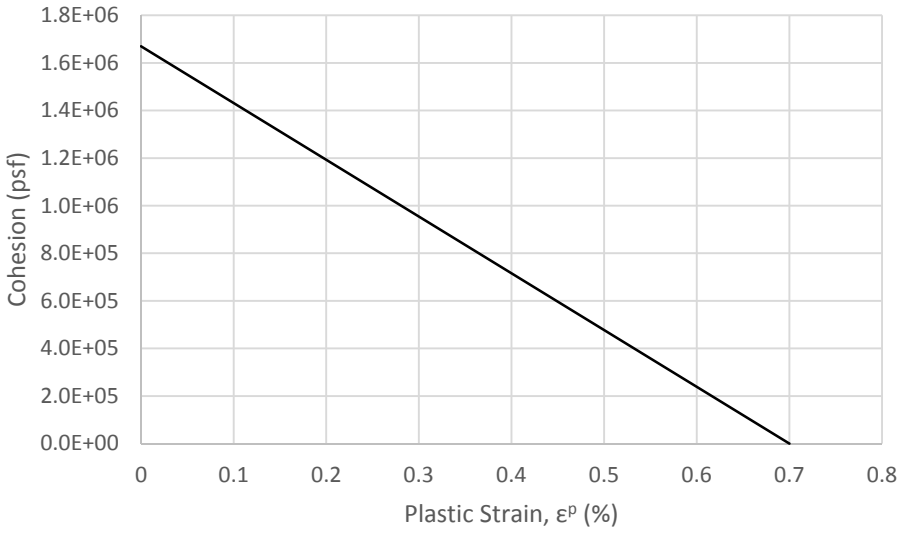

(a)

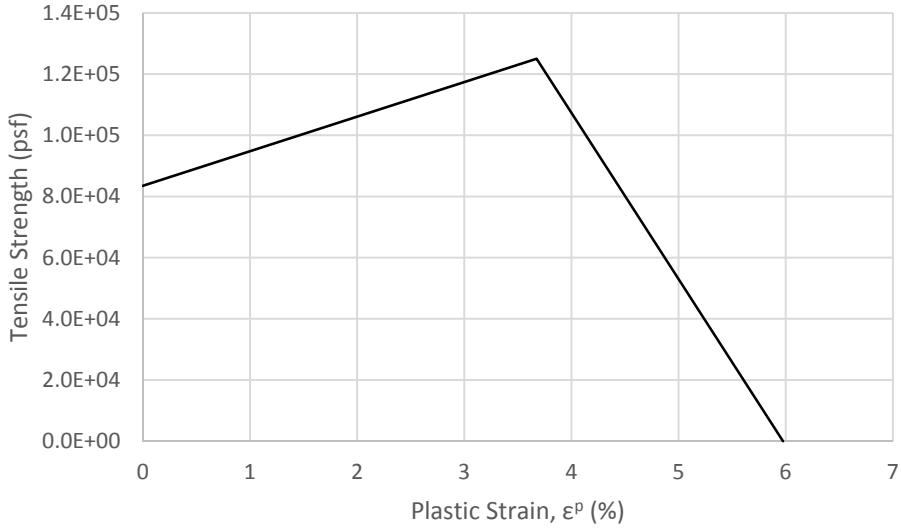

(b)

Figure 4-10, (a) Cohesion and (b) tensile strength functions for modeling ECC with strain hardening/softening constitutive model

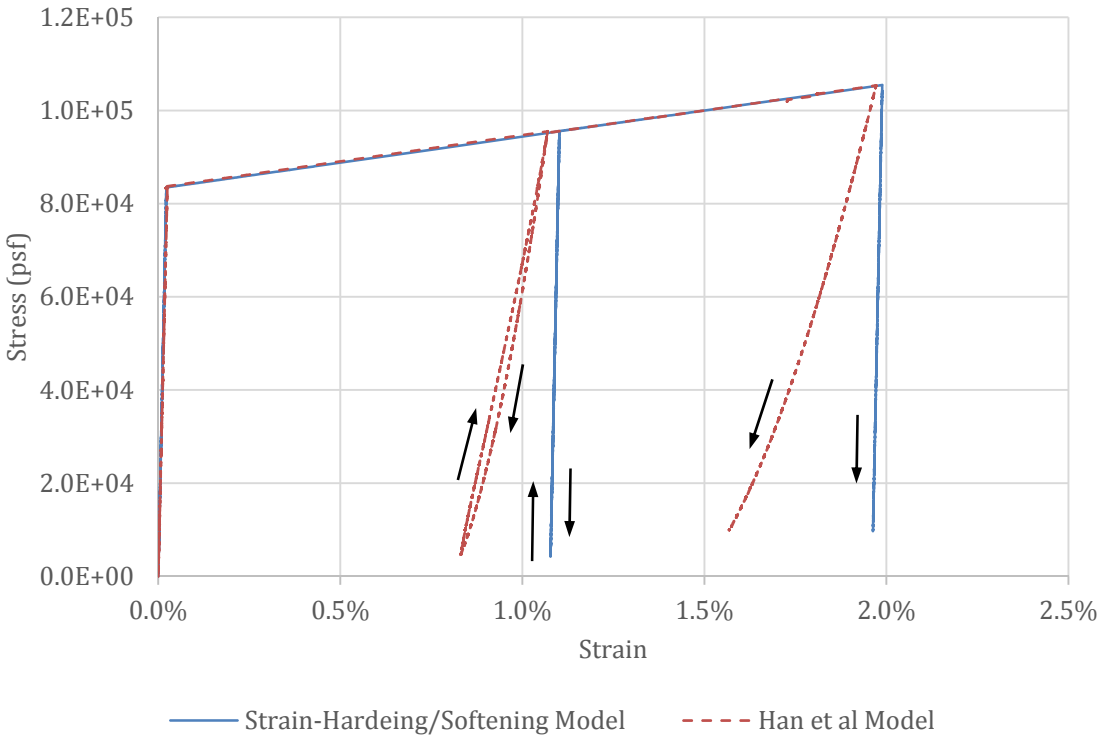

Figure 4-11, Stress strain curves for ECC using strain-hardening/softening model, subject to tensile hardening, unloading, and reloading

CHAPTER 5

Dynamic Response of ECC Levee Cutoff Walls

Having developed a candidate mix design for ECC for levee cutoff walls, the subsequent step in this feasibility study was to investigate the loading that is placed on an ECC cutoff wall during a seismic event to help further refine the ECC mix and understand the dynamic response of this type of cutoff walls. A set of numerical analyses were conducted, in which a levee was modeled with an ECC cutoff wall and was subject to earthquake shaking. The primary purpose of these analyses was to assess the adequacy of the strength parameters of the ECC mix design. These analyses also served the purpose of investigating the overall dynamic response with an ECC cutoff wall. In this chapter, details of the setup and scope of the numerical modeling are presented, followed by presentation of the analysis results.

5.1 Numerical Model and Analysis Setup

Several components of the setup for the numerical analysis of levees with ECC cutoff walls were adopted from the parametric analyses that were presented in previous chapters. An overview of the analyses is presented here, but the reader is referred to Chapters 2 and 3 for further details on certain components of the setup.

In order to investigate the behavior of an ECC cutoff wall under a range of soil conditions, three levee profiles were modeled in this analysis. For each profile, the levee had the same geometry as the previous parametric analyses, with a height of 35 feet, a crest width of 15 feet, and 3:1 (H:V) slopes. From the parametric analyses of levees founded on non-liquefiable soils, the clay profile with linearly increasing strength, Profile 3, was retained for this analysis. Both levees from the analyses of levees founded on liquefiable soils, Levee A and Levee B, were used in this analysis. Figure 5-1 presents a summary of the key parameters of each of these levees.

The cutoff wall length of 65 feet was also retained from the previous analyses. The cutoff wall was modeled using finite difference zones, with a total wall thickness of 1 foot. This thickness was selected as the likely minimum thickness that would be feasible for the given construction method. In order to model the slender wall element using finite difference zones, the finite difference grid was revised to minimize the contrast in element size between the wall and surrounding soil. Figure 5-2 shows the finite difference grid in the vicinity of the cutoff wall. The wall elements were connected to the surrounding soil elements with an unglued interface. The strain-hardening softening model available in FLAC (Itasca 2011) was used to model the ECC material. Figure 5-3 presents the tensile and compressive stress-strain curves that were used as input for the material model, based on the strength testing of the current ECC mix design. (See Chapter 4 for further details regarding modeling the behavior of ECC.)

All aspects of the initial stress state calculation and dynamic analysis setup were the same as in the previous parametric analysis. The reader is referred to Chapter 2 for details on the setup of Profile 3 and Chapter 3 for details on the setup of Levee A and Levee B. The ground motion inputs from the analyses of levees founded on liquefiable soils, NGA0728, NGA0150, and NGA0901 were also used for the analyses of levees with ECC cutoff walls.

5.2 Analysis Results

As was discussed in previous chapters, the dynamic response of levees founded on non-liquefiable soils was significantly different from the response of those founded on liquefiable soils. For this reason, the results of the analyses with ECC cutoff walls are presented separately in the following sections for levees founded on non-liquefiable and liquefiable soils.

5.2.1 ECC Cutoff Walls in Non-liquefiable Levees

For the analyses of the clay profile (Profile 3) with an ECC cutoff wall, the general response of the levee was largely the same as with a sheet pile cutoff wall. This is illustrated by the surface displacements for two of the ground motion inputs in Figure 5-4. For both of the ground motion inputs, the horizontal surface displacements are very similar for the analyses modeling an ECC cutoff wall and a sheet pile wall. The same was true for the other parameters that have been studied throughout the parametric analyses in this study. The reader is referred to Chapter 2, *Dynamic Response of Levees with Conventional Cutoff Walls* for further explanation of how the presence of a cutoff wall affects the dynamic response of a levee founded on non-liquefiable soils.

For this portion of the analyses, the results of primary interest to this study are the demands and response of the cutoff wall itself. Figure 5-5 shows contours of maximum shear strains in the ECC cutoff wall for each of the ground motion input analyses. The shear strains within the wall remained relatively low (below 0.01%) for each of the ground motions. For all three motions, the maximum strains occurred below the interface between the levee and the foundation soils, suggesting that the tip of the wall behaves in a fixed manner. Figure 5-6 presents the maximum tensile strains and associated stresses that the wall experienced during each of the ground motions.

The prescribed stress-strain curve for the material model is included for reference. For the analyses with Profile 3, the wall remained well within the elastic region of the loading curve (cracking initiates at approximately 0.025% tensile strain). These strains are however beyond the tensile strain capacity of many conventional concretes. These results suggest that, for levees founded on non-liquefiable soils, the current ECC mix design is more than adequate, in terms of tensile strength and strain capacity.

5.2.2 ECC Cutoff Walls in Levees Founded on Liquefiable Soils

In addition to Profile 3, both liquefiable soil profiles, Levee A and Levee B, were analyzed with ECC cutoff walls. As with Profile 3, the general dynamic response of the levee was very similar for an ECC cutoff wall and a sheet pile wall. Since liquefaction governs the overall response of the levee in this case, the similarity in results for the two wall types is illustrated with the liquefaction extents. Figures 5-7 and 5-8 present example comparisons of the liquefaction extents for the two wall types for Levee A and Levee B, respectively. Liquefaction extents were determined by computing the excess pore pressure ratio, R_u. UBCSAND zones with R_u values greater than 0.7 were considered liquefied. (In these figures, it appears that the upper layer (10 feet) of foundation soil is liquefied, but these zones are not modeled with UBCSAND and have excess pore pressure ratios greater than 0.7, but less than 1.0. This layer was not modeled as a liquefiable layer, and is *not* liquefied, despite the extent indicated.) For a discussion of the general aspects of the response of levees with cutoff walls founded on liquefiable soils, the reader is referred to Chapter 3, *Dynamic Response of Levees Founded on Liquefiable Soils with Conventional Cutoff Walls.*

As was observed for the analyses of levees founded on liquefiable soils with steel sheet pile cutoff walls, liquefaction resulted in significantly higher demands on the ECC wall. Figure 5-9 shows contours of maximum tensile strains within the ECC cutoff wall for the Levee A analyses. Figure 5-10 presents the same for the Levee B analyses. With all three input motions for Levee A, the maximum tensile strains occur near the midpoint of the wall length and are of similar magnitude. For Levee A, none of the soils liquefied in the region beneath the levee, so the wall remained in a fixed condition at depth. The location of the maximum strain suggests that relative movement between the levee and the foundation soils are the main cause of the wall demand. For Levee B, however, the tensile strains are higher in magnitude (by roughly on order) and occur closer to the tip of the cutoff wall. This is most pronounced for input motions NGA0728 and NGA0901, for which the uppermost layers of foundation soils liquefied beneath the entire width of the levee. The shift in the location of highest wall demand is a result of the soil liquefaction below the levee, but not all the way to the wall tip, allowing for some fixity. It is also important to observe here that, although input motion NGA0901 has a greater liquefaction extent than input motion NGA0728, the strains are highest for input motion NGA0728. This again illustrates that the greatest demands are placed on the cutoff wall for 'intermediate' liquefaction, as opposed to the most extensive liquefaction.

The maximum cutoff wall tensile strains observed for the levees founded on liquefiable soils are well in excess of the tensile elastic region of ECC. Figure 5-11 presents the maximum tensile strains for each input motion for all three levees (both liquefiable and non-liquefiable) and the associated stress. The stresses and strains are plotted against the tensile stress-strain curve for the current ECC mix design, for reference. For all of the liquefiable profiles, the cutoff wall entered the tensile-hardening portion of the response, although none entered the strain-softening behavior.

In order to assess the adequacy of the current mix design, it is also important to consider the wall demands in the context of the overall performance of the levee. Figure 5-12 presents the maximum cutoff wall tensile strains versus the maximum vertical crest displacement resulting from the same input motion. The purpose of this figure is to illustrate that even though the tensile strains for some of the analyses are approaching the strain-softening region, it would not likely be worthwhile to tailor the ECC mix for a higher tensile strain capacity. These high wall demands only occur for extremely large levee displacements, at which point the cutoff wall no longer serves its intended purpose, since the levee has already failed and would require extensive repairs, regardless of the wall.

5.3 Conclusions of Analyses of Dynamic Response of ECC Levee Cutoff Walls

Finite difference numerical analyses were performed to investigate the response of an ECC cutoff wall embedded in an earthen levee, subject to ground shaking. Three levee profiles, founded on both non-liquefiable and liquefiable soils were analyzed using a selection of recorded ground motion inputs.

The primary purpose of these analyses was to assess the adequacy of the current ECC mix design in terms of strength demands. The following observations were made:

- In levees founded on non-liquefiable soils, the ECC cutoff wall experienced maximum tensile strains well within the elastic region of the material response.
- Significantly higher maximum tensile strains were observed for levees founded on liquefiable soils. The cutoff wall experienced tensile strains that entered the strain-

hardening region of the material response, although strain-softening behavior was not observed.

- The results of these analyses suggest that the current ECC mix design would indeed be adequate, in terms of strength capabilities, for use as a levee cutoff wall material. The broad separation of wall demands between the levees founded on liquefiable and non-liquefiable soils raises the potential option of proposing two separate mix designs. A mix design with lower tensile cracking strain and tensile strain capacity could perhaps be tailored and recommended for levees founded on non-liquefiable soils while the current mix design can be recommended for levees founded on liquefiable soils. Additional validation of the results and these recommendations is needed through some type of physical modeling of levees with ECC cutoff walls (e.g. centrifuge testing, shake table testing, etc.)

In addition to the observations regarding the demands of the ECC cutoff wall, the analyses also provide information about the dynamic response of levees with cutoff walls. The overall response of the levee was observed to be largely the same for levees with an ECC cutoff wall and levees with a steel sheet pile cutoff wall.

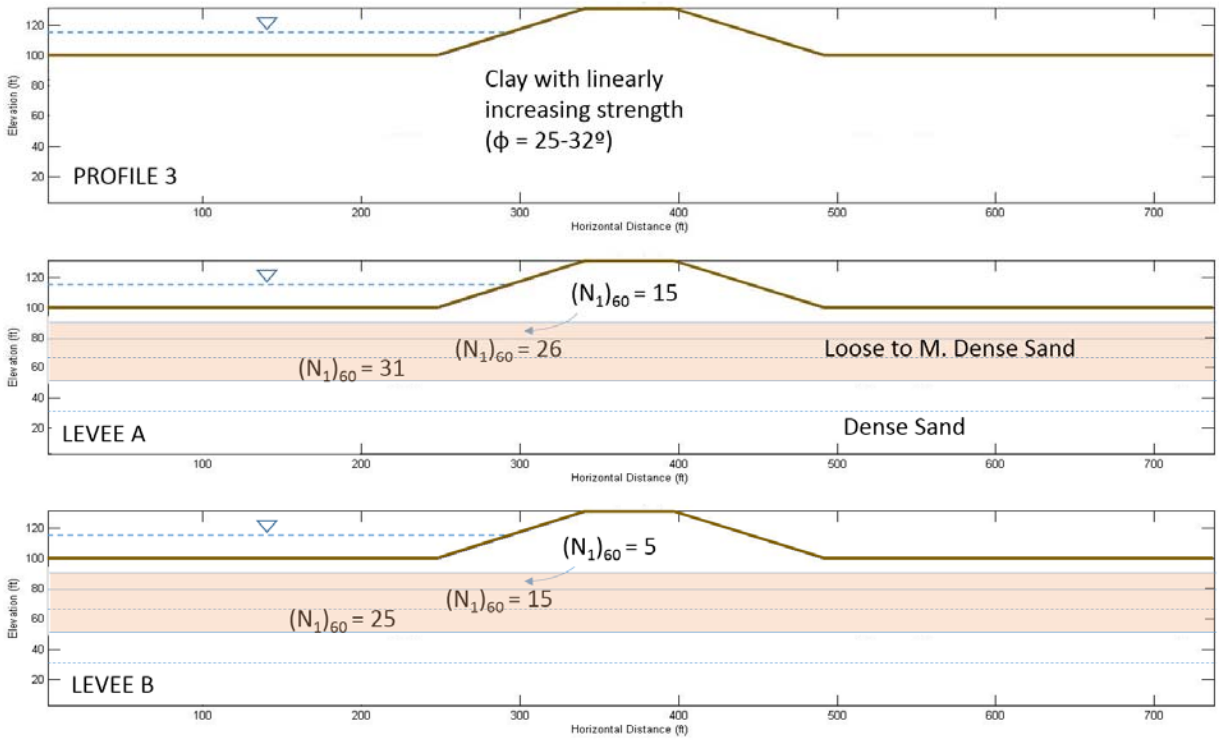

Figure 5-1, Levee profiles analyzed with ECC cutoff walls

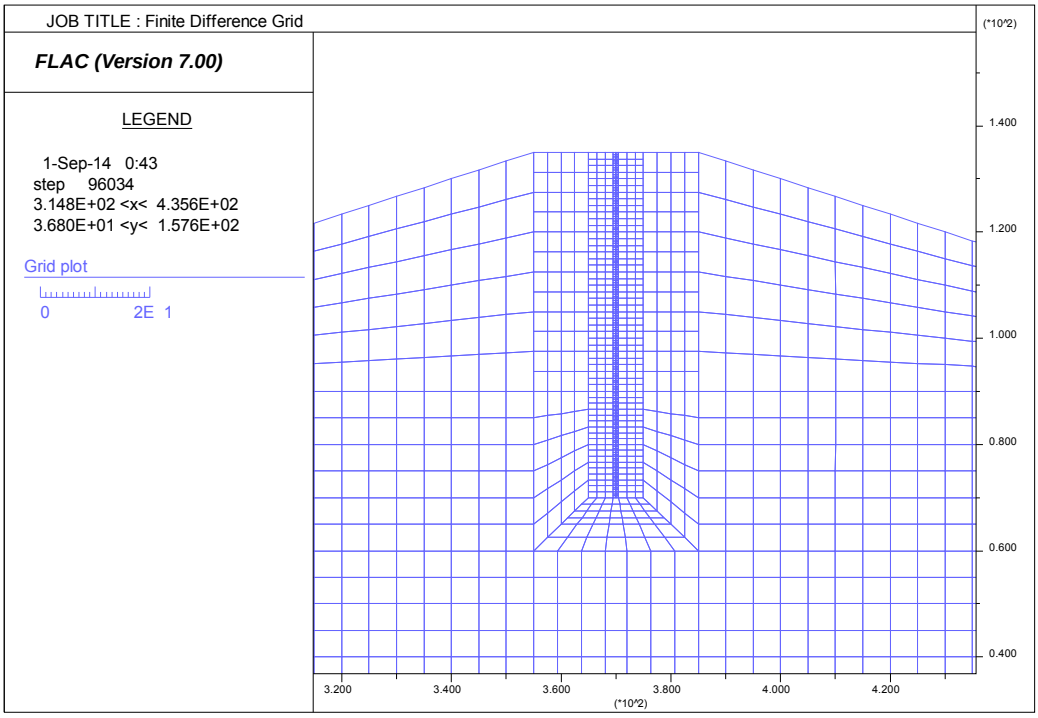

Figure 5-2, Finite difference grid used to model levee with ECC cutoff wall

(a)

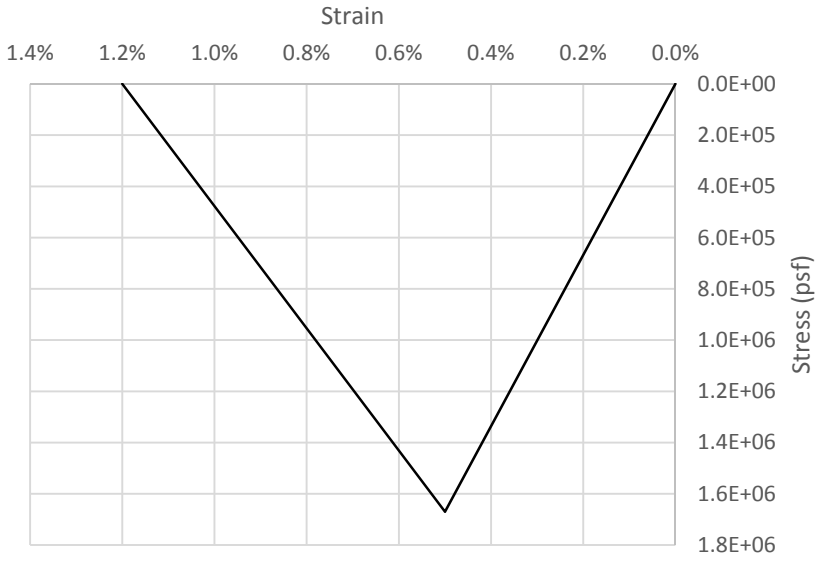

(b)

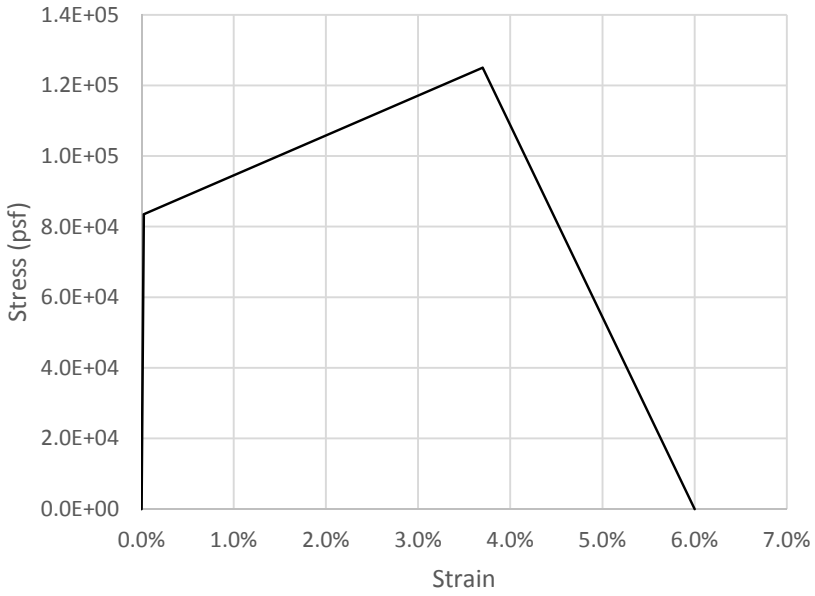

Figure 5-3, Stress-strain curves used to model ECC (a) compressive behavior and (b) tensile behavior

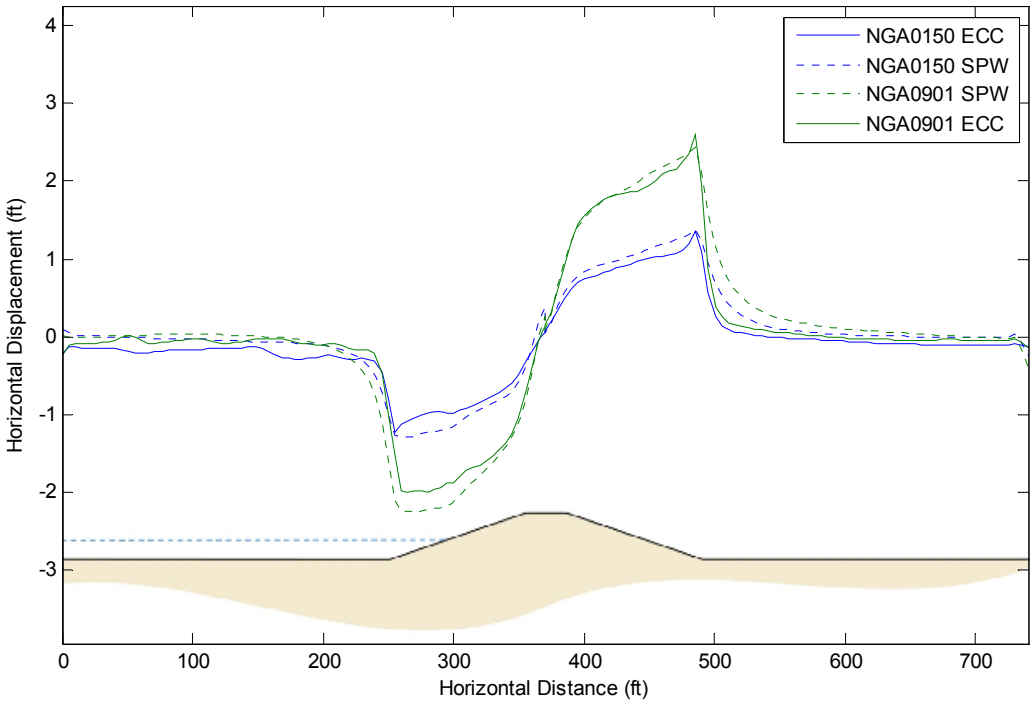

Figure 5-4, Comparison of horizontal surface displacements for Profile 3 with sheet pile cutoff wall and ECC cutoff wall

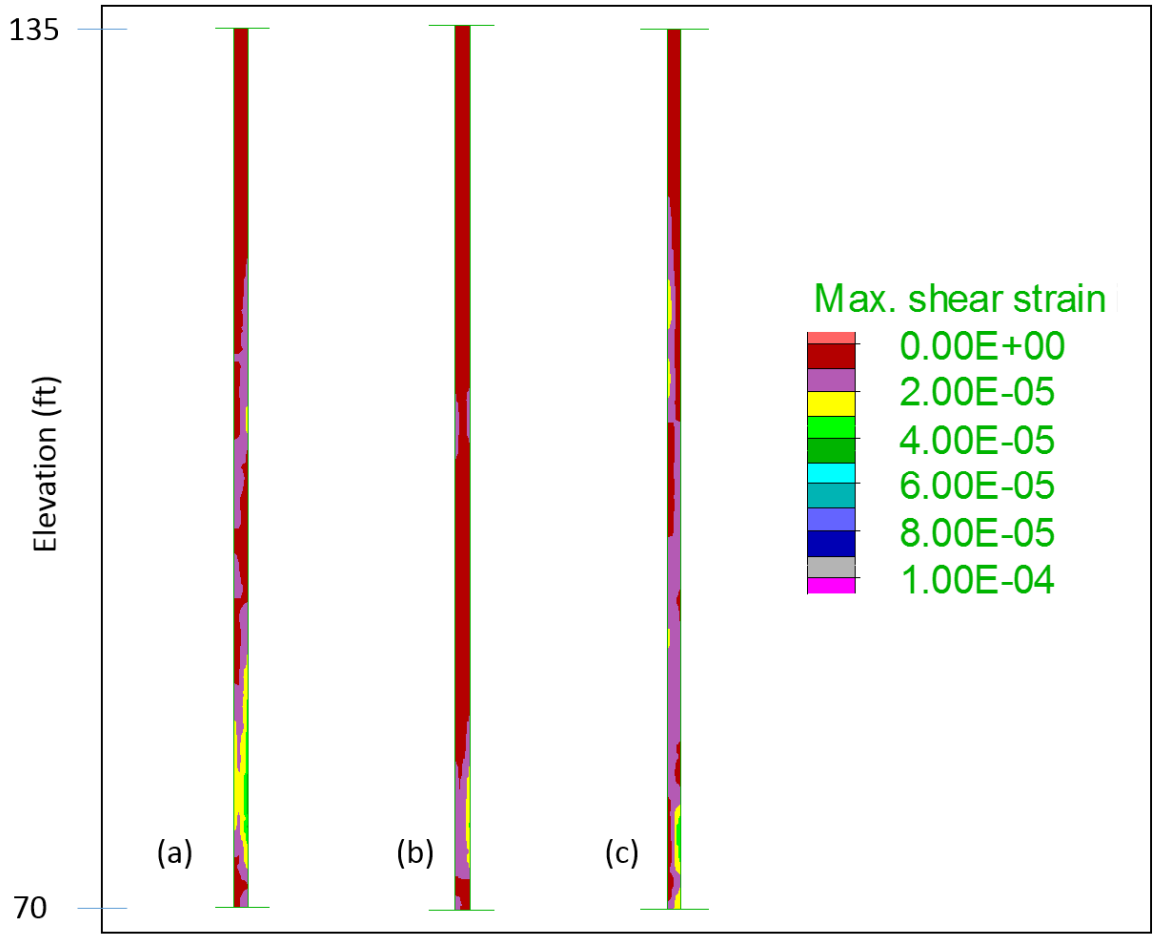

Figure 5-5, Contours of maximum shear strain within the cutoff wall in Profile 3 analyses for input motion (a) NGA0728, (b) NGA0150, and (c) NGA0901

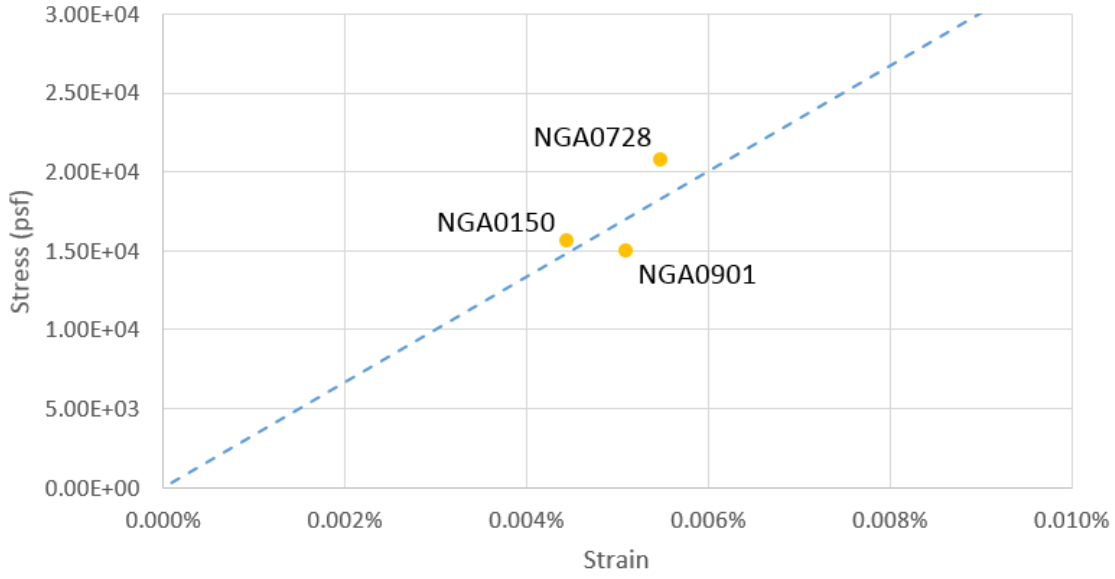

Figure 5-6, Maximum ECC cutoff wall tensile strains and associated stresses for Profile 3 with various input motions.

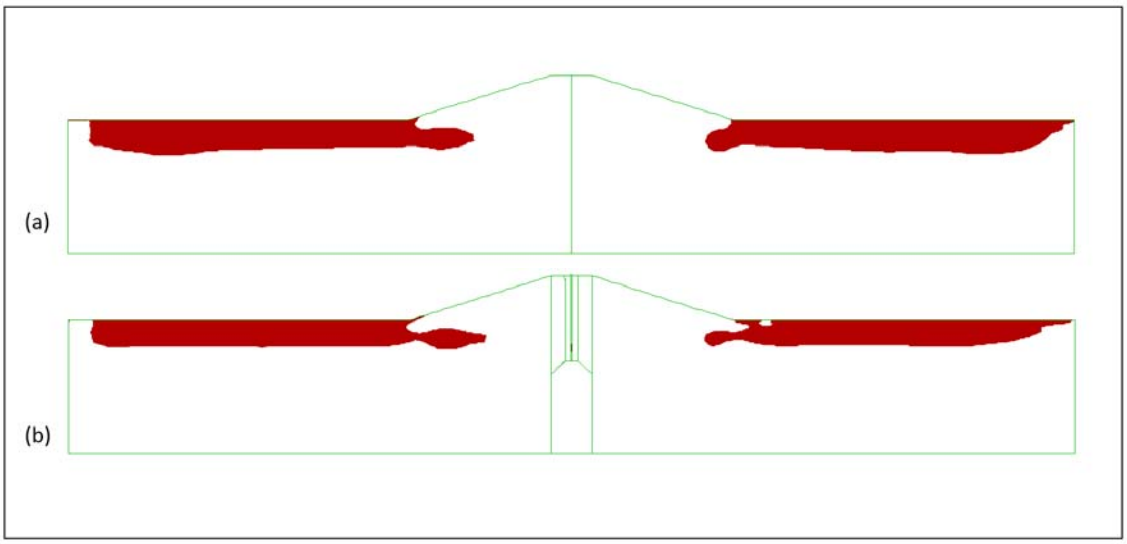

Figure 5-7, Liquefaction extents for Levee A with input motion NGA0150 with (a) a sheet pile cutoff wall and (b) an ECC cutoff wall

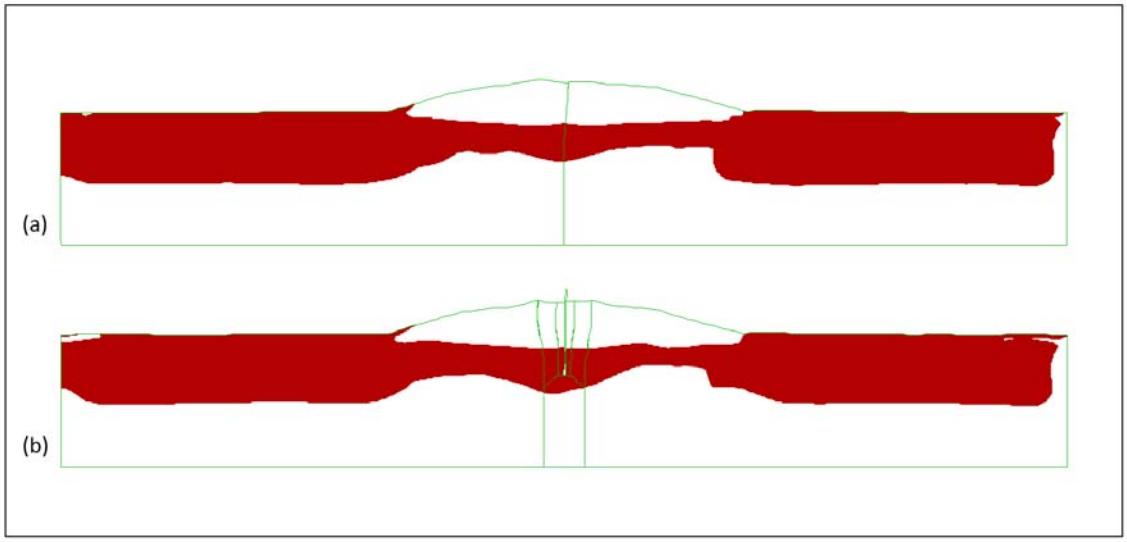

Figure 5-8, Liquefaction extents for Levee B with input motion NGA0901 with (a) a sheet pile cutoff wall and (b) an ECC cutoff wall

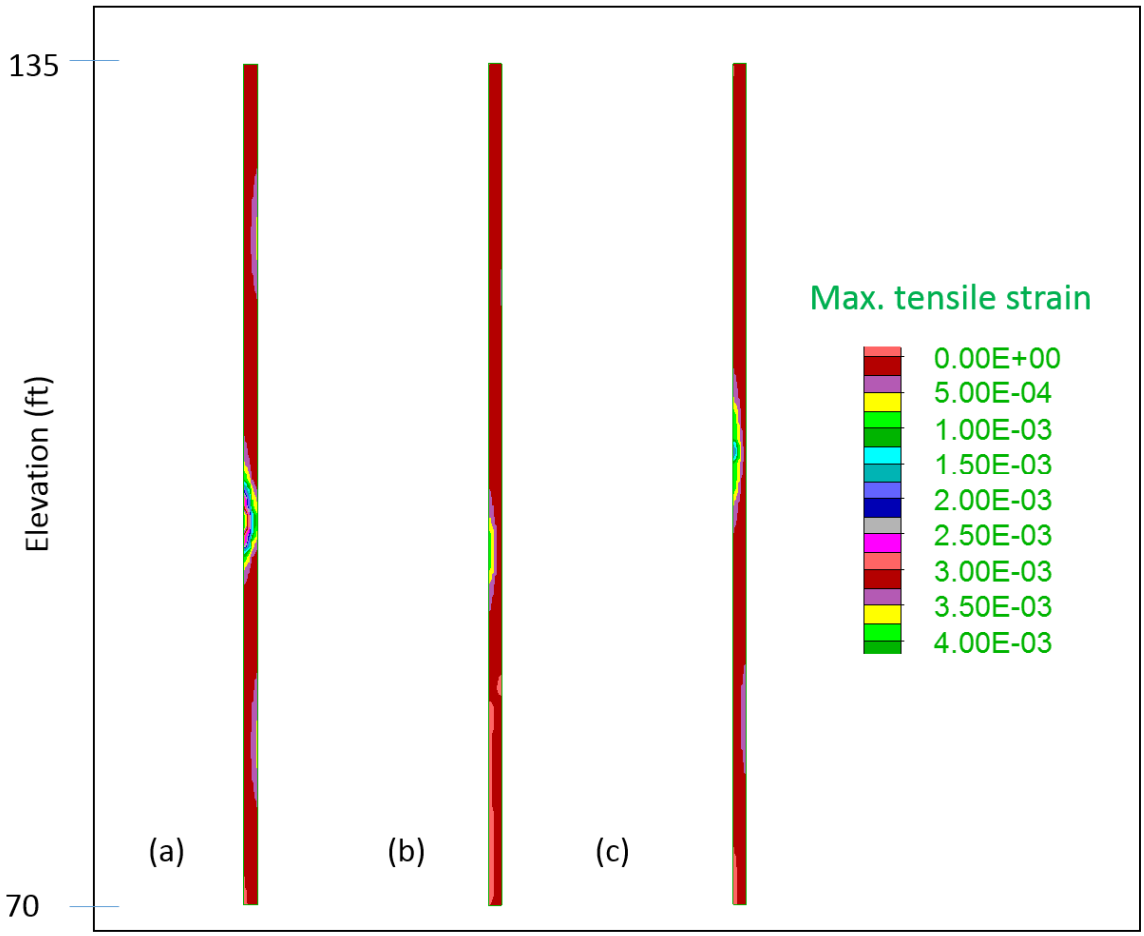

Figure 5-9, Contours of maximum tensile strain within the cutoff wall in Levee A analyses for input motion (a) NGA0728, (b) NGA0150, and (c) NGA0901

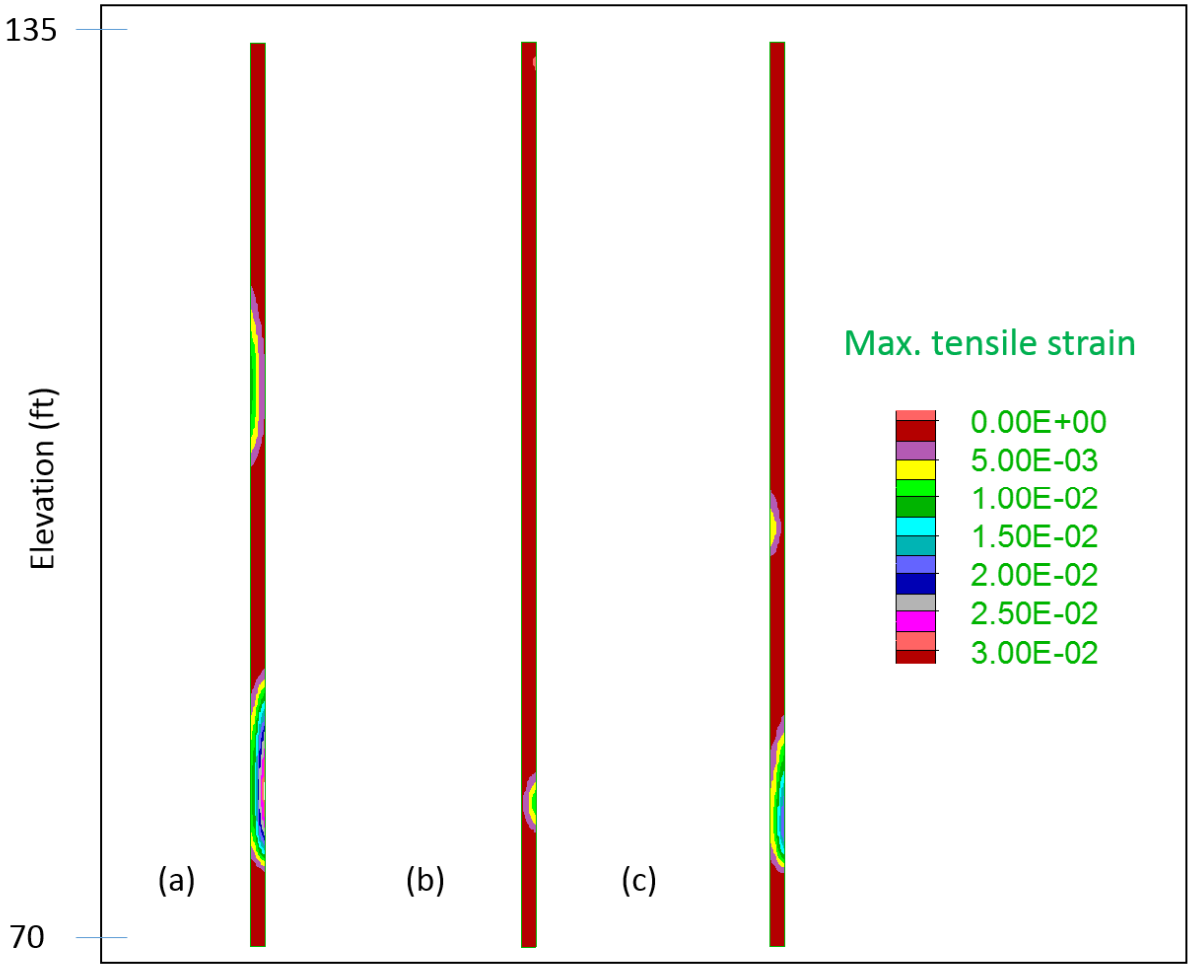

Figure 5-10, Contours of maximum tensile strain within the cutoff wall in Levee B analyses for input motion (a) NGA0728, (b) NGA0150, and (c) NGA0901

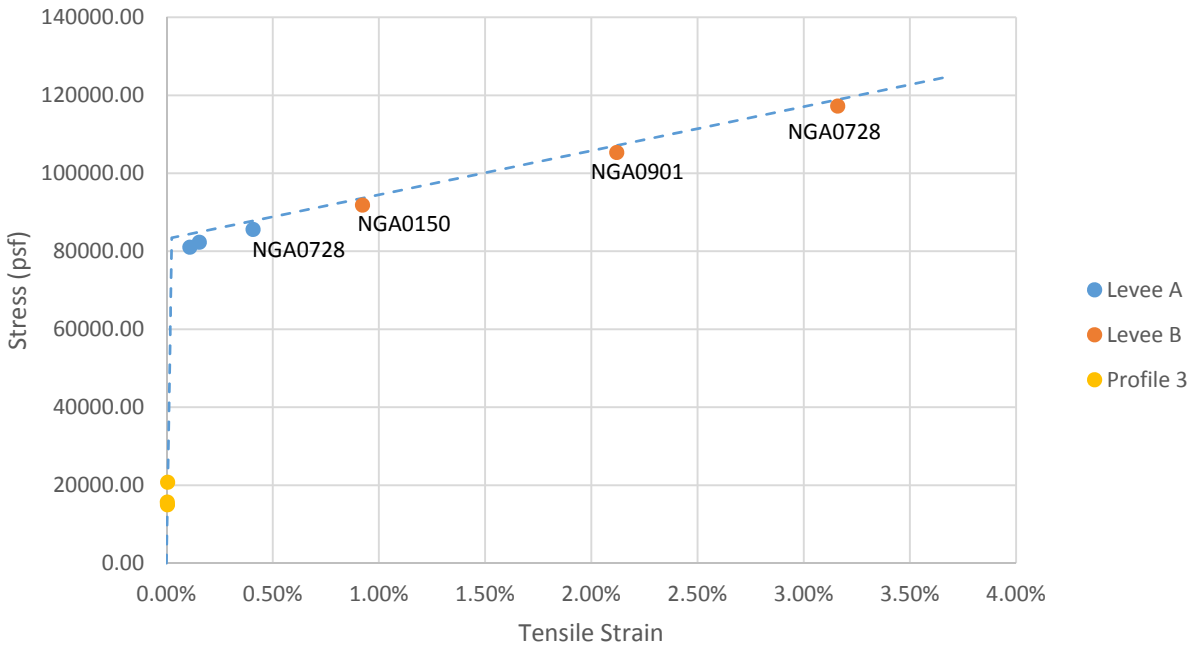

Figure 5-11, Maximum ECC cutoff wall tensile strains and associated stresses for Levee A, Levee B, and Profile 3 with various input motions.

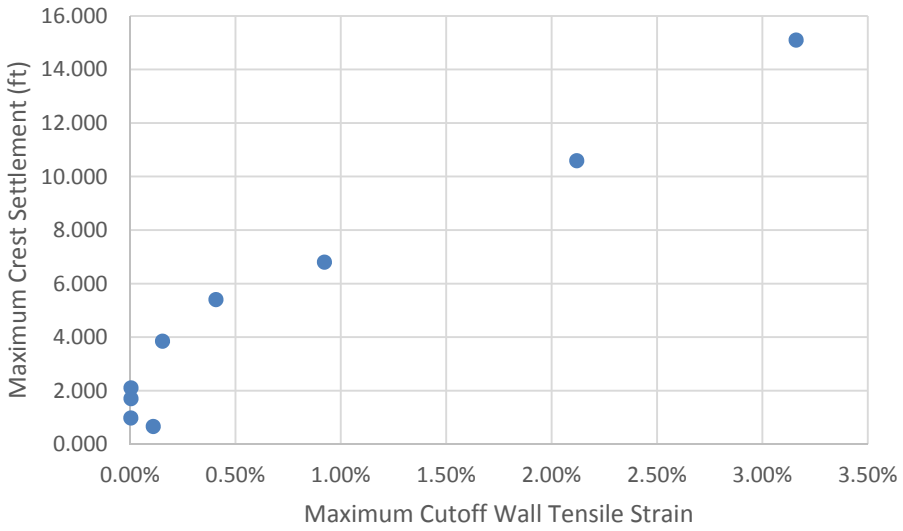

Figure 5-12, Maximum levee crest settlement versus maximum ECC cutoff wall tensile strain

CHAPTER 6

Conclusions

Flood protection systems are a vital component of our nation's infrastructure and recent natural disasters, as well as recent investigations, have shown that many of our levees are at risk. Cutoff walls are a key component for mitigating under- and through-seepage in levees, but many are inadequate in their current state. Furthermore, seismic hazards pose a serious threat to levees and conventional cutoff walls are not well suited to withstand seismic activity. In an effort to address the need for more advanced cutoff wall materials for levees in seismic regions, a feasibility study was conducted to investigate the use of an engineering cementitious composite (ECC) as a levee cutoff wall material. The initial portion of this study focused on characterizing the dynamic response of levees with conventional cutoff walls. Two sets of numerical modeling parametric analyses were conducted to investigate how the presence of a cutoff wall affects the dynamic response of a levee and what type of demands are placed on the cutoff wall during the seismic event. One set of analyses was for levees founded on non-liquefiable soils and the other was for levees founded on liquefiable soils. In collaboration with materials science researchers, an ECC material was then tailored for use in the construction of levee cutoff walls. The results of materials testing on the resulting candidate mix design were then used as input in further numerical

modeling, in which the dynamic response of levees with ECC cutoff walls was investigated. This numerical model was used to assess the feasibility of the candidate mix design. The following sections present the key conclusions of this study and recommendations for future research.

6.1 Conclusions

This study yielded several conclusions, both with respect to the feasibility of using the proposed material in levee cutoff walls, as well concerning the dynamic response of levees with cutoff walls. The main conclusion, addressing the primary focus of this study, is that ECC is a feasible material option for high performance cutoff walls for levees in seismic regions. Table 6-1 presents a summary of the key aspects of the final candidate mix design. The results of the numerical modeling indicate that the structural demands placed on an ECC levee cutoff wall by an expected range of seismic events are within the capacity of the proposed material. The proposed mix design has also been shown to be feasible in terms of economics and constructability, with a material cost well within the target cost and fresh properties consistent with other materials that are implemented using the slurry construction method. In addition, the tailoring process also showed that the environmental impact of the material can be decreased with a variety of mix alterations.

Table 6-1, Levee cutoff wall ECC mix proportions, strength parameters, and cost

Mix proportions	
Cement	1
Fly Ash	4.6
Polystyrene Bead	0.115
Water	1.4
Polypropylene Fiber (by volume)	2.00
Water Reducing Admixture	0.039
Strength Parameters	
Tensile Cracking Strain	0.025%
Tensile Cracking Stress	4.0 MPa
Peak Tensile Strain	3.7%
Peak Tensile Stress	5.99 MPa
Material Cost	
$ 6.47 per square foot of wall (1 foot thickness)	

In addition to demonstrating the feasibility of ECC as a cutoff wall material, this study has also resulted in findings related to the dynamic response of levees with cutoff walls. These are listed below, separately for levees founded on non-liquefiable soils and levees founded on liquefiable soils:

Levees founded on non-liquefiable soils

- Based on the results of the parametric analysis, the presence of an embedded cutoff wall does alter the dynamic response of a levee, as compared to a levee without a cutoff wall. Shear strain contours indicate that the wall results in a change in the geometry of the dynamic failure surface, by forcing the entry point of the landside failure surface to the landside of the levee crest centerline.

- Comparison of the analyses performed using simplified dynamic inputs with the analyses for actual ground motion recordings indicated that Ricker wavelet pulses and simple sinusoidal inputs are very good indicators of trends and behaviors observed for actual earthquakes.

- The ratio of vertical to horizontal slope displacement was observed to deviate significantly from the commonly assumed value of 0.7 and was observed to by systematically different for levees with and without cutoff walls. For analyses of clay profiles with Ricker wavelet inputs, the ratio was observed to vary between 0.25 and 1.2. The ratio was consistently lower (by approximately 0.1) for levees with sheet pile cutoff walls, as opposed to levees with no cutoff wall. The average value of the ratio for levees with no cutoff wall ranged between 0.7 and 0.9 and the average value of the ratio for levees with a steel sheet pile cutoff wall ranged between 0.6 and 0.8.

- Comparison of horizontal slope displacements for ground motion recording inputs with simplified relationships for Newmark-type displacements (Shewbridge et al 2009) indicate that the simplified relationship tends to overestimate displacements for levees with cutoff walls. The overestimation was observed to be as greater as 80%. Very little difference (less than 5%) was observed in horizontal displacements between levees with steel sheet pile cutoff walls and levees with soil cement bentonite cutoff walls.

- Levee crest settlements (as percentages of combined levee height and foundation thickness) computed for analyses of clay profiles with Ricker wavelet inputs, agreed very well with case history data presented by Swaisgood (2003). For levees with steel sheet pile cutoff walls, computed crest settlements were consistently between 10% and 20% lower than for levees with no cutoff wall. When compared to the regression equation presented by

Swaisgood (2003) for crest settlement as a function of PGA and earthquake magnitude, the presence of a cutoff wall results in a decrease in crest settlement roughly equivalent to the decrease in settlement due to a decrease in earthquake magnitude of approximately 0.3.

- Input frequency was observed to have a significant effect on crest settlements, with lower frequencies resulting in higher settlements. For a given input PGA a change in frequency from 5 Hz to 1 Hz resulted in an increase in crest settlement by more than 1 order of magnitude. For a given Arias Intensity, a change in frequency from 5 Hz to 1 Hz resulted in an increase in crest settlement by approximately 1 order of magnitude (e.g 16 cm to 160 cm).
- It was observed that the earth pressures on deep portions of the cutoff wall behave similarly to what has been observed for braced retaining structures. However, at shallower locations, particularly within the levee itself, the wall pressures were strongly influenced by adjacent levee slope movements. A simple monotonically increasing lateral earth pressure profile is not adequate to characterize the dynamic wall pressures, as this was seen to under-predict lateral earth pressures at shallow locations, by as much as approximately 100%.

Levees founded on liquefiable soils

- The effect of the presence of a cutoff wall on the dynamic displacements of a levee was seen to vary, depending on the foundation soils. For Levee A (the denser of the two levees), no systematic difference was observed in horizontal displacements between levees with and without cutoff walls. The difference in horizontal displacements (normalized by displacements for a levee with no wall) between the two cases ranged from -10% to 10%

and averaged approximately 0%. For Levee B, the presence of a wall was seen to result in a reduction in horizontal displacements by 15% on average, but as high as 32%.

- Similar behavior was observed for vertical crest displacements. For Levee A, there was little difference between levees with and with cutoff walls. The difference ranged from -8% to 11%, with an average of approximately 2%. For Levee B, however, the presence of a cutoff wall resulted in a reduction of vertical displacements of 15%, on average.
- No consistent difference was observed for the ratio of vertical to horizontal displacements for levees with and without cutoff walls. However, the value of the ratio was observed to range between 0.45 and 1.0 and varied for different numbers of cycles of loading, although it converged to 0.7 for input motions with greater than 9 cycles of loading. For Levee A, the ratio was seen to range between 0.45 and 0.7 and increased as the number of cycles of loading increased. For Levee B, the ratio ranged between 0.65 and 1.0 and decreased as the number of cycles of loading increased.
- The results of the analyses conducted in this study indicate that the presence of a cutoff wall does affect the triggering of liquefaction in the soils beneath the levee, resulting in more liquefaction than for levees with no cutoff walls. The portion of liquefiable soil that experienced liquefaction (as indicated by values of excess pore pressure ratio) was seen to increase by as much as 35% upon inclusion of a cutoff wall. The increase in liquefaction due to the presence of a cutoff wall was more prominent for Levee A (denser) than for Levee B. This increase in liquefaction is likely the result of two factors: 1) the presence of the cutoff wall results in a change in the initial static stress state within the levee, which results in a reduction in cyclic resistance, and 2) the presence of the cutoff wall may hinder dissipation of excess pore pressures generated during shaking.

- With regard to the structural demands placed on the cutoff wall during and after shaking, it was observed that the worst-case scenario occurs for cased of intermediate liquefaction (in the context of this study). The greatest cutoff wall demands were observed when only portions of the soil beneath the levee liquefied, as opposed to cases with very widespread liquefaction beneath the levee.

6.2 Recommendations for Future Research

Through the course of this feasibility study, several items have been revealed which warrant further study. Recommendations for further development of the proposed ECC material, as well as recommendations for further research on the dynamic response of levees with cutoff walls, are presented here.

6.2.1 Recommendations for Further Development of Levee Cutoff Wall ECC

- As described in Chapter 4, ECC specimens that were strained beyond 1% tensile strain exhibited permeability that was greater than the desired minimum for cutoff wall applications. This shortcoming in the current mix design should be remedied before proceeding with the levee cutoff wall ECC.
- The numerical modeling of levees founded on non-liquefiable soils with ECC cutoff walls indicated that the ECC did not experience strains beyond the elastic region of the material. The ECC walls in levees founded on liquefiable soils however did. Therefore it may be advantageous to tailor a separate grade of levee cutoff wall ECC for levees founded on non-liquefiable soils, and reduce the material cost and environmental impact.

- Previous studies have shown that vegetation and burrowing animals are potentially very destructive to slurry type cutoff walls. Investigation into how vegetation and plant roots interact with cracked ECC would be valuable. Also, coatings used to protect cutoff walls from burrowing animals should be tested on ECC.
- Several assumptions were made regarding the cyclic behavior of the ECC, based on previous studies of cyclic behavior of other high performance fiber reinforced cementitious composites. However, for this feasibility study, no cyclic testing was conducted as part of the material tailoring process. Cyclic material testing should be conducted to verify the assumptions made regarding the behavior of ECC under fully reversed cyclic loading. Once cyclic testing has been conducted, numerical modeling should be repeated, using a constitutive model that captures the observed cyclic behavior.
- The feasibility study presented here has relied solely on numerical modeling to investigate the response of the ECC cutoff wall. Physical testing, such as shake table testing or centrifuge testing, should be conducted to validate the results of the numerical modeling.

6.2.2 Recommendations for Future Research on the Dynamic Response of Levees with Cutoff Walls

- This study has only investigated one levee geometry and one cutoff wall geometry. Even though most levees are fairly similar, levees of other height, with different slopes, and asymmetry should be investigated. Also other cutoff wall lengths and placements within the levee should be studied.

- There is a need for field and case history data of the seismic response of earthen levees. Such data would be valuable for validating the results of the parametric analyses presented as part of this feasibility study.
- The parametric analysis of levees with cutoff walls founded on liquefiable soils indicated that the presence of a cutoff wall results in more liquefaction than for levees without cutoff walls. However, the results of this study do not provide a definitive answer regarding the mechanism responsible for this difference. Further study into this observed effect of a cutoff wall, including physical testing, should be conducted, in order to revise existing simplified liquefaction triggering evaluation procedures.
- Due to the computationally expensive numerical analysis tools used in this study, a relatively small number of ground motions was investigated. In order to provide recommendations for revision of existing simplified procedures, with regard to the presence of a cutoff wall, broader parametric analyses should be conducted with other numerical methods.

REFERENCES

Athanasopoulos-Zekkos, A. and R. B. Seed (2013). "Simplified methodology for consideration of 2D dynamic response of levees in liquefaction triggering evaluation." Journal of Geotechnical and Geoenvironmental Engineering **139**(11): 1911-1922.

Athanasopoulos-Zekkos, A. and Saadi, M. (2012). "Ground Motion Selection for Liquefaction Evaluation Analysis of Earthen Levees." Earthquake Spectra **28**(4): 1331-1351.

Aveston, J. and A. Kelly (1973). "Theory of multiple fracture of fibrous composites." Journal of Materials Science **8**: 352-362.

Aveston, J., A. Cooper, A. Kelly (1971). The Properties of Fibre Composites, IPC Science and Technology Press Ltd.

Baxter, D. and G. Filz (2007). Deformation predictions of ground adjacent to soil-bentonite cutoff walls using the finite element method. Geo-Denver 2007: New Peaks in Geotechnics, Denver, CO, ASCE.

Beaty, M. and P. M. Byrne (1998). An effective stress model for predicting liquefaction behaviour of sand. Geotechnical Earthquake Engineering and Soil Dynamics III, Seattle, WA, ASCE.

Beaty, M. and P. M. Byrne (2000). A synthesized approach for predicting liquefaction and resulting displacements. Twelfth World Conference on Earthquake Engineering, Auckland, New Zealand.

Bjerrum, L. and N. Simons (1960). Comparison of shear strength characteristics of normally consolidated clays. Conference on Shear Strength of Cohesive Clays, New York, NY, ASCE.

Byrne, P. M. (1991). A Cyclic Shear-Volume Coupling and Pore-Pressure Model for Sand. Second International Conference on Recent Advances in Geotechnical Earthquake Engineering and Soil Dynamics, St. Louis, Missouri 47-55.

Byrne, P. M., S. S. Park, M. Beaty, M.K. Sharp, L. Gonzalez, T. Abdoun (2004). "Numerical modeling of liquefaction and comparison with centrifuge tests." Canadian Geotechnical Journal **41**(2): 193-211.

Dafalias, Y. F. (1986). "Bounding Surface Plasticity. I: Mathematical Foundation and Hypoplasticity." Journal of Engineering Mechanics **112**(9): 966-987.

Di Laora, R., A. Mandolini, G. Mylonakis (2012). "Insight on kinematic bending of flexibile piles in layered soil." Soil Dynamics and Earthquake Engineering **43**: 309-322.

Evans, J. C. (1991). "Geotechnics of Hazardous Waste Control Systems," Chapter 20, Foundation Engineering Handbook, 2nd Edition, Ed. H. Y. Fang, Von Nostrand Reinhold Company, New York, NY.

Feenstra, P. H., J. G. Rots, A. Arnesen, J.G. Teigen, K.V. Hoiseth (1998). A 3D constitutive model for concrete based on a co-rotational concept. Computational Modelling of Concrete Structures. R. d. Borst, Bicanic, Mang and Menschke. Rotterdam, Balkema**:** 13-22.

Fischer, G. and V. C. Li (2002). "Effect of matrix ductility on deformation behavior of steel reinforced ECC flexural memebers under reversed cyclic loading conditions." ACI Structures Journal **99**(6): 781-790.

Golder (2011). Seismic Design Guidelines for Dikes, British Columbia Ministry of Forests, Lands and Natural Resource Operations - Flood Safety Section.

Han, T.-S., P. H. Feenstra, S.L. Billington (2002). Constitutive Model for Highly Ductile Fiber-Reinforced Cementitious Composites. Ithaca, NY, Cornell University.

Han, T.-S., P. H. Feenstra, S.L. Billington (2003). "Simulation of Highly Ductile Fiber-Reinforced Cement-Based Composite Components Under Cyclic Loading." ACI Structural Journal **100**(6): 749-757.

Harder, L. et al. (2009) "Investigation of Tree Root Penetration into a Levee Soil-Cement-Bentonite Slurry Cutoff Wall"

Harder, L. F. and R. Boulanger (1997). Application of K_sigma and K_alpha Correction Factors. NCEER Workshop on Evaluation of Liquefaction Resistance of Soils.

ILH (2013). The International Levee Handbook. London, UK, CIRIA.

Independent Levee Investigation Team (ILIT) (2006). "Investigation of the performance of the New Orleans regional flood protection systems during Hurricane Katrina." *Final Report*., <http://www.ce.berkeley.edu/~new_orleans/> Jully 31, 2006.

Itasca (2011). FLAC - Fast Lagrangian Analysis of Continua, Version 7.0, User's Guide. Minneapolis, MN, Itasca Consulting Group.

Kesner, K. E., S. L. Billington, K. S. Douglas (2003). "Cyclic Response of Highly Ductile Fiber-Reinforced Cement-Based Composites." ACI Materials Journal **100**(5): 381-390.

Lee, B. Y. (2011). Feasibility Study of High-Performance Cut-off Walls for Levees in Seismic Regions: Dynamic Wall Analyses and Ductile Slurry Development. Ann Arbor, University of Michigan.

Lepech, M. D. and V. C. Li (2009). "Water permeability of engineered cementitious composites." Cement & Concrete Composites **31**: 744-753.

Li, V. C. (2003). "On Engineered Cementitious Composites (ECC)." Journal of Advanced Concrete Technology **1**(3): 215-230.

Li, V. C. (2008). Engineered Cementitious Composites (ECC) - Material, Structural, and Durability Performance. Concrete Construction Engineering Handbook. E. Nawy, CRC Press.

Li, V. C. and C. Leung (1992). "Steady-State and Multiple Cracking of Short Random Fiber Composites." Journal of Engineering Mechanics **118**(11): 2246-2264.

Li, V. C. and H.-C. Wu (1992). "Conditions for pseudo strain-hardening in fiber reinforced brittle matrix composites." Applied Mechanics Review **45**(8): 390-398.

Li, V. C., S. Wang, et al. (2001). "Tensile Strain-Hardening Behavior of Polyvinyl Alcohol Engineered Cementitious Composite (PVA-ECC)." ACI Materials Journal **98**(6): 483-492.

Lobbestael, A. J. and A. Athanasopoulos-Zekkos (2013). The effect of input frequency on dynamic soil-structure interaction of levees and cutoff walls. Geo-Congress 2013: Stability and Performance of Slopes and Embankments III, San Diego, CA, ASCE.

Lobbestael, A.J. and Athanasopoulos-Zekkos, A. (2014). "Characterization of the Dynamic Response of Earthen Levees with Cutoff Walls – A Finite Difference Method Study." Soil Dynamics and Earthquake Engineering (under review).

Lobbestael, A.J. and Athanasopoulos-Zekkos, A. (2015). “Soil-Structure Interaction in Levees with Cutoff Walls Founded on Liquefiable Soils.” XVI European Conference on Soil Mechancis and Geotechncial Engineering, Edinburgh, Scotland (under review).

Makdisi, F. and H. B. Seed (1978). "Simplified procedure for estimating dam and embankment earthquake-induced deformations." Journal of the Geotechnical Engineering Division - ASCE **104**(7): 849-867.

Marshall, D. B. and B. N. Cox (1988). "A J-Integral Method for Calculating Steady-State Matrix Cracking Stresses in Composites." Mechanics of Materials **7**: 127-133.

Martin, G. R., W. D. L. Finn, H. B. Seed (1975). "Fundamentals of Liquefaction under Cyclic Loading." Journal of the Geotechnical Engineering Division - ASCE **101**(GT5): 423-438.

Mejia, L. H. and E. M. Dawson (2006). Earthquake deconvolution for FLAC. 4th International FLAC Symposium on Numerical Modeling in Geomechanics.

Millet, R. A., Perez, J. Y., Davidson, R. R. (1992). “USA Practice Slurry Wall Specifications 10 years Later,” Slurry Walls: Design, Construction and Quality Control, ASTM STP 1129, David B. Paul, Richard R. Davidson and Nicholas J. Cavalli, Eds., American Society of Testing and Materials, Philadelphia.

Mononobe, N. and M. Matsuo (1929). On the determination of earth pressures during earthquakes. Worlde Engineering Congress.

NEES EOT (2014), "Seismic Stability of Levees Resting Atop Peat Soil," https://nees.org/resources/7515.

Okabe, S. (1924). "General theory on earth pressure and seismic stability of retaining wall and dam." Journal of Japan Society of Civil Engineers **10**(6): 1277-1323.

Olson, S. M. and T. D. Stark (2002). "Liquefied strength ratio from liquefaction flow failure case histories." Canadian Geotechnical Journal **39**: 629-647.

Papadimitriou, A. G., C. D. Bouckovalas, et al. (2002). "Plasticity model for sand under small and large cyclic strains." Journal of Geotechnical and Geoenvironmental Engineering **127**(11): 973-983.

PEER (2011). NGA Strong Motion Database.

Petersen, M. D., M. P. Moschetti, P. M. Powers, C. S. Mueller, K. M. Haller, A. D. Frankel, Zeng, Yuehua, Razaeian, Sanaz, S. C. Harmsen, O. S. Boyd, Field, Ned, Chen, Rui, K. S. Rukstales, Luco, Nico, R. L. Wheeler, R. A. Williams, A.H. Olsen (2014). Documentation

for the 2014 update of the United States national seismic hazard maps: U.S. Geological Survey Open-File Report 2014-1091, United State Geological Survey**:** 243.

Rathje, E. M., N. A. Abrahamson, J. D. Bray (1998). "Simplified frequency content estimates of earthquake ground motions." Journal of Geotechnical and Geoenvironmental Engineering **124**(2): 150-159.

Razmkhah, A., M. Kamalian, R. Golrokh (2008). Parametric analysis of the seismic response of irregular topographic features. Geotechnical Earthquake Engineering and Soil Dynamics IV, GSP 181, ASCE.

Ricker, N. (1940). "The form and nature of seismic waves and the structure of seismograms." Geophysics **5**(4): 348-366.

Seed, H. B. and I. M. Idriss (1970). Soil moduli and damping factors for dynamic response analyses. Berkeley, CA, University of California.

Seed, H. B. and I. M. Idriss (1971). "Simplified procedure for evaluating soil liquefaction potential." Journal of the Soil Mechanics adn Foundations Division - ASCE **97**(SM9): 1249-1273.

Seed, H.B., Idriss, I.M., Makdisi, F., and Banerjee, N. (1975). Representation of irregular stress time histories by equivalent uniform stress series in liquefaction analyses, EERC 75-29, Earthquake Engineering Research Center, University of California, Berkeley.

Seed, R. B. and L. F. Harder (1990). SPT-based analysis of cyclic pore pressure generation and undrained residual strength. H. B. Seed Memorial Symposium, Vancouver, British Columbia, BiTech Publishing.

Seed, R. B., K. O. Cetin, R. E. S. Moss, A. M .Kammerer, J. Wu, J. M. Pestana, M. F. Riemer, R. B. Sancio, J. D. Bray, R. E. Kayen, A. Faris (2003). Recent Advances in Soil Liquefaction Engineering: A Unified and Consistent Framework. Berkeley, CA, College of Engineering, University of California.

Seed, R. B., R. G. Bea, et al. R. I Abdelmalak, Athanasopoulos-Zekkos, Adda,G. P. Boutwell,J.-L. Briaud, C. Cheung, D. Cobos-Roa, L. Ehrensing, A. V. Govindasamy, L. F. Harder Jr., K. S. Inkabi, J. Nicks, Pestana, J.M., J. Porter, K. Rhee, Riemer, M.F., Rogers, J.D., Storesund, R., Vera-Grunauer, X., and Wartman, J. (2008). "New Orleans and Hurricane Katrina. I: Introduction, Overview, and the East Flank." Journal of Geotechnical and Geoenvironmental Engineering **134**(5): 701-717.

Seed, R. B., R. G. Bea, Athanasopoulos-Zekkos, Adda, G. P. Boutwell, Bray, J. D., C. Cheung, D. Cobos-Roa, J. Cohen-Waeber, B.D. Collins, L. F. Harder Jr., R. E. Kayen, Pestana, J.M.,

Riemer, M.F., Rogers, J.D., Storesund, R., Vera-Grunauer, X., and Wartman, J. (2008). "New Orleans and Hurricane Katrina. IV: Orleans East Bank (Metro) Protected Basin." Journal of Geotechnical and Geoenvironmental Engineering **134**(5): 762-779.

Seed, R. B., R. G. Bea, Athanasopoulos-Zekkos, Adda, G. P. Boutwell, Bray, J. D., C. Cheung, D. Cobos-Roa, L. Ehrensing, L. F. Harder Jr., Pestana, J.M., Riemer, M.F., Rogers, J.D., Storesund, R., Vera-Grunauer, X., and Wartman, J. (2008). "New Orleans and Hurricane Katrina. II: The Central Region and the Lower Ninth Ward." Journal of Geotechnical and Geoenvironmental Engineering **135**(5): 718-739.

Seed, R. B., R. G. Bea, Athanasopoulos-Zekkos, Adda, G. P. Boutwell, Bray, J. D., C. Cheung, D. Cobos-Roa, L. F. Harder Jr., R. E. S. Moss, Pestana, J.M., Riemer, M.F., Rogers, J.D., Storesund, R., Vera-Grunauer, X., and Wartman, J. (2008). "New Orleans and Hurricane Katrina. III: The 17th Street Drainage Canal." Journal of Geotechnical and Geoenvironmental Engineering **134**(5): 740-761.

Shewbridge, S., J. Wu, S. Punyamurthula, J. Vargas, S. Mahnke, and M. Inamine (2009). Simplified Approach to Assess Levee Seismic Vulnerability. 29th Annual USSD Conference. Nashville, Tennessee, United States Society on Dams.

Sitar, N., R. G. Mikola, and G. Candia (2012). Seismically induced lateral earth pressures on retaining structures and basement walls. Geo-Congress 2012: State of the Art and Practice in Geotechnical Engineering, Oakland, CA, ASCE.

Stark, T. D. and G. Mesri (1992). "Undrained Shear Strength of Liquefied Sands for Stability Analysis." Journal of Geotechnical Engineering **118**: 1727-1147.

Stark, T. D., M. Beaty, P. M. Byrne, G. Castro, F. Walberg, V. Perlea, P. Axtell, J. Dillon, W. Empson and D. Mathews (2012). "Seismic deformation analysis of Tuttle Creek Dam." Canadian Geotechnical Journal **49**: 323-343.

Swaisgood, J. R. (2003). Embankment dam deformations caused by earthquakes. 2003 Pacific Conference on Earthquake Engineering. Christchurch, New Zealand, National Society for Earthquake Engineering.

Tsompanakis, Y. (2009). Issues related to the dynamic interaction of retainings walls and retained soil layer. Coupled Site and SSI Effects with Application to Seismic Risk Mitigation. T. Schanz and R. Iankov, Springer Science.

URS. (2007). “Phase 1 technical memorandum draft 2 – Seismology.” Delta Risk Management Strategy Project, San Francisco, CA.

USACE (2013). Guidelines for Seismic Evaluation of Levees. D. o. t. Army. Washington, DC, U.S. Army Corps of Engineers.

Veletsos, A. and S. Younan (1997). "Dynamic Response of Cantilever Retaining Walls." Journal of Geotechnical and Geoenvironmental Engineering **123**(2): 161-172.

Vucetic, M. and R. Dobry (1991). "Effect of soil plasticity on cyclic response." Journal of the Geotechnical Engineering Division - ASCE **111**(1): 89-107.

Yang, E.-H. (2008). Designign Functionalities into ECC Materials via Micromechanics. Doctor of Philosophy, University of Michigan.

Youd, T. L. and M. J. Bennett (1983). "Liquefaction Sites, Imperial Valley, California." Journal of Geotechnical Engineering **109**(3): 440-457.